

SERI/STR-231-1860  
DE83011967

April 1983

# New Thermal Energy Storage Concepts for Solar Thermal Applications

## Final Subcontract Report

Randy Petri  
Estela T. Ong  
Terry D. Claar  
Leonard G. Marianowski

Institute of Gas Technology  
Chicago, Illinois

Prepared under Subcontract No. XP-0-9371-2



# SERI

**Solar Energy Research Institute**

A Division of Midwest Research Institute

1617 Cole Boulevard  
Golden, Colorado 80401

Operated for the  
**U.S. Department of Energy**  
under Contract No. EG-77-C-01-4042

Printed in the United States of America  
Available from:  
National Technical Information Service  
U.S. Department of Commerce  
5285 Port Royal Road  
Springfield, VA 22161  
Price:  
Microfiche \$4.50  
Printed Copy \$11.50

#### **NOTICE**

This report was prepared as an account of work sponsored by the United States Government. Neither the United States nor the United States Department of Energy, nor any of their employees, nor any of their contractors, subcontractors, or their employees, makes any warranty, express or implied, or assumes any legal liability or responsibility for the accuracy, completeness or usefulness of any information, apparatus, product or process disclosed, or represents that its use would not infringe privately owned rights.

**SERI/STR-231-1860  
DE83011967**

**April 1983**

# **New Thermal Energy Storage Concepts for Solar Thermal Applications**

## **Final Subcontract Report**

**Randy Petri  
Estela T. Ong  
Terry D. Claar  
Leonard G. Marianowski**

**Institute of Gas Technology  
Chicago, Illinois**

**Prepared under Subcontract No. XP-0-9371-2**

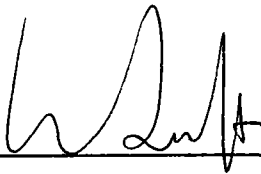
SECTION 1.0

FOREWORD

This report describes the results of work done by the Institute of Gas Technology under subcontract XP-0-9371-2 to the Solar Energy Research Institute, as part of task 1298, in WPA 348-82, in the Energy Storage program. The work was performed over the period 06/15/81 to 07/01/82.

Funds for this work were provided by the Division of Energy Storage Technology of the U. S. Department of Energy.

Approved for the  
SOLAR ENERGY RESEARCH INSTITUTE



---

Werner Luft, Manager  
Solar Energy Storage Program



---

Clayton S. Smith, Manager  
Solar Fuels and Chemicals Research Division

## SECTION 2.0

### SUMMARY

This report presents the results of an investigation into the feasibility of an advanced composite salt/ceramic thermal energy storage media concept for high-temperature solar thermal storage applications. This novel approach involves retention and immobilization of phase-change salts within porous ceramic matrices by capillary action. Composite media pellets, bricks, or other suitable shapes may be used in direct-contact heat recovery/storage applications with compatible fluids, thus eliminating expensive heat exchanger tubes required in molten salt storage systems utilizing shell-and-tube designs. Higher heat transfer rates are also expected based on the ability to control and minimize the thickness of solidified salt zones.

A composite material consisting of  $\text{Na}_2\text{CO}_3\text{-BaCO}_3$  salt (715°C melting point) supported by MgO ceramic particles was selected as a model material for experimental processing, stability, and behavior studies. Techniques developed for processing of composite carbonate/ceramic powders by spray drying and for fabrication of high-density pellets by cold pressing/sintering are described. The results of high-temperature stability studies have demonstrated the ability of the media to retain significant volume fractions of molten carbonate and to maintain their shape and structural integrity after repeated thermal cycling. Thermal charge/discharge cycling results are also presented for laboratory-scale tests on media pellets in a packed-bed configuration.

Preliminary economic analyses indicate that significant reductions in storage system cost and volume requirements may be realized with composite carbonate/salt media relative to storage based on refractories such as MgO or  $\text{Al}_2\text{O}_3$ . Further research and development efforts directed toward optimization of media composition, development of cost-effective commercial processing methods, and demonstration of long-term endurance are recommended.

## SECTION 3.0

### TABLE OF CONTENTS

|   | <u>Page</u> |
|---|-------------|
| 1.0 Foreword.....   | iii         |
| 2.0 Summary.....  | v           |
| 6.0 Background and Introduction.....  | 1           |
| 7.0 Technical Discussion.....   | 5           |
| 7.1 Task 1.0. Establishment of Concept Feasibility.....                                   | 5           |
| 7.1.1 Subtask 1.1. Materials Selection.....   | 5           |
| 7.1.2 Subtask 1.2. Development of Materials Processing and<br>Fabrication Techniques..... | 7           |
| 7.1.3 Subtask 1.3. Evaluation of Composite Materials<br>Behavior.....                     | 17          |
| 7.1.4 Summary of Composite Materials Behavior.....  | 29          |
| 7.2 Task 2.0. Proof-of-Concept Testing.....   | 30          |
| 7.2.1 Subtask 2.1. Laboratory-Scale Module Design and<br>Fabrication.....                 | 30          |
| 7.2.2 Subtask 2.2. Laboratory-Scale Testing and Evaluation..                              | 32          |
| 7.2.3 Performance Evaluation.....   | 38          |
| 7.2.4 Subtask 2.3. Post-Test Examination.....   | 52          |
| 7.3 Task 3.0. Economic Analyses.....  | 52          |
| 8.0 Task 4.0 Summary and Recommendations.....   | 68          |
| 8.1 Summary.....  | 68          |
| 8.2 Recommendations for Future Research.....  | 69          |
| 9.0 References Cited.....   | 71          |
| Appendix. Conversion Factors.....   | 73          |

## SECTION 4.0

### LIST OF FIGURES

|      |  | <u>Page</u> |
|------|--|-------------|
| 6-1  | Air Brayton Cycle Solar Thermal Power Plant/Storage Schematic....  | 2           |
| 6-2  | Schematic Microstructure of Composite TES Media:<br>Molten Salt Supported by Ceramic Matrix.....   | 4           |
| 7-1  | Enthalpy Contents of Selected Sensible- and Latent-Heat<br>Storage Materials.....  | 6           |
| 7-2  | Stork-Bowen Laboratory-Scale Spray Drying Facility At IGT.....   | 9           |
| 7-3  | Processing of Composite Carbonate/Ceramic Media.....   | 10          |
| 7-4  | $\text{Na}_2\text{CO}_3\text{-BaCO}_3/\text{NaAlO}_2$ Powder Prepared By Spray Drying and<br>Firing at $850^\circ\text{C}$ for 5 Hours (SN57BN-1A).....  | 13          |
| 7-5  | Cold-Pressing Characteristics of Spray Dried $\text{Na}_2\text{CO}_3\text{-BaCO}_3/\text{NaAlO}_2$<br>Powders With PVA + Ethylene Glycol Binder (SN57BN-1A).....   | 14          |
| 7-6  | Compaction and Sintering Behaviors of $\text{Na}_2\text{CO}_3\text{-BaCO}_2/\text{MgO}$<br>Composites (SM51AN-A1).....   | 15          |
| 7-7  | As-Fabricated $\text{Na}_2\text{CO}_3\text{-BaCO}_2/\text{MgO}$ Pellets Used for Laboratory-Scale<br>TES Testing.....  | 18          |
| 7-8  | Changes in Composite TES Pellets Heated in Air.....  | 20          |
| 7-9  | SEM Fractographs of $\text{Na}_2\text{CO}_3\text{-BaCO}_3/\text{NaAlO}_2$ Pellet Heated at $850^\circ\text{C}$<br>for 350 Hours and Two Thermal Cycles to R.T. (SN57BN-1A).....  | 21          |
| 7-10 | SEM Micrographs of Fracture Surface From $\text{Na}_2\text{CO}_3\text{-BaCO}_3/\text{MgO}$<br>Pellet Tested at $800^\circ\text{C}$ for 200 Hours (SM51BN-1A).....  | 23          |
| 7-11 | $\text{Na}_2\text{CO}_3\text{-BaCO}_3/\text{MgO}$ (SM51BN-1A) Pellets After a Total of 510<br>Hours at $800^\circ\text{C}$ With 22 Thermal Cycles.....   | 24          |
| 7-12 | SEM Fractograph of $\text{Na}_2\text{CO}_3\text{-BaCO}_3/\text{MgO}$ Pellet Sintered 2 Hours<br>at $1100^\circ\text{C}$ and Tested 1115 Hours (at $800^\circ\text{C}$ for 510 Hours)<br>With 22 Thermal Cycles to Near Room Temperature, All in Air..... | 25          |
| 7-13 | Six Possible Contact Stresses in a Packed Bed of Pellets.....  | 27          |
| 7-14 | Modified Reynolds Number Versus Temperature For Various Ambient<br>Inlet Air Flow Rates Through 3.54-Inch-Diameter Bed.....  | 31          |
| 7-15 | Four-Station TES Laboratory-Scale Test Stand.....  | 33          |
| 7-16 | Cross Section of Laboratory-Scale TES Test Cannister.....  | 34          |

SECTION 4.0

LIST OF FIGURES, Cont.

|      | <u>Page</u>   |
|------|---|
| 7-17 | Laboratory-Scale TES Test Cannister..... 35   |
| 7-18 | Schematic Diagram of Laboratory-Scale TES Module..... 37  |
| 7-19 | Cold-Pressed and Sintered Composite Na <sub>2</sub> CO <sub>3</sub> -BaCO <sub>3</sub> /MgO TES<br>Pellets Loaded Into TES Test Cannister..... 40                                   |
| 7-20 | Typical Discharge Performance of Laboratory-Scale TES Unit<br>Containing Composite 51 Wt % Na <sub>2</sub> CO <sub>3</sub> -BaCO <sub>3</sub> /49 Wt % MgO Media..... 42            |
| 7-21 | Reynolds Number Versus Temperature For Various Inlet Air Flow<br>Rates Through a 0.5-Inch Tube..... 43  |
| 7-22 | Composite Media Discharge Performance at 200 SCF/h Air Flow<br>Rate on Run 4 (149 Hours of Operation)..... 44   |
| 7-23 | Composite Media Discharge Performance at 200 SCF/h Air Flow<br>Rate on Cycle 13 (314 Hours of Operation)..... 45  |
| 7-24 | Typical Discharge Performance of Na <sub>2</sub> CO <sub>3</sub> -BaCO <sub>3</sub> System at 180 ft <sup>3</sup> /h<br>Air Flow Rate..... 46                                       |
| 7-25 | Discharge Air Outlet Temperatures Versus Time for 51 Wt %<br>Na <sub>2</sub> CO <sub>3</sub> -BaCO <sub>3</sub> /49 Wt % MgO Composite System At 200 SCF/h Air<br>Flow Rate..... 47 |
| 7-26 | Temperature Profile in Bed During Fourth Cycle at 200 SCF/h<br>Air Flow Rate..... 49  |
| 7-27 | Lifetime Discharge Performance of 51 Wt % Na <sub>2</sub> CO <sub>3</sub> -BaCO <sub>3</sub> /<br>49 Wt % MgO Media Packed Bed..... 50  |
| 7-28 | TES Composite Bed Pressure Drop as a Function of Air Flow Rate<br>for Pre- and Post-Test Conditions..... 53   |
| 7-29 | Post-Test Appearance of TES Test Cannister and Composite Media... 56  |
| 7-30 | Estimated Materials Costs for Na <sub>2</sub> CO <sub>3</sub> /Ceramic Composites..... 57   |
| 7-31 | Storage Media Cost in Dollars per Million Btu Stored as a<br>Function of Temperature Swing for Baseline and Composite Media... 59   |
| 7-32 | Volume Requirements per Unit of Energy Stored as a Function of<br>Temperature Swing for Baseline and Composite Media..... 60  |



SECTION 5.0

LIST OF TABLES

|      | <u>Page</u>  |
|------|--|
| 7-1  | Congruent Melting Carbonate Compositions..... 8  |
| 7-2  | Characteristics of Composite TES Media Powders..... 12   |
| 7-3  | Mass and Thermal Capacity Sizing of Laboratory-Scale TES Bed..... 36   |
| 7-4  | Pellet and Packed-Bed Characteristics..... 39  |
| 7-5  | Lifetime Average Heat Flux Discharge Performance for 51 Wt %<br>NaBaCO <sub>3</sub> /49 Wt % MgO Composite Media..... 51                                 |
| 7-6  | Pre- and Post-Test Composite Media Characteristics..... 54   |
| 7-7  | Pre- and Post-Test Chemical Analysis of 51 Wt % NaBaCO <sub>3</sub> /<br>49 Wt % MgO Composite System..... 55  |
| 7-8  | Comparison of Composite Media and Baseline (Solid Sensible)<br>Storage Requirements, $\Delta T = 250^{\circ}\text{C}$ ( $450^{\circ}\text{F}$ )..... 62  |
| 7-9  | Composite Versus Baseline Ratio and Percent Savings for Media<br>(Fabricated), $\Delta T = 250^{\circ}\text{C}$ ( $450^{\circ}\text{F}$ )..... 63        |
| 7-10 | Comparative Impact of Volume Reduction on Projected System<br>Containment Cost, $\Delta T = 250^{\circ}\text{C}$ ( $450^{\circ}\text{F}$ )..... 65       |
| 7-11 | Preliminary Thermal Storage Economic Evaluation for Sensible and<br>Direct-Contact Composite Storage Systems (Two 75-MWe Gross<br>Power Modules)..... 67 |

## SECTION 6.0

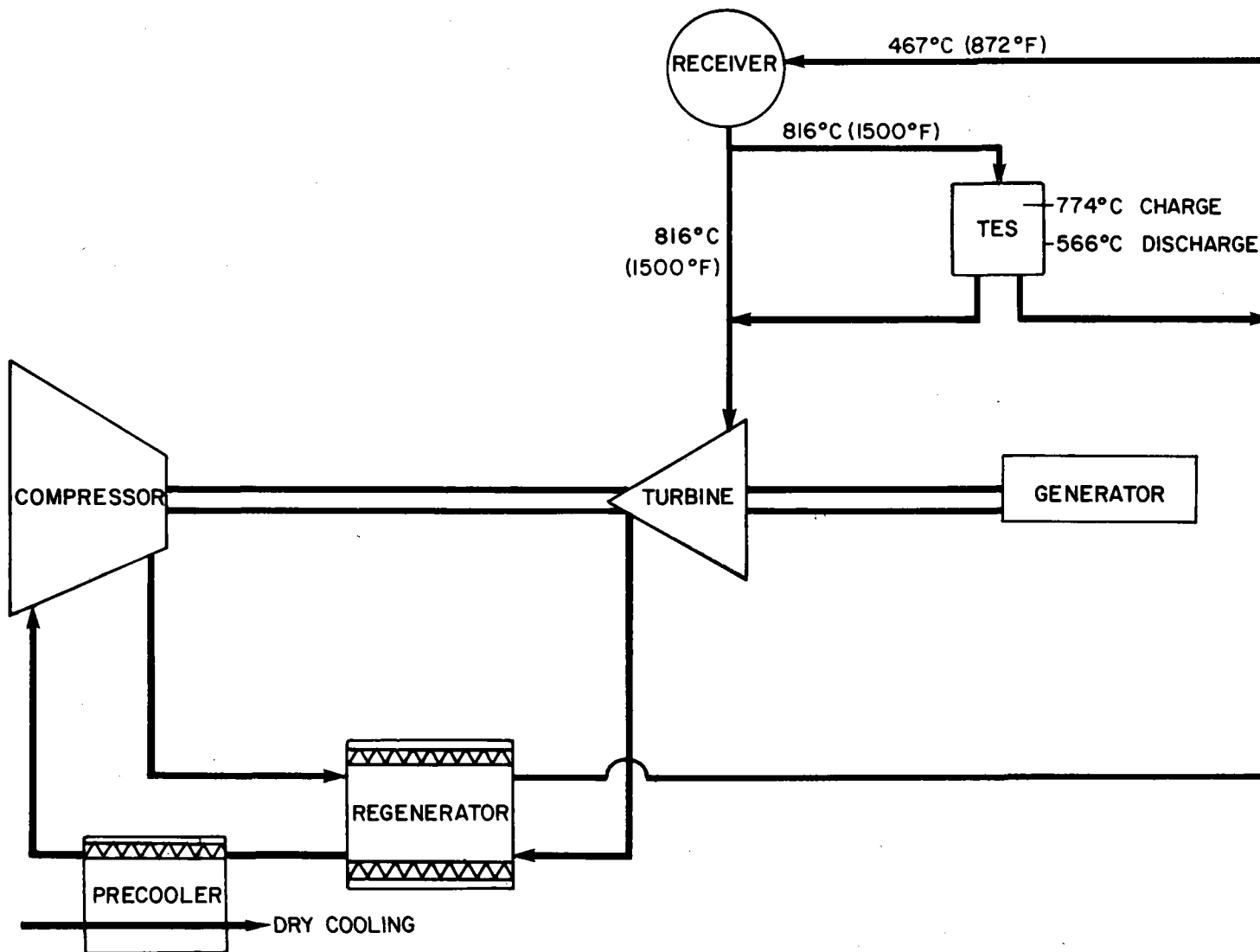
### BACKGROUND AND INTRODUCTION

This report presents the results of a program conducted by the Institute of Gas Technology (IGT) entitled "New Thermal Energy Storage Concepts for Solar Thermal Applications." The program was performed for the U.S. Department of Energy and managed by the Solar Energy Research Institute under Subcontract No. XP-0-9371-2.

Numerous thermal energy storage (TES) technologies are under development for application in solar thermal power systems to provide for continuous operation during nonsolar hours and during periods of variable insolation, as outlined in Reference 1. First-generation TES subsystems include dual media oil/rocks and oil thermoclines. Second-generation TES technology development is focusing on storage subsystems for solar receivers cooled by water/steam, molten salts, liquid metals, organic fluids, or gases. The objective of the current effort is to investigate the technoeconomic feasibility of an advanced composite salt/ceramic TES media concept that offers potential cost/performance benefits over second-generation solar Brayton TES technologies and that will provide an advanced TES technology base for application in future solar thermal systems.

One of the advanced solar thermal power systems to which this advanced media concept may be applicable is a high-temperature Brayton cycle system, illustrated schematically in Figure 6-1. This system consists of a high-temperature central receiver integrated with a closed cycle air Brayton subsystem and a TES subsystem. The primary air flow circuit from the receiver is through the turbine, recuperator (low-pressure side), pre-cooler, compressor, recuperator (high-pressure side), and back to the receiver. The alternative TES loop extends solar-plant electricity production into non-insolation hours. The 3.45 MPa (500 psia) air working fluid is heated to a temperature of 816°C (1500°F) in the central receiver. The heated air is used to charge the storage subsystem to a temperature of 774°C (1425°F). During discharge, the storage system is cooled to approximately 566°C (1050°F).

A number of technology development and systems studies have been conducted on latent-heat storage using inorganic salt phase-change materials (e.g. carbonates, chlorides, fluorides, hydroxides, and nitrates). In general, the results of these efforts have shown the advantages of latent-heat systems in providing high energy storage densities and availability of stored latent heat at constant temperature. Most efforts have focused on containment of molten salts in a shell-and-tube heat exchanger configuration. But passive tube-intensive designs have inherent heat transfer performance limitations caused by growth of solid salt layers on external heat exchanger tube surfaces during thermal discharge. Attempts to improve thermal performance through use of high-conductivity extended surfaces and active concepts using mechanical salt scrapers have met with limited success. Another drawback of tube-intensive latent-heat designs is that systems for very-high-temperature (>700°C) applications require the use of superalloy heat exchanger tube materials for adequate strength and corrosion resistance, significantly increasing capital costs.



A79122779

Figure 6-1. AIR BRAYTON CYCLE SOLAR THERMAL POWER PLANT/STORAGE SCHEMATIC

Work conducted under previous TES development programs at IGT has demonstrated the attractive properties and stability of alkali metal/alkaline earth metal carbonates as latent-heat phase-change storage media, as indicated in References 2 through 6. Various carbonate compositions with melting points covering the range of 397° to 898°C (747° to 1648°F) have been evaluated for materials compatibility and TES performance as free melts in shell-and-tube heat exchanger configurations utilizing austenitic stainless-steel or nickel-base superalloy materials of construction. An engineering-scale TES module of 25 MJ (24,000 Btu) thermal capacity (latent plus sensible) has also been designed, fabricated, and tested with 59 kg (130 lb) of  $\text{LiKCO}_3$  salt, which melts congruently at 505°C (941°F) with a heat of fusion of 344 kJ/kg (148 Btu/lb). The module showed very stable thermal performance and excellent compatibility between salt and AISI 316 stainless-steel containment vessel and heat exchanger tube materials during 5650 hours of testing and 129 charge/discharge cycles over the temperature range 480° to 535°C (896° to 995°F). Although the 300-series austenitic stainless steels have been found to be generally compatible with molten carbonates at temperatures up to 700°C (1292°F), superalloys or coatings are required for long-term operation at higher temperatures, significantly increasing the cost of a TES subsystem.

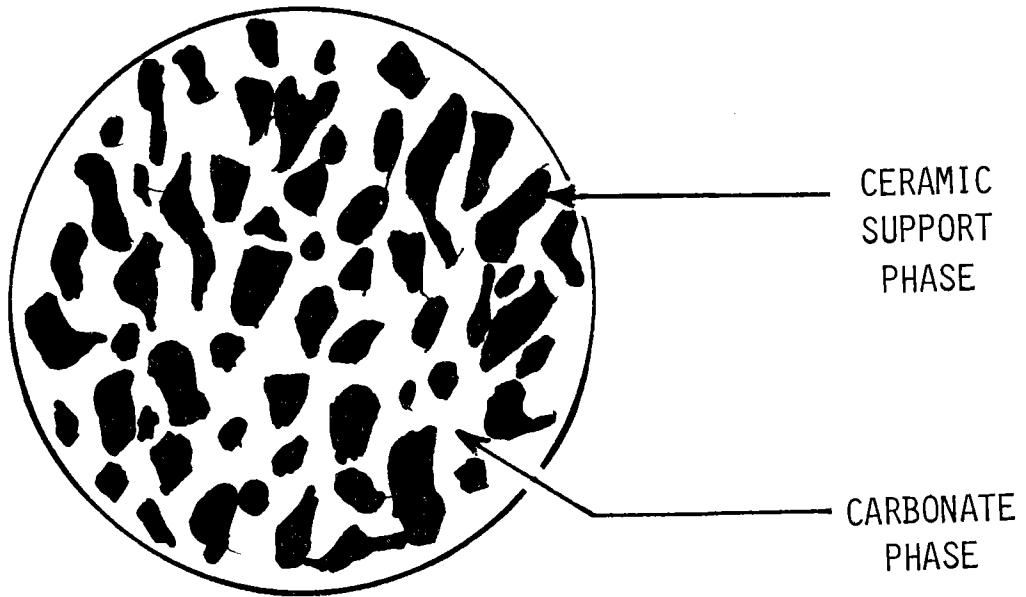
The objective of the current study was to assess the potential of an advanced media concept that takes advantage of the attractive properties of phase-change materials, thus eliminating the performance and cost limitations associated with tube-intensive systems.

This novel composite-media concept involves retention and immobilization of phase-change salts within porous ceramic matrices.\* The ceramic phase may consist of a distribution of discrete submicron-sized particles, as shown in the schematic microstructure of Figure 6-2, or as an interconnected phase in a partially sintered porous body. The molten salt is retained within the void space defined by the ceramic network, primarily by capillary forces. The volume fraction of molten salt that can be retained is determined by characteristics of the support material (particle size and shape distributions, specific surface area), salt properties (surface tension, viscosity), and wetting behavior between molten salt and ceramic. The feasibility of retaining 65-volume-percent (65 vol %) molten alkali carbonates within a ceramic particle matrix at 700°C has been experimentally demonstrated. Retention of higher volume fractions of liquid is possible by optimization of ceramic support characteristics and media processing conditions.

Immobilization of the molten salt within the porous ceramic structure permits operation of the composite pellets, bricks, or other suitable shapes in direct contact with compatible fluids, thus eliminating expensive heat exchanger tubes required in shell-and-tube designs. Such a direct-contact heat exchanger design could consist of composite media shapes fabricated as cylindrical pellets, briquettes, spheres, etc., and utilized in a packed-bed arrangement. Alternatively, composite materials could be formed as brick shapes and stacked in a regular array similar to a checkerwork regenerator. High heat transfer rates are expected from both control and minimization of solidified salt thicknesses and elimination of thermal resistances associated with heat exchanger tubes. Media shapes and sizes can be readily varied to optimize heat transfer surface/volume ratio and bed packing density.

---

\* IGT has filed a patent application on this concept.



A83040424

Figure 6-2. SCHEMATIC MICROSTRUCTURE OF COMPOSITE TES MEDIA:  
MOLTEN SALT SUPPORTED BY CERAMIC MATRIX

## SECTION 7.0

### TECHNICAL DISCUSSION

#### 7.1 TASK 1.0. ESTABLISHMENT OF CONCEPT FEASIBILITY

The overall objective of this program was to investigate, develop, and assess the feasibility of an innovative, direct-contact, TES heat exchange concept utilizing phase-change salts contained within a porous ceramic matrix for solar applications. This effort addressed the materials development and lab-scale proof-of-concept testing essential to the improvement and further refinement of the cost/predictive performance evaluations for an advanced, latent/sensible media, direct heat exchange concept.

This task involved development and testing of TES materials, powder processing/composite-shape fabrication, and evaluation of composite media behavior critical to assessing and understanding the operational feasibility of a direct-contact latent/sensible TES concept. In addition, the results from a parallel DOE-funded program (ORNL/UCC Subcontract No. 86X-9400-1C) focusing on industrial TES applications of this advanced concept were made available to this program.

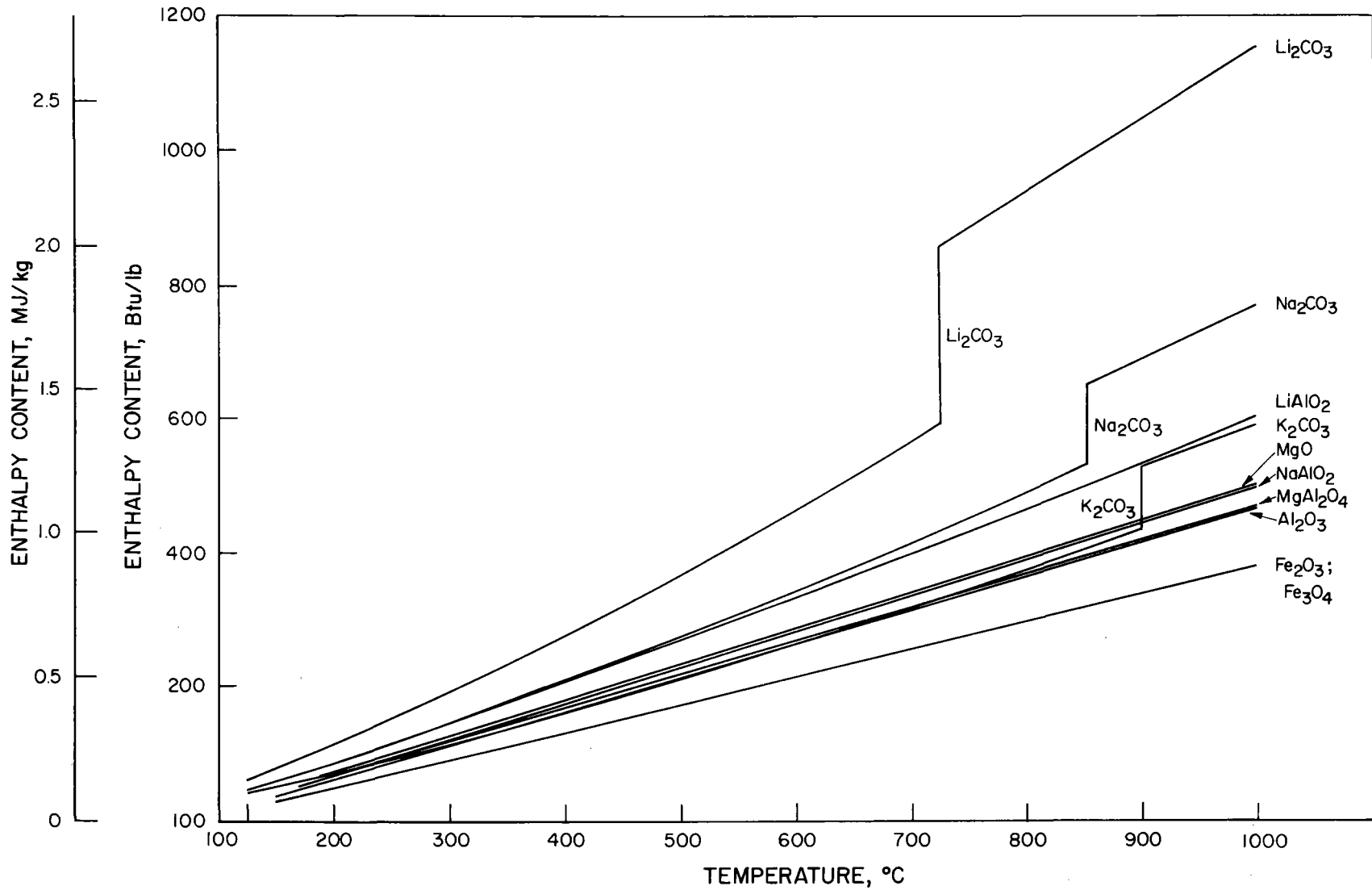
The technical feasibility of this approach will depend on a number of key factors:

- Ability of the ceramic support to retain adequate amounts of molten salt by capillary action, with minimal chemical interaction between salt and ceramic. Creepage of molten salt from the porous shape must be minimal.
- Chemical compatibility of the molten salts with solar TES charge/discharge fluids to minimize vaporization losses or changes in salt chemistry, melting behavior, surface tension, and other critical physical properties.
- Sufficient strength to maintain physical integrity under the stresses imposed by the system design.

##### 7.1.1 Subtask 1.1. Materials Selection

One possible solar application of the concept is in storage for solar Brayton power systems operating at 700° to 900°C (1292° to 1652°F) with air or helium working fluids. Mixtures of alkali metal/alkaline earth metal carbonates were selected for development and evaluation based on the availability of moderate-cost carbonate compositions with melting temperatures in this range, attractive heats of fusion, and their high-temperature thermochemical stabilities in both inert and oxidizing environments. Ceramic support materials were selected from among metal oxides and aluminates. Figure 7-1 shows enthalpy curves for several candidate latent- and sensible-heat materials.

Ten congruently melting carbonate mixtures based on  $\text{Li}_2\text{CO}_3$ ,  $\text{Na}_2\text{CO}_3$ , and  $\text{K}_2\text{CO}_3$  were identified, having melting points (mp's) covering the temperature range



A80112884

Figure 7-1. ENTHALPY CONTENTS OF SELECTED SENSIBLE- AND LATENT-HEAT STORAGE MATERIALS

397° to 858°C (747° to 1576°F). A summary of selected properties of these carbonate compositions is given in Table 7-1. Emphasis was given to salt compositions having mp's above approximately 700°C (~1300°F), applicable to thermal storage for solar Brayton power systems. Specifically, the 48-weight-percent (48 wt %) Na<sub>2</sub>CO<sub>3</sub>-52 wt % BaCO<sub>3</sub> having an mp of ~715°C was selected for process development under this project, while the 50 wt % Na<sub>2</sub>CO<sub>3</sub>-50 wt % K<sub>2</sub>CO<sub>3</sub> composition and Na<sub>2</sub>CO<sub>3</sub> were studied under the parallel industrial TES program. The Na<sub>2</sub>CO<sub>3</sub>-BaCO<sub>3</sub> salt had been tested under a previous TES program at IGT as a phase-change salt material in a lab-scale TES unit with a central heat exchanger tube. It showed good stability during repeated thermal cycling and exhibited thermal arrests over the 712° to 717°C temperature range. Also under that program, the Na<sub>2</sub>CO<sub>3</sub>-BaCO<sub>3</sub> salt was determined by Dynatech R&D Company to have an mp of 716°C and a heat of fusion of 185 kJ/kg (79.6 Btu/lb). These salt property results were confirmed under this program using a Perkin-Elmer DSC-2 differential scanning calorimeter, from which an mp of 707°C and a heat of fusion of 175.8 kJ/kg (75.6 Btu/lb) were measured.

The ceramic support materials (sensible-heat phase) that were considered included metal oxides, aluminates, ferrites, and titanates. The functions of the ceramic phase are to retain the molten carbonate salt and to provide sensible heat to the composite media. The most critical property of the ceramic support material is expected to be its chemical stability in the high-temperature carbonate environment. Significant chemical reaction or solubility of the ceramic in the molten carbonate will affect the long-term carbonate retention property and structural integrity of the composite. Other selection criteria for the ceramic support material include specific heat, cost, and ability to prepare as fine particulates or porous bodies.

For supporting the Na<sub>2</sub>CO<sub>3</sub>-BaCO<sub>3</sub> salt, MgO and NaAlO<sub>2</sub> were experimentally evaluated as support particles, based on their expected low solubilities in molten carbonates [7,8,9] and on the lower cost of these materials relative to the titanate and zirconate families.

#### 7.1.2 Subtask 1.2. Development of Materials Processing and Fabrication Techniques

Processing of the composite media powders and shapes containing carbonate and ceramic support materials was based on IGT's extensive experience in preparation of similar materials for high-temperature molten carbonate fuel cell applications. A spray drying process was developed for preparation of the carbonate/ceramic powders, based on its ability to produce intimately dispersed, homogeneous powders with good flowability. Spray drying was performed using the Stork-Bowen laboratory-scale spray dryer pictured in Figure 7-2. The spray dried powders may be fabricated into high-density TES pellets by a number of ceramic-forming processes, including die pressing, extrusion, or briquetting. Figure 7-3 is a flow diagram showing the various composite media processing steps.

Composite powders of the Na<sub>2</sub>CO<sub>3</sub>-BaCO<sub>3</sub>/NaAlO<sub>2</sub> and Na<sub>2</sub>CO<sub>3</sub>-BaCO<sub>3</sub>/MgO compositions were prepared by spray drying aqueous slurries of the carbonate salt and ceramic support raw materials. The technical-grade materials used to provide cost-effective TES media included Stauffer Lite Na<sub>2</sub>CO<sub>3</sub>, Foote Mineral BaCO<sub>3</sub>, Nalco 680P Na<sub>2</sub>Al<sub>2</sub>O<sub>4</sub>·3H<sub>2</sub>O, and Basic Chemicals Magox 98HR Fine MgO. The

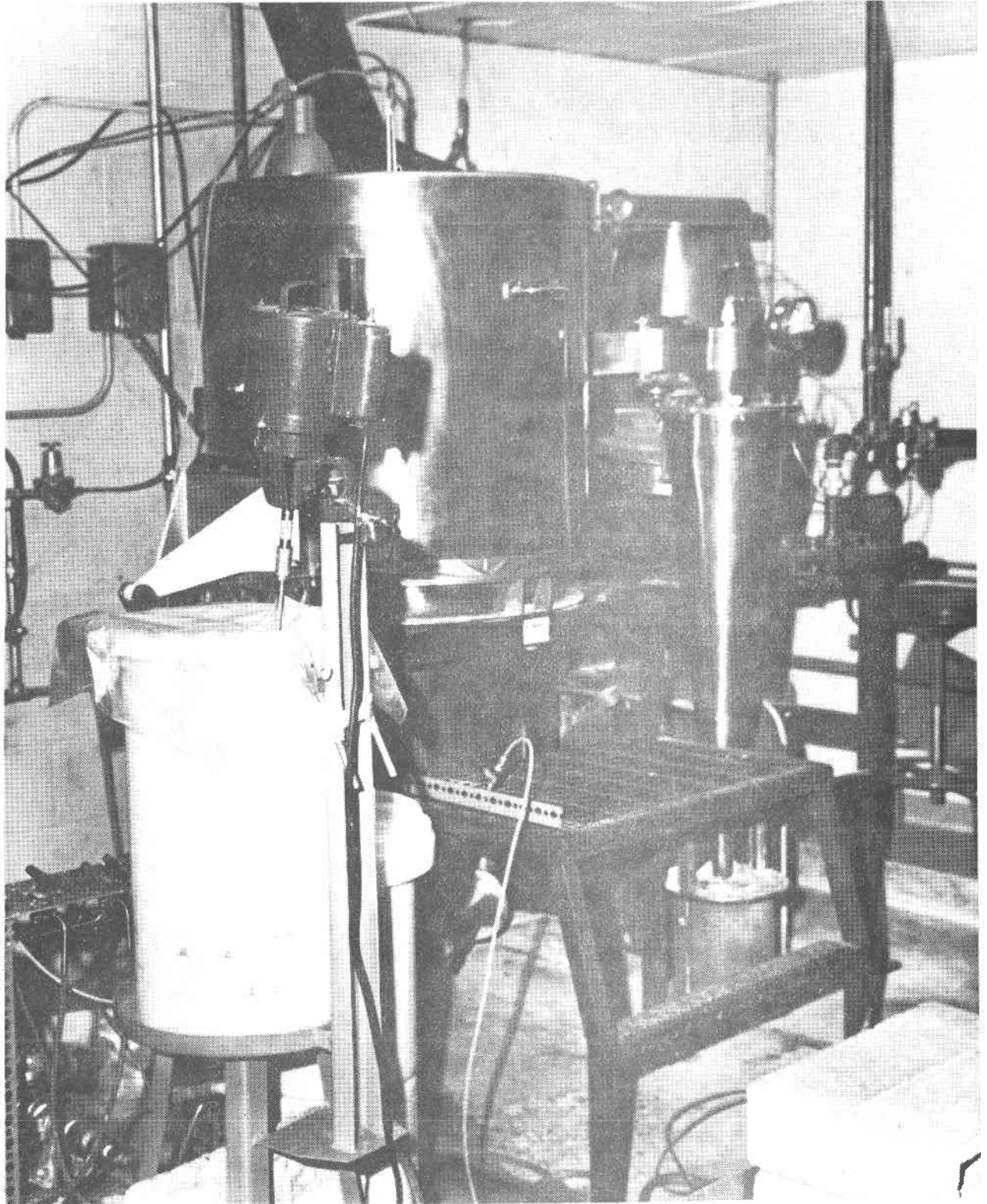


Table 7-1. CONGRUENT MELTING CARBONATE COMPOSITIONS

| Composition, wt %   | mp, |        | $\Delta H_f$ , |          | Cost, |                       | J/\$ (Btu/\$ <sup>b</sup> ) |        |
|---|-----|--------|----------------|----------|-------|-----------------------|-----------------------------|--------|
|   | °C  | (°F)   | J/kg           | (Btu/lb) | \$/kg | (\$/lb <sup>a</sup> ) |                             |        |
| 32 Li <sub>2</sub> CO <sub>3</sub> -33 Na <sub>2</sub> CO <sub>3</sub> -35 K <sub>2</sub> CO <sub>3</sub> | 397 | (747)  | 276,794        | (119)    | 1.01  | (0.46)                | 273,260                     | (259)  |
| 46.6 Li <sub>2</sub> CO <sub>3</sub> -53.4 K <sub>2</sub> CO <sub>3</sub>                                 | 488 | (910)  | 390,768        | (168)    | 1.48  | (0.67)                | 264,819                     | (251)  |
| 44.3 Li <sub>2</sub> CO <sub>3</sub> -55.7 Na <sub>2</sub> CO <sub>3</sub>                                | 496 | (925)  | 393,094        | (169)    | 1.21  | (0.55)                | 323,902                     | (307)  |
| 28.5 Li <sub>2</sub> CO <sub>3</sub> -71.5 K <sub>2</sub> CO <sub>3</sub>                                 | 498 | (928)  | 316,336        | (136)    | 1.06  | (0.48)                | 298,581                     | (283)  |
| 35.0 Li <sub>2</sub> CO <sub>3</sub> -65.0 K <sub>2</sub> CO <sub>3</sub>                                 | 505 | (941)  | 344,248        | (148)    | 1.21  | (0.55)                | 283,810                     | (269)  |
| ∞ 55.7 Li <sub>2</sub> CO <sub>3</sub> -44.3 CaCO <sub>3</sub>  | 662 | (1224) | --             | --       | 1.52  | (0.69)                | --                          | --     |
| 47.8 Na <sub>2</sub> CO <sub>3</sub> -52.2 BaCO <sub>3</sub>  | 715 | (1319) | 186,080        | (80)     | 0.24  | (0.11)                | 710,053                     | (673)  |
| 50 Na <sub>2</sub> CO <sub>3</sub> -50 K <sub>2</sub> CO <sub>3</sub>                                     | 710 | (1310) | 162,820        | (70)     | 0.24  | (0.11)                | 671,016                     | (636)  |
| Li <sub>2</sub> CO <sub>3</sub>   | 723 | (1330) | 607,086        | (261)    | 2.67  | (1.21)                | 227,892                     | (216)  |
| Na <sub>2</sub> CO <sub>3</sub>   | 858 | (1576) | 265,164        | (114)    | 0.07  | (0.03)                | 4,009,213                   | (3800) |
| K <sub>2</sub> CO <sub>3</sub>  | 898 | (1648) | 200,036        | (86)     | 0.42  | (0.19)                | 477,940                     | (453)  |

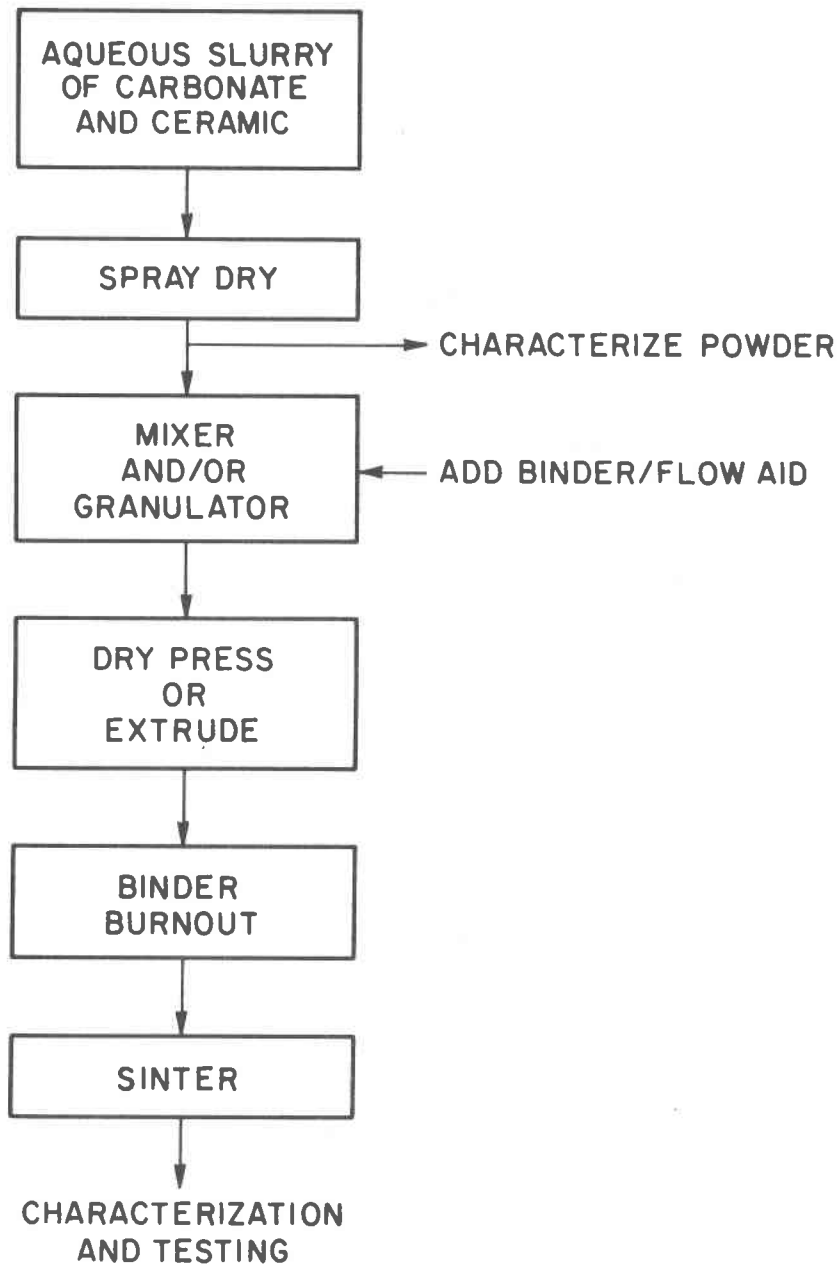
<sup>a</sup> Costs from Chemical Marketing Reporter, June 16, 1980.

<sup>b</sup> Based on heat of fusion only; sensible heats neglected.



P83040425

Figure 7-2. STORK-BOWEN LABORATORY-SCALE  
SPRAY DRYING FACILITY AT IGT



A83020287

Figure 7-3. PROCESSING OF COMPOSITE CARBONATE/CERAMIC MEDIA

$\text{Na}_2\text{Al}_2\text{O}_4 \cdot 3\text{H}_2\text{O}$  and  $\text{Na}_2\text{CO}_3$  were soluble in water, while the  $\text{BaCO}_3$  and  $\text{MgO}$  were dispersed in water to form an aqueous slurry for spray drying. Characteristics of composite powders prepared by spray drying are listed in Table 7-2. The weight percent of carbonate salt in the materials was adjusted so that the composite shapes contained ~60 vol % molten salt phase. Powder Batch SN57BN-1A ( $\text{Na}_2\text{CO}_3\text{-BaCO}_3/\text{NaAlO}_2$ ) was fired at  $850^\circ\text{C}$  for 5 hours under a  $\text{CO}_2$  environment to complete the  $\text{NaAlO}_2$  formation process, to ensure full carbonation of the salt phase and to remove any residual moisture. Micrographs of the final powder (Figure 7-4) show spherical agglomerates typical of a spray dried powder (left) and submicron-sized  $\text{NaAlO}_2$  (right) coated by molten salt. The spray dried powder batches SM51BN-1A and -2A ( $\text{Na}_2\text{CO}_3\text{-BaCO}_3/\text{MgO}$ ) did not undergo any high-temperature treatment prior to use, since the starting materials were already in the forms that are required in the final powder. X-ray diffraction analysis of these latter two powders showed the presence of  $\text{Mg}(\text{OH})_2$ , which was eliminated without difficulty after the powder was pressed into pellets and subsequently heated for densification.

The composite powders were consolidated into pellets to provide high density for evaluation of salt retention capability, thermal cycling response, and packed-bed behavior. The compaction behaviors of both types of powders described above were investigated using steel dies and a laboratory press. Pellet densification behavior under various sintering conditions was also studied.

For the  $\text{Na}_2\text{CO}_3\text{-BaCO}_3/\text{NaAlO}_2$  powder (Batch SN57BN-1A), a binder solution of polyvinyl alcohol and ethylene glycol in water was mixed with the powder prior to cold pressing in a 2-cm (0.8-in.) steel die. Pellets of approximately 5 g (0.011 lb) in weight were pressed at pressures of from 34.5 to 206.8 MPa (5,000 to 30,000 psi). The binder-free pellet densities ranged from 65% to 78% of theoretical density, as shown in Figure 7-5. Without adding binder to the powder, a 14-g (0.03-lb) pellet pressed at 206.8 MPa (30,000 psi) in a 2.84-cm (1.12-in.) steel die achieved only 73% of the theoretical density, comparable to the 2.03-cm (0.8-in.) diameter pellets pressed at 82.7 MPa (12,000 psi) with binders. Pellets with various green densities were then heat treated under several conditions to determine their densification behavior. First the pellets were heated in vacuum at  $850^\circ\text{C}$  ( $1562^\circ\text{F}$ ) for 2 hours. Except for elimination of the binder, no changes in weight, dimensions, and densities were observed. The pellets were then heated in air at  $850^\circ\text{C}$  for 50 hours. Weight losses of 3.5% to 4.5% were observed. The pellets turned yellow-green in color and their densities increased proportionally to their initial as-pressed densities (Figure 7-5). No visible cracks and only very minor shape deformations were observed from these specimens. Further longer-term thermal stability tests were performed on these pellets in air at  $850^\circ\text{C}$  and will be discussed in Section 1.3.

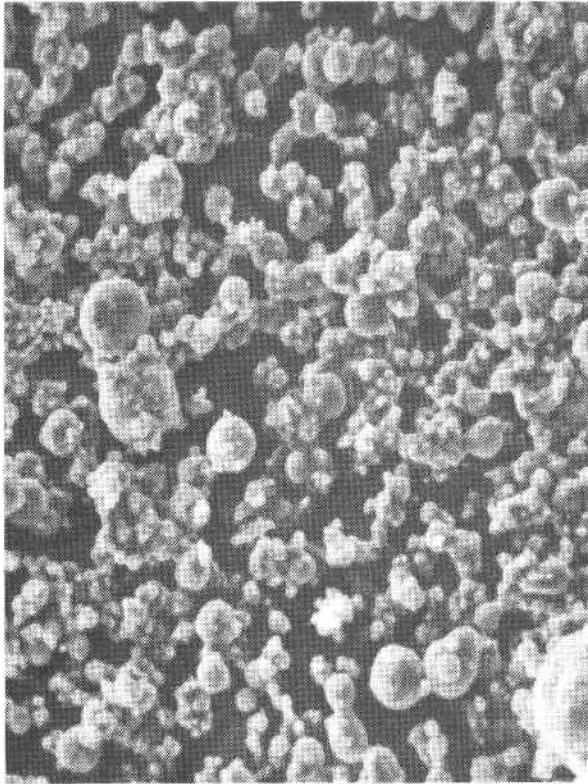
Pellets from  $\text{Na}_2\text{CO}_3\text{-BaCO}_3/\text{MgO}$  powder (Batch SM51BN-1A) required relatively high ejection forces to remove pellets from the die after pressing, and it was found that substantial amounts of binder solution (polyvinyl alcohol and ethylene glycol in water) needed to be added to the powder to significantly reduce this ejection force. The presence of such high binder contents in effect limits the binder-free pellet density that can be achieved during cold pressing. Hence, the compaction behavior of SM51BN-1A powder under cold pressure was determined on as-spray-dried powder without any binder additive and is presented in Figure 7-6. These pellets, which weighed ~15 g (0.033 lb)

Table 7-2. CHARACTERISTICS OF COMPOSITE TES MEDIA POWDERS

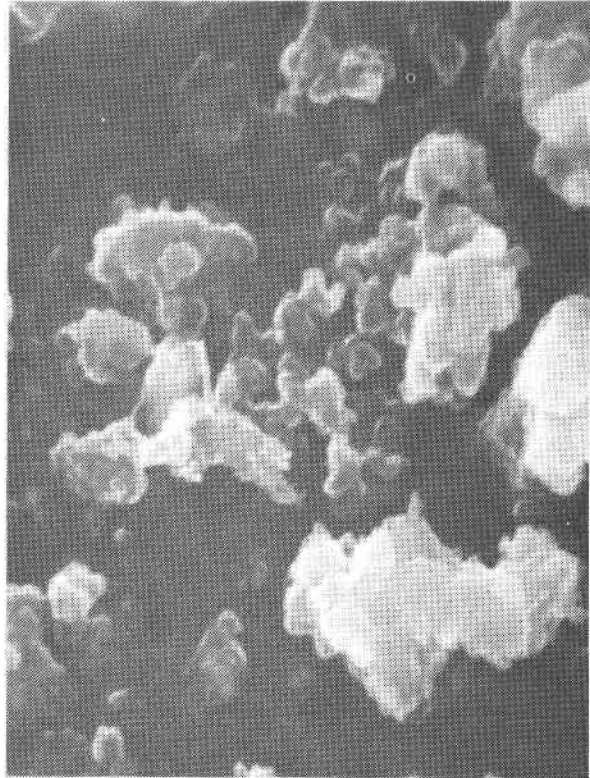
|   | Powder Batch<br>SN57BN-1A  | Powder Batch<br>SM51BN-1A and -2A   |
|---|--|---|
| Composition, <sup>a</sup> wt %  | 43% NaAlO <sub>2</sub><br>29.8% BaCO <sub>3</sub><br>27.2% Na <sub>2</sub> CO <sub>3</sub>                               | 49% MgO<br>26.6% BaCO <sub>3</sub><br>24.4% Na <sub>2</sub> CO <sub>3</sub> |
| Starting Materials  | Na <sub>2</sub> CO <sub>3</sub> , BaCO <sub>3</sub> , Na <sub>2</sub> Al <sub>2</sub> O <sub>4</sub> · 3H <sub>2</sub> O | Na <sub>2</sub> CO <sub>3</sub> , BaCO <sub>3</sub> , MgO                   |
| Powder Treatments After<br>Spray Drying                                 | 5 hours at 850°C in CO <sub>2</sub>  | None  |
| Composite Theoretical Density<br>at Room Temperature, g/cm <sup>3</sup> | 3.00   | 3.41  |

<sup>a</sup> The compositions were such that the carbonate to ceramic volume ratio was 60/40 above the salt melting point.

53ER/RPE/65055ta



50  $\mu$ m



1  $\mu$ m

P81102123

Figure 7-4.  $\text{Na}_2\text{CO}_3\text{-BaCO}_3/\text{NaAlO}_2$  POWDER PREPARED BY SPRAY DRYING AND FIRING AT  $850^\circ\text{C}$  FOR 5 HOURS (SN57BN-1A)

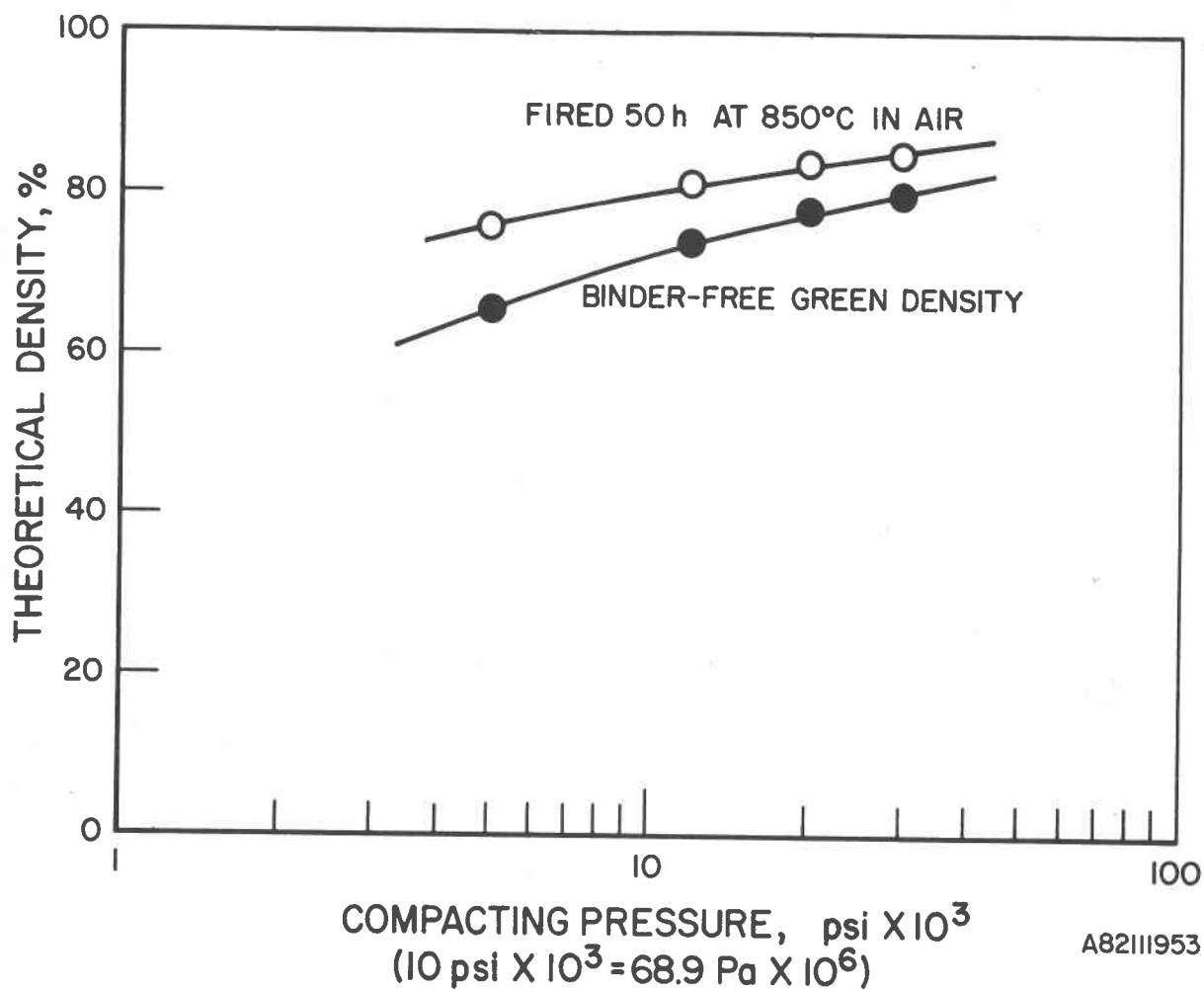


Figure 7-5. COLD-PRESSING CHARACTERISTICS OF SPRAY DRIED  $\text{Na}_2\text{CO}_3\text{-BaCO}_3/\text{NaAlO}_2$  POWDERS WITH PVA + ETHYLENE GLYCOL BINDER (SN57BN-1A)

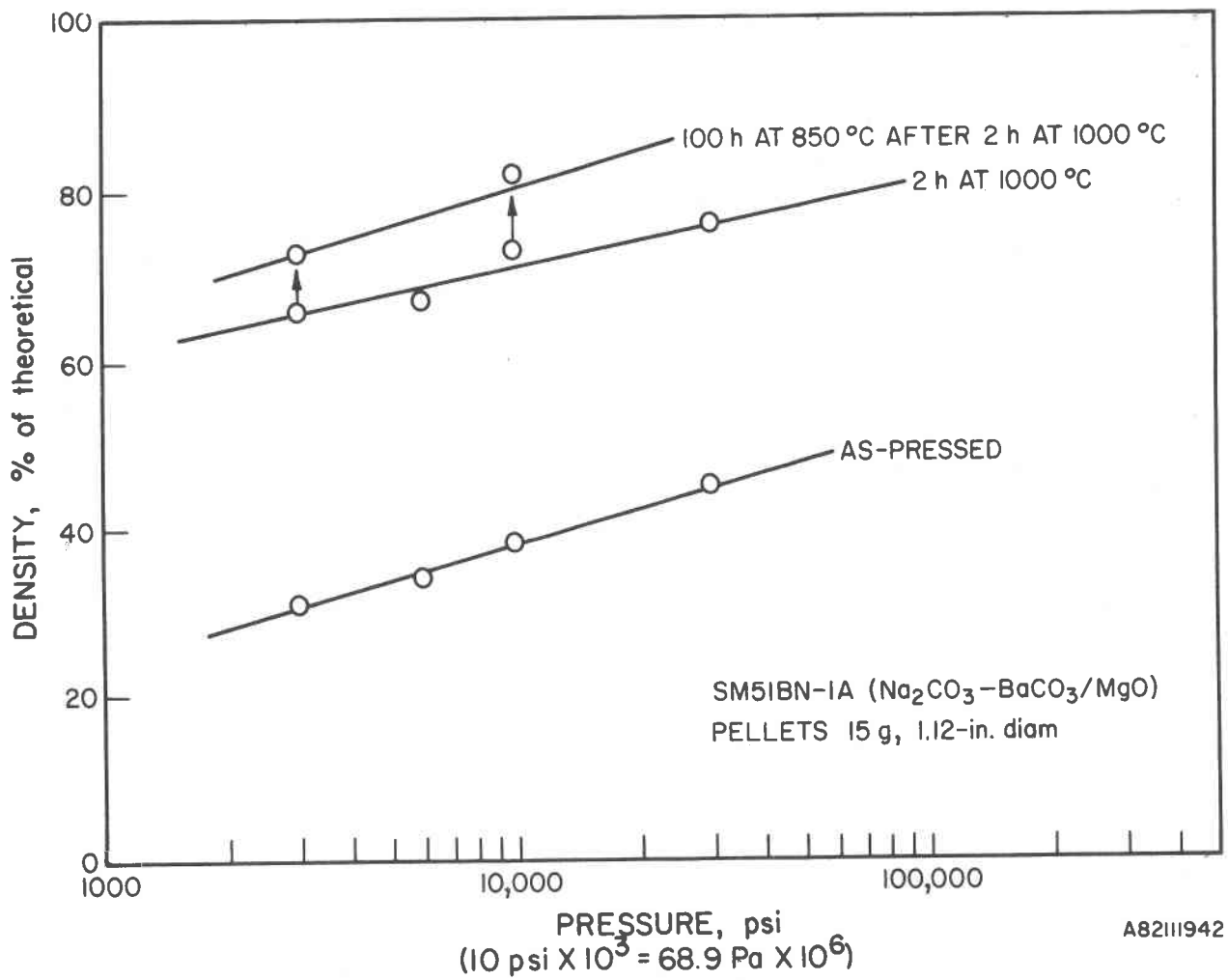


Figure 7-6. COMPACTION AND SINTERING BEHAVIORS OF  $\text{Na}_2\text{CO}_3$ - $\text{BaCO}_3$ /MgO COMPOSITES (SM51AN-1A)



and had diameters of 2.84 cm (1.12 in.), were pressed in a split die, thus eliminating the use of ejection forces to remove them from the die.

$\text{Na}_2\text{CO}_3\text{-BaCO}_3/\text{MgO}$  pellets pressed from Batch SM51BN-1A powder without binder under different pressures were heat treated in air at  $1000^\circ\text{C}$  ( $1832^\circ\text{F}$ ) for 2 hours to promote densification. An average weight loss of 9.5% was observed, although only 7.5% volatiles were determined from chemical analyses of the powder. The pellets turned green, but no cracks or shape deformations were visually detected. The pellet densities increased significantly during this thermal treatment as shown in Figure 7-6. But because further densification of the pellets was observed during subsequent stability tests at  $850^\circ\text{C}$  ( $1362^\circ\text{F}$ ) (also shown in Figure 7-6), further optimization of the sintering conditions was performed to obtain physically more stable, higher density pellets. These conditions were determined on 2.84-cm (1.12-in.) diameter pellets pressed at 206.8 MPa (30,000 psi) to a nominal green density of 42% of the theoretical (theoretical density =  $3.41 \text{ g/cm}^3$ ). The sintering schedules of  $1100^\circ\text{C}$  ( $2012^\circ\text{F}$ ) for 2 hours or  $1150^\circ\text{C}$  ( $2102^\circ\text{F}$ ) for 1 hour in air both yielded pellet densities of 92% of theoretical at room temperature, which corresponds to ~100% of the theoretical density at temperatures above the salt melting point, because of volume expansion of the salt upon melting.

Based on the good thermal stability in air of  $\text{Na}_2\text{CO}_3\text{-BaCO}_3/\text{MgO}$  pellets, to be discussed under Section 7.1.3, this composite was adopted for use in the TES testing for industrial applications under the parallel program at IGT managed by Oak Ridge National Laboratory. Because of the broader scope of the industrial program, additional studies on the behavior characteristics and media fabrication techniques were performed under that program. The results from those studies were implemented on this solar TES program for fabrication of the  $\text{Na}_2\text{CO}_3\text{-BaCO}_3/\text{MgO}$  pellets used in the laboratory-scale TES testing in this project, using a modified fabrication procedure described below.

The  $\text{Na}_2\text{CO}_3\text{-BaCO}_3/\text{MgO}$  composite media pellets tested in the laboratory-scale direct-contact TES system were fabricated from a 6-kg (13.2-lb) batch of powder (Batch SM51BN-2A) processed by spray drying, as described above. The pellets were fabricated by dry pressing using a Parr hand pellet press, after the powder was granulated to improve flowability and bulk density. The granulation process was developed under the media fabrication studies performed for the industrial TES program. The powder was first mixed with a binder solution of polyvinyl alcohol and ethylene glycol in water to form a mixture of 35 wt % binder solution and 65 wt % powder. After thorough mixing using a mortar and pestle, the mixture was sieved through a 20-mesh screen. Using a 1.3-cm (0.5-in.) standard punch and die set for the Parr press, as-pressed pellets measured about 1.3 cm (0.5 in.) in diameter by 1-cm (0.4-in.) high and weighed approximately 2.3 g (0.005 lb). The as-pressed pellet densities were about 31% of the theoretical. The pellets were then dried in an air oven at  $110^\circ\text{C}$  ( $230^\circ\text{F}$ ) for 18 hours, during which time most of the moisture was driven off. Subsequently, the binder burnout was done in an air oven at a rate of  $25^\circ\text{C}/\text{hour}$  ( $45^\circ\text{F}/\text{h}$ ) to  $600^\circ\text{C}$  ( $1112^\circ\text{F}$ ). The pellets were then cooled down and transferred to a high-temperature furnace for sintering at  $1150^\circ\text{C}$  ( $2102^\circ\text{F}$ ) for 1 hour under a  $\text{CO}_2$  atmosphere. The partial pressure of  $\text{CO}_2$  was provided to prevent carbonate decomposition at this high sintering temperature. The sintered pellets were about 0.89 cm (0.35 in.) in diameter by 0.71 cm (0.28 in.) in height having an average density of 87% of the theoretical. The color of the pellets ranged from light green to light

beige. The green pellets were produced before the outlet of the CO<sub>2</sub> flow tube was modified to provide a more uniform CO<sub>2</sub> flow distribution in the furnace. This modification involved loosely covering the CO<sub>2</sub> inlet tube with a thin layer of fibrous ceramic material to disperse the gas stream. This diffuser was effective in providing a more uniform CO<sub>2</sub> atmosphere, thus producing the light-colored pellets. The greenish pellets had a slightly higher density (90% of theoretical) than the beige pellets (80% to 85% of theoretical). A photograph of the as-sintered pellets is shown in Figure 7-7.

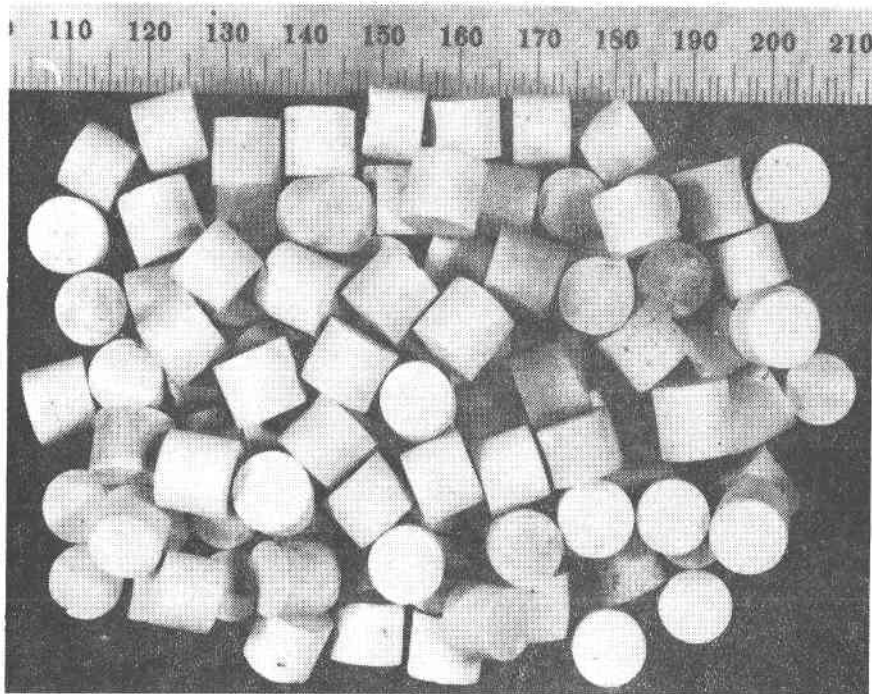
### 7.1.3 Subtask 1.3. Evaluation of Composite Materials Behavior

Evaluations of these composite carbonate/ceramic storage media were performed for materials compatibility screening and for identification and resolution of significant materials stability issues. These evaluations were based on support particle compatibility with molten Na<sub>2</sub>CO<sub>3</sub>-BaCO<sub>3</sub>, and stabilities of support material, carbonate salt, and the composite materials under anticipated test environments. Calculations were also performed to estimate the stresses expected to be encountered by the composite pellets in a packed-bed storage system configuration.

The stability of pellets in air at temperatures above the salt melting point was evaluated by determining changes in pellet characteristics and chemical composition after different test periods, by weight and dimensional measurements, chemical analyses, and scanning electron microscopy (SEM). Contact stresses in a packed bed of pellets were estimated and compared to pellet strengths that were measured on Na<sub>2</sub>CO<sub>3</sub>-BaCO<sub>3</sub>/MgO pellets under the industrial TES program.

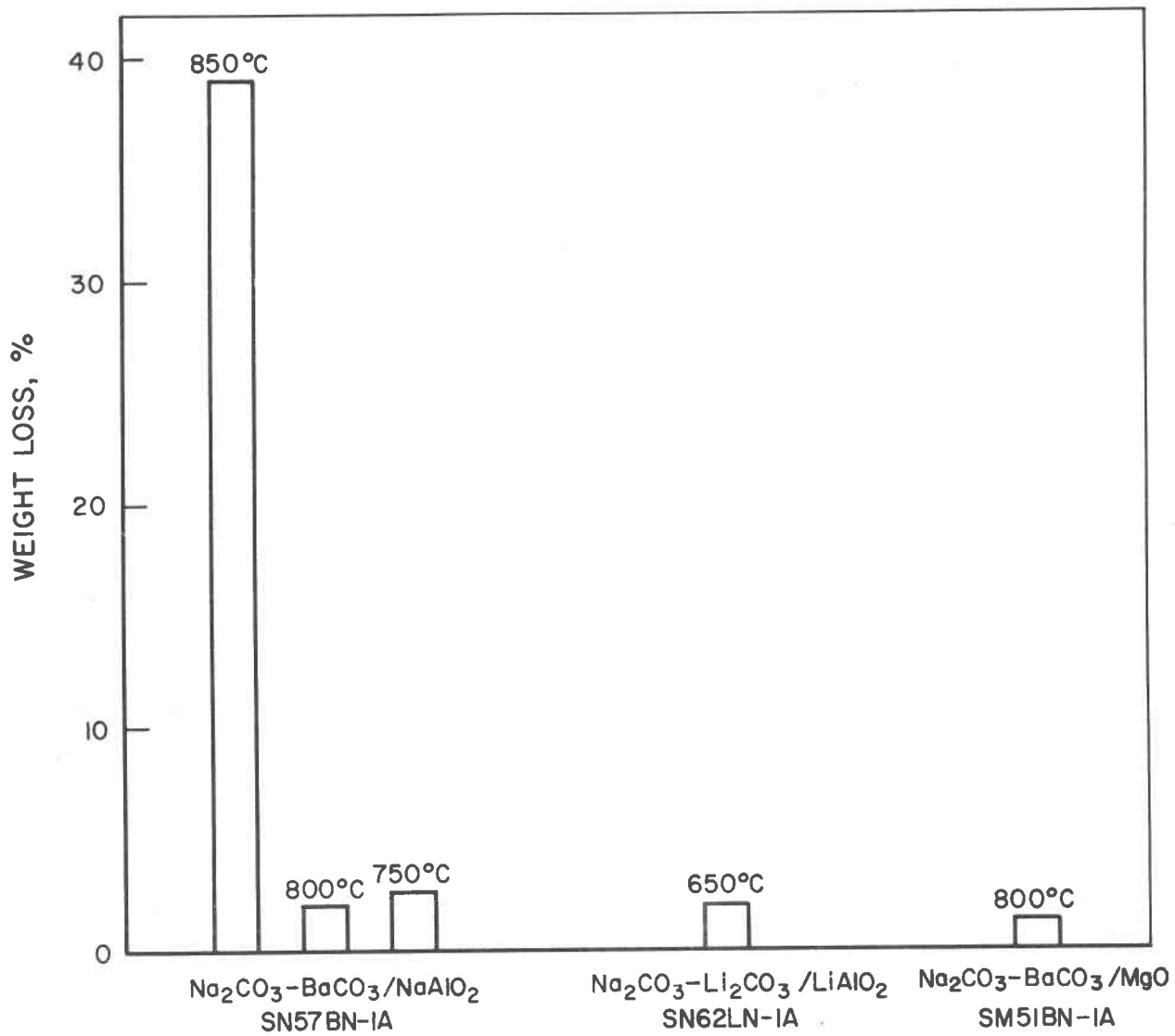
The Na<sub>2</sub>CO<sub>3</sub>-BaCO<sub>3</sub>/NaAlO<sub>2</sub> pellets from Batch SN57BN-1A that were pressed at various pressures and heated at 850°C (1562°F) in vacuum for 2 hours and at 850°C in air for 50 hours (see Figure 7-5 for pellet density at different test stages) were further heated in air at 850°C for another 422 hours, for a total of 472 hours. Starting from the as-pressed condition, the pellets lost an average total weight of 18%. The pellets remained yellow-green in color, but no cracking or shape deformation occurred. X-ray diffraction analysis of one of the tested pellets showed patterns for NaAlO<sub>2</sub>, Na<sub>2</sub>CO<sub>3</sub>-BaCO<sub>3</sub> salt, and Ba<sub>7</sub>Al<sub>2</sub>O<sub>10</sub>.

Two other 2-cm (0.8-in.) diameter pellets were pressed at 206.8 MPa (30,000 psi) from Batch SN57BN-1A powder containing 10% of an organic binder (Claden B-62). The binder-free green density was 70% of the theoretical. These pellets were tested in air at 850°C and cooled to room temperature in the furnace (approximately 20 hours cool-down time) for weight and dimensional measurements after 50, 150, and 350 hours of testing. Samples were obtained from one pellet for chemical analysis after each cooldown. The weight loss results are shown in Figure 7-8. Post-test chemical analyses revealed that the Al/Ba molar ratio remained practically constant (~4.5:1 throughout 350 hours), but the Na/Ba molar ratio decreased with time (from 8:1 to 4.5:1 after 350 hours), indicating a preferential loss of Na<sub>2</sub>CO<sub>3</sub> from the pellets. Only 58% of the remaining salt phase was carbonated after 350 hours, as measured by CO<sub>2</sub> evolution from the sample, indicating carbonate decomposition under these test conditions. A breakdown of the observed weight losses was estimated from the chemical analysis results. The initial 17% weight loss after 50 hours of



P83040426

Figure 7-7. AS-FABRICATED  $\text{Na}_2\text{CO}_3\text{-BaCO}_2/\text{MgO}$  PELLETS USED FOR LABORATORY-SCALE TES TESTING



A83030340

Figure 7-8. CHANGES IN COMPOSITE TES PELLETS HEATED IN AIR

test was due to binder burnout (10%) and  $\text{Na}_2\text{CO}_3$  loss (7%) by creepage, reaction with  $\text{Al}_2\text{O}_3$  container material, and/or vaporization. During the period from 50 to 350 hours of test, the incremental 16% weight loss was estimated to be a result of  $\text{CO}_2$  loss (5% possibly due to formation of  $\text{Ba}_7\text{Al}_2\text{O}_{10}$  or carbonate decomposition) and continued  $\text{Na}_2\text{CO}_3$  loss (11%).

Also shown for comparison in Figure 7-8 is the weight loss bar for pellets of a reference molten  $\text{Na}_2\text{CO}_3$ - $\text{Li}_2\text{CO}_3$  eutectic (496°C, 925°F mp) supported by  $\text{LiAlO}_2$  (Batch SN62LN-1A), tested for 350 hours at 650°C (1202°F) in air. The stability of this composite material, which was developed for fuel cell applications at a temperature of ~150°C (270°F) above the salt mp, demonstrates the good composite materials stability that can be achieved by proper selection of compatible salt and ceramic materials and use of supports having the required physical characteristics.

Scanning electron micrographs of a fractured surface of a  $\text{Na}_2\text{CO}_3$ - $\text{BaCO}_3$ / $\text{NaAlO}_2$  pellet that was tested for 350 hours at 850°C (1562°F) are shown in Figure 7-9. A comparison of these micrographs with those from the as-prepared powder (Figure 7-4) indicates that  $\text{NaAlO}_2$  particle growth has occurred under these test conditions. This coarsening phenomenon adversely affects the carbonate retention and mechanical properties of composites.

The stability of  $\text{Na}_2\text{CO}_3$ - $\text{BaCO}_3$ / $\text{NaAlO}_2$  (Batch SN57BN-1A) pellets in air was also investigated at temperatures of 750° and 800°C (1382° and 1472°F). Weight losses of only 2.5% after 500 hours were accounted at both test temperatures, which were significant improvements over those observed for the 850°C test. Moreover, no color change, shape deformation, or cracking was observed. X-ray diffraction analysis, however, indicated formation of  $\text{BaAl}_2\text{O}_4$  at these lower test temperatures by reaction of  $\text{BaCO}_3$  in the molten salt phase with the  $\text{NaAlO}_2$  support initially present in composites.

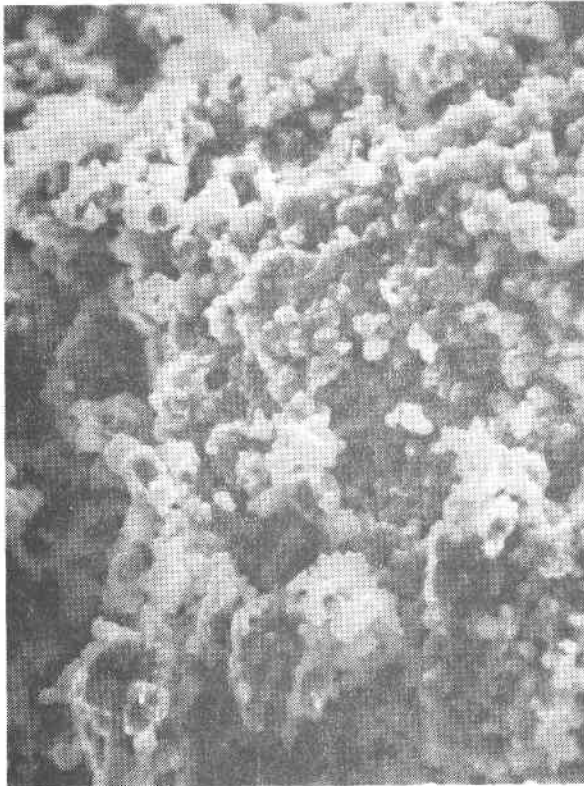
Barium aluminates exist with a wide range of stoichiometry [10], represented as  $x\text{BaO}\cdot\text{Al}_2\text{O}_3$ , with x ranging from 1 to 10. Weight losses due to  $\text{CO}_2$  evolution would be expected for conversion of  $\text{NaAlO}_2$  to barium aluminate via reaction with  $\text{BaCO}_3$ . That is —



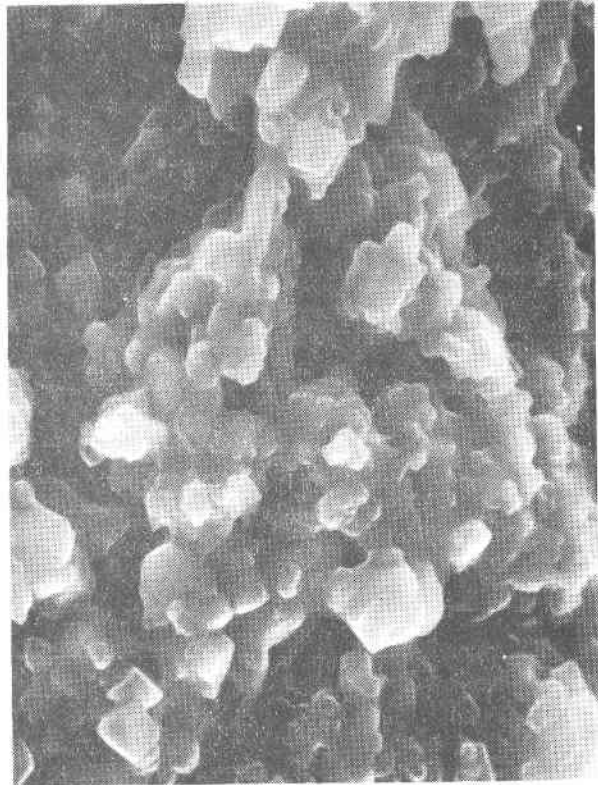
The thermodynamics of this reaction could be determined by systematic thermogravimetric studies of the  $\text{Na}_2\text{CO}_3$ - $\text{BaCO}_3$ - $\text{NaAlO}_2$ - $\text{CO}_2$  system to define the stability regime for  $\text{NaAlO}_2$  and the various  $x\text{BaO}\cdot\text{Al}_2\text{O}_3$  compounds as a function of temperature, gas composition, and melt composition.

Similar stability tests were performed on pellets pressed and sintered from  $\text{Na}_2\text{CO}_3$ - $\text{BaCO}_3$ / $\text{MgO}$  powder (Batch SM51BN-1A) to assess the ability of  $\text{MgO}$  particles to support molten  $\text{Na}_2\text{CO}_3$ - $\text{BaCO}_3$  salt. The powder processing and pellet fabrication procedures were described in Section 7.1.2.

Two sintered pellets nominally 15 g (0.033 lb) in weight and 2.54 cm (1 in.) in diameter x 1.3 cm (0.5 in.) in height with densities of 67% and 76% of the theoretical were obtained by cold pressing Batch SM51BN-1A powder at 41.4 and 206.8 MPa (6,000 and 30,000 psi) pressures, respectively, followed by sintering in air at 1000°C (1832°F) for 2 hours. They were tested in air at



20  $\mu$  m



5  $\mu$  m

P81102122

Figure 7-9. SEM FRACTOGRAPHS OF  $\text{Na}_2\text{CO}_3\text{-BaCO}_3/\text{NaAlO}_2$  PELLET HEATED AT  $850^\circ\text{C}$  FOR 350 HOURS AND TWO THERMAL CYCLES TO R.T. (SN57BN-1A)

800°C (1472°C) for 200 hours. No significant weight loss (~0.5%) (Figure 7-8), dimensional change, shape deformation, or cracks were observed.

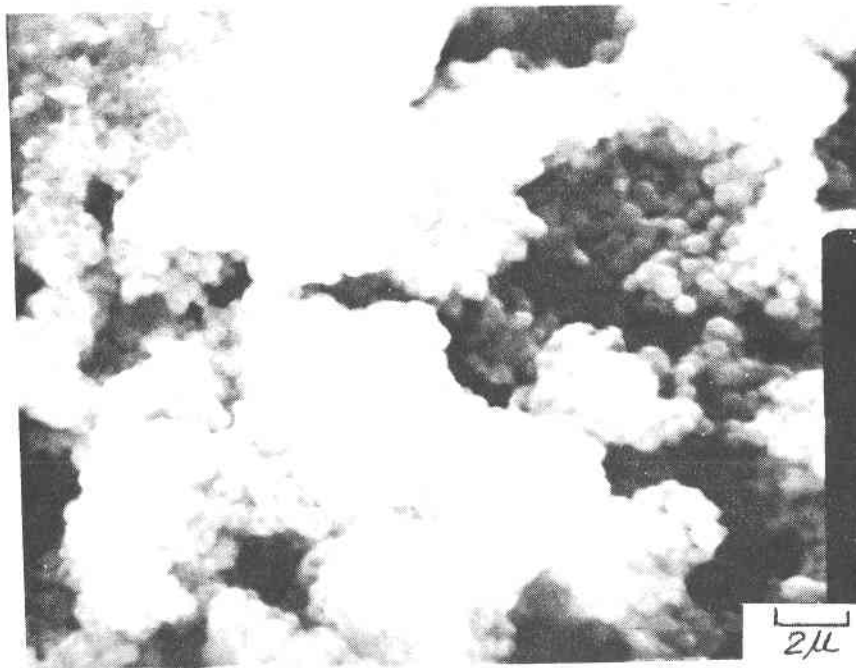
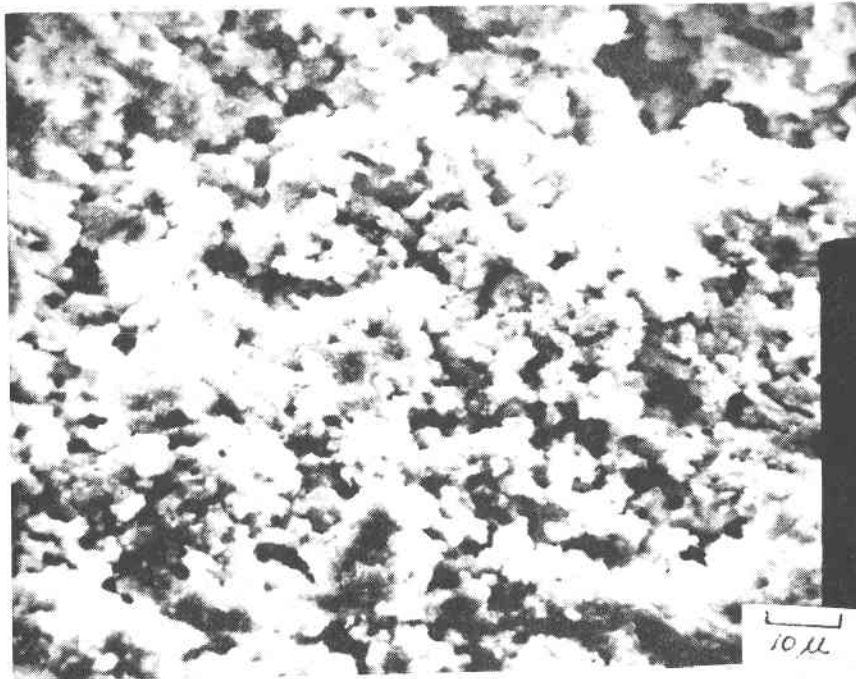
Two other pellets fabricated and sintered similarly but pressed at 20.7 and 69 MPa (3,000 and 10,000 psi) pressures (hence producing sintered densities of 66% and 73% of the theoretical, respectively) were tested in air at 850°C (1562°F). After 100 hours, no significant weight loss (<0.5%), shape deformation, or cracks were observed. Pellet shrinkage was observed, causing densification to 75% and 82% of the theoretical pellet density.

X-ray diffraction patterns of pellets tested at 800° and 850°C showed evidence of only MgO and Na<sub>2</sub>CO<sub>3</sub>-BaCO<sub>3</sub> salt mixture. Chemical analyses showed that the chemical compositions of the tested pellets were similar to the hydrate- and moisture-free as-spray-dried powder. SEM micrographs of a fracture surface of a pellet tested at 800°C for 2 hours (Figure 7-10) show relatively uniform composite microstructure with MgO particle sizes of approximately 0.5 μm.

Longer-term stability tests of Na<sub>2</sub>CO<sub>3</sub>-BaCO<sub>3</sub>/MgO pellets in air with repeated thermal cycles were also performed. Two pellets of similar size to those described above were pressed at 206.8 MPa (30,000 psi) and sintered in air at 1050° and 1100°C (1922° and 2012°F) for 2 hours, yielding densities of 84% and 92% of the theoretical. They were then placed on a dense alumina plate and heated in a Lindberg three-zone vertical furnace in air to 800°C. Thermal cycling was performed by cooling the pellets in the furnace to ambient temperature (25° to 75°C) in about 15 hours, and then reheating them back to 800°C in ~2 hours (~375°C/hour heat rate). A total of 22 thermal cycles were performed within a total hold time period of 510 hours at 800°C over a total elapsed test period of 1115 hours. At the end of this test only 1.2% weight loss was observed, and no dimensional change, shape deformation, or cracking was observed. A photograph of the thermal-cycled pellets appears in Figure 7-11. An SEM fractograph of one of the tested pellets is shown in Figure 7-12. The slightly larger MgO particles observed for this sample, as compared to that shown in Figure 7-10, may be due to particle coarsening as tests continued and/or relatively different particle sizes developed during the different pellet sintering processes used (2 hours at 1000°C for the pellet shown in Figure 7-10 and 2 hours at 1100°C for that shown in Figure 7-12). Based on the superior stability in air exhibited by the Na<sub>2</sub>CO<sub>3</sub>-BaCO<sub>3</sub>/MgO pellets, this composite was selected for laboratory-scale charge/discharge testing to be discussed in Task 2.

In this advanced storage media concept, the composite media shapes could be utilized as a packed bed of media pellets or as a regular arrangement of brick shapes, with passages for flow of charge/discharge gases provided by the interstices between shapes. Because stresses will be exerted upon the media shapes by the mass of media situated above them in a storage system, the media must possess adequate strength and creep resistance to ensure long-term structural integrity.

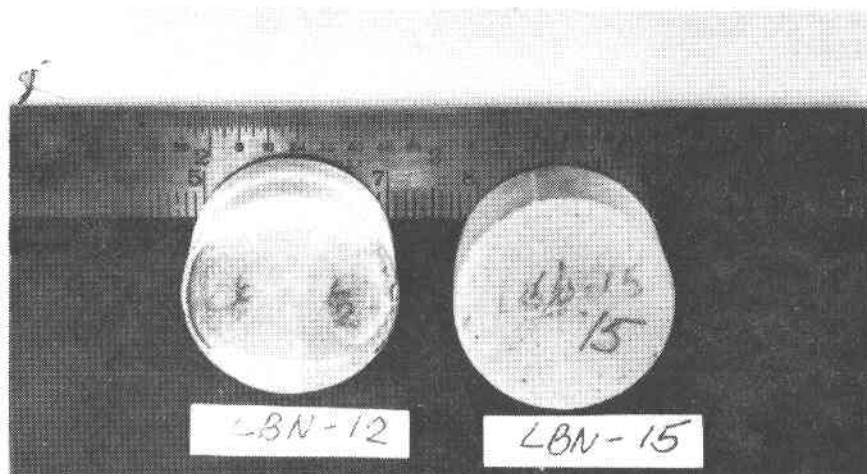
Under this development program, analyses have been performed to estimate the stresses that would be imposed on composite pellets arranged in a packed-bed storage system configuration. In this concept, cylindrical pellets of uniform height and diameter would be randomly loaded inside a storage containment vessel to a packing density of approximately 60%. Such a configuration would



P83040431

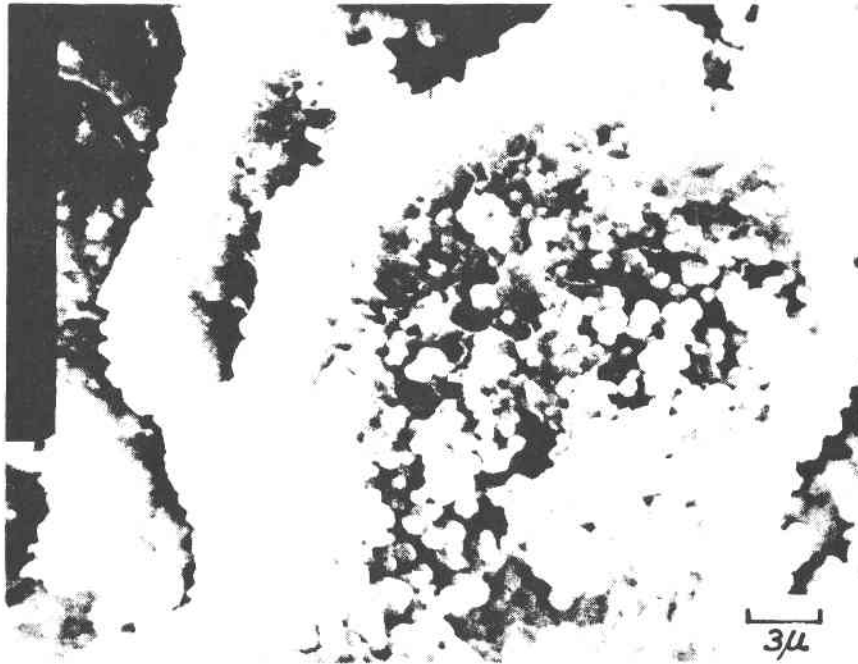
Figure 7-10. SEM MICROGRAPHS OF FRACTURE SURFACE FROM  $\text{Na}_2\text{CO}_3\text{-BaCO}_3/\text{MgO}$  PELLET TESTED AT  $800^\circ\text{C}$  FOR 200 HOURS (SM51BN-1A)





P83040427

Figure 7-11.  $\text{Na}_2\text{CO}_3\text{-BaCO}_3/\text{MgO}$  (SM51 BN-1A) PELLETS AFTER A TOTAL OF 510 HOURS AT  $800^\circ\text{C}$  WITH 22 THERMAL CYCLES



P83040433

Figure 7-12. SEM FRACTOGRAPH OF  $\text{Na}_2\text{CO}_3\text{-BaCO}_3/\text{MgO}$  PELLET  
SINTERED 2 HOURS AT  $1100^\circ\text{C}$  AND TESTED 1,115 HOURS  
(AT  $800^\circ\text{C}$  FOR 510 HOURS) WITH 22 THERMAL CYCLES  
TO NEAR ROOM TEMPERATURE, ALL IN AIR

lead to several different types of pellet interactions and contact stress levels.

At least six cylindrical pellet contact arrangements are possible, as shown in Figure 7-13. Case 1 involves the simple case of a pellet being loaded by force P on its face in contact with another pellet face or with a supporting plate. This type of loading results in a nominal pellet stress of —

$$\sigma = \frac{P}{A} \quad (1)$$

where P is the load applied to the contact area A. Case 2 involves a line contact resembling a roller on a flat surface. The contact stress for this case according to Timoshenko [11] for elastic media behavior is —

$$\sigma = 0.59 \sqrt{\frac{PE}{d\ell}} \quad (2)$$

where d and  $\ell$  are pellet diameter and height, respectively, while E is the modulus of elasticity of the pellet. When the cylindrical axes of the two pellets shown in Case 4 are mutually parallel to each other, there is also a line contact with a uniform stress, also derived in Reference 11, of —

$$\sigma = 0.83 \sqrt{\frac{PE}{d\ell}} \quad (3)$$

where  $\ell$  is the length of contact. As shown in Figure 7-13 for Case 4,  $\sigma$  takes on a range of values, depending on the relative orientation of the cylindrical axes of the pellets.

The other pellet arrangements shown in Figure 7-13 (Cases 3, 5, and 6) involve point contacts. Stresses at point contacts follow the general equation —

$$\sigma = 0.94 \sqrt[3]{\frac{fPE^2}{d}} \quad (4)$$

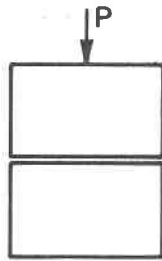
where f is a factor depending on the two contacting geometries. The factor f increases in magnitude as the contact point becomes sharper. For spheres, f would have a value of 1 for Case 5, 0.42 for Case 6, and 0.25 for Case 3. More complicated geometrical derivations would be involved in solving for f values corresponding to contacting pellet edges. Spherical contact point approximations are being used for the present estimation of contact stresses.

The total load exerted on a layer of pellets by a packed bed of height h above it is —

$$P_t = \rho hA \quad (5)$$

where  $\rho$  = media mass packing density, h = bed height, and A = cross-sectional area of packed bed. This total load,  $P_t$ , is distributed among the pellets in the given layer; the nominal load, P, supported by the average pellet in this layer is then —

$$P = \frac{P_t}{N_A} \quad (6)$$



(1) FACE-TO-FACE CONTACT

$$\sigma = \frac{P}{A}$$



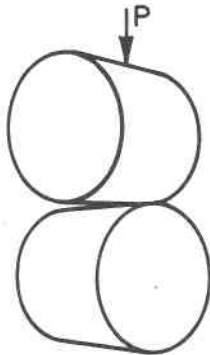
(2) SIDE-TO-FACE CONTACT

$$\sigma = 0.059 \sqrt{\frac{PE}{dl}}$$



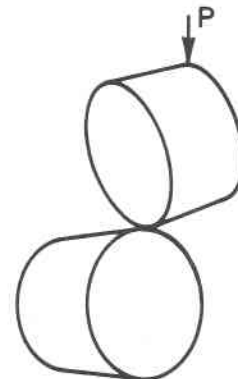
(3) EDGE-TO-FACE CONTACT

$$\sigma = 0.98 \sqrt[3]{\frac{fPE^2}{d^2}}$$



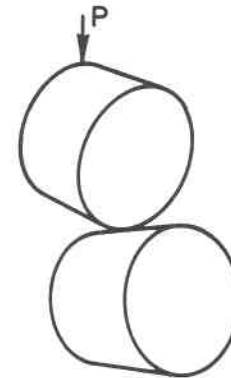
(4) SIDE-TO-SIDE CONTACT

$$0.83 \sqrt{\frac{PE}{dl}} \leq \sigma \leq 0.59 \sqrt[3]{\frac{PE^2}{d^2}}$$



(5) EDGE-TO-EDGE CONTACT

$$\sigma = 0.98 \sqrt[3]{\frac{fPE^2}{d^2}}$$



(6) EDGE-TO-SIDE CONTACT

$$\sigma = 0.98 \sqrt[3]{\frac{fPE^2}{d^2}}$$

A82081456

Figure 7-13. SIX POSSIBLE CONTACT STRESSES IN A PACKED BED OF PELLETS

where  $N_A$  is the average number of pellets per unit cross-sectional area in the bed. Although statistical analyses of various assumed pellet packing configurations may be used to estimate  $N_A$ , to a first approximation it can be shown that —

$$P = \approx \rho h d^2$$

for cylindrical pellets with an  $\ell/d$  ratio of  $\sim 1$ .

Estimates of various contact stresses have been obtained for a packed bed of  $\text{Na}_2\text{CO}_3$ - $\text{BaCO}_3$ /MgO pellets on the following bases —

$$\rho = 1882 \text{ kg/m}^3 \text{ (0.068 lb/in.}^3\text{)}$$

$$d = 2.54 \text{ cm (1 in.)}$$

$$\ell = 2.54 \text{ cm (1 in.)}$$

$$h = 30.5 \text{ cm (12 in.)}$$

$$f = 1$$

$$E = 68.9 \text{ MPa (1} \times 10^4 \text{ psi) above salt mp}$$

$$E = 6,894 \text{ MPa (1} \times 10^6 \text{ psi) at room temperature}$$

The values of pellet moduli of elasticity,  $E$ , given above were experimentally determined on  $\text{Na}_2\text{CO}_3$ - $\text{BaCO}_3$ /MgO pellets under the industrial TES program.

For 3 dm (1 ft) of bed height, the maximum contact stress is estimated to be that of Case 5, which is  $\sim 3$  MPa ( $\sim 440$  psi) above the salt mp and 70 MPa ( $\sim 10,000$  psi) at room temperature. The line stress as in Case 2, on the other hand, is just 0.4 MPa (55 psi) at temperatures above the salt mp and 3.9 MPa (560 psi) at room temperature, while the pellet face-loading stress shown in Case 1 is less than 7 kPa (1 psi) and is independent of  $E$  and, hence, temperature. Although stresses at point contacts are high, occurrence of point contacts in a packed bed of pellet is statistically low and may be neglected for practical reasons.

In case of brittle materials (as for the composite pellets at room temperature), local failure at points will occur when the contact stress exceeds the material compressive strength. However, for plastic materials (as for the pellets above the salt mp), when the contact stress exceeds the yield strength of the material, plastic deformation occurs at contact points until the stress is reduced to a stable level. The compressive strength of  $\text{Na}_2\text{CO}_3$ - $\text{BaCO}_3$ /MgO pellets was measured under the industrial TES program to be 152 to 180 MPa (22,000 to 26,000 psi) at room temperature and 2 MPa ( $\sim 300$  psi) above the salt mp. Preliminary evaluation of the limited pellet mechanical property data presently available indicate that the  $\text{Na}_2\text{CO}_3$ - $\text{BaCO}_3$ /MgO media utilized in this study should provide a stable packed bed configuration at least 1.5 m (5 ft) in height. However, more extensive studies on media mechanical properties as a function of temperature, carbonate salt content, loading configuration, and time need to be performed before more definitive conclusions can be made regarding the long-term integrity of a packed bed of composite carbonate/ceramic TES pellets.

#### 7.1.4 Summary of Composite Materials Behavior

The feasibility of an advanced composite salt/ceramic thermal storage media was identified in Task 1.3. The most promising\* materials and processes tested were selected for further testing in Task 2.

In summary, the Task 1.3 scoping studies revealed that the stability of the TES media (pellets) was dependent on, in a decreasing order:

- Ceramic support phase selection
- Pre-test pellet processing temperatures (densification/sintering)
- Testing temperature.

Of the numerous ceramic support media considered, MgO and NaAlO<sub>2</sub> were tested. MgO was found to be the more stable support matrix at all the conditions tested using Na<sub>2</sub>CO<sub>3</sub>-BaCO<sub>3</sub> salt mixtures. For example, when NaAlO<sub>2</sub> was tested at 850°C for 472 hours, an 18% weight loss was observed. Post-test examination showed that a portion of the BaCO<sub>3</sub> reacted with the NaAlO<sub>2</sub> to form Ba<sub>7</sub>Al<sub>2</sub>O<sub>10</sub>. Another test conducted for 350 hours at 850°C exhibited similar weight losses (~16%). Chemical analysis indicated that this 16% loss was divided as follows: 5% to Ba<sub>7</sub>Al<sub>2</sub>O<sub>10</sub> formation and 11% to Na<sub>2</sub>CO<sub>3</sub> loss. The carbonate loss could be explained by coarsening (particle growth, as observed in post-test SEM examination) of the NaAlO<sub>2</sub> support structure, i.e., loss in capillary retention forces. When the testing temperature was reduced to 750° and 800°C, the weight losses for Na<sub>2</sub>CO<sub>3</sub>-BaCO<sub>3</sub>/NaAlO<sub>2</sub> composites were reduced to 2.5% after 500 hours of testing. Qualitatively we would infer that this improved stability was caused by reduced morphological changes occurring at the lower test temperatures, resulting in better carbonate retention properties.

When the Na<sub>2</sub>CO<sub>3</sub>-BaCO<sub>3</sub> salt mixtures were tested with MgO supports, superior stabilities were obtained for all conditions tested. For example, pellets tested at 800° and 850°C for periods up to 200 hours demonstrated 0.5% weight loss. X-ray analysis revealed only Na<sub>2</sub>CO<sub>3</sub>, BaCO<sub>3</sub> and MgO; i.e., no salt reactions with the MgO support matrix were observed. Another test that operated in a cycling mode (22 thermal cycles through 1115 hours total and 510 hours at 800°C) resulted in about 1% weight loss. Comparison of the ceramic support morphologies after testing showed that, in general, the temperature used for densifying the pellets prior to testing has an effect (as expected) on the particle size: Higher densifying temperatures produce larger particles and therefore potentially decreased carbonate retention properties. As a result, the lowest temperatures consistent with sufficient densification are desired.

The combination of these initial scoping studies and the experience gained from developing electrolyte tiles for molten carbonate fuel cells indicates the importance of the morphology of the ceramic support material when used in composite matrices. Based on the promising results of this program, we

---

\* Scoping results only, not optimized or fully developed.

feel that by continued materials/processing/fabrication development, the carbonate losses can be further reduced to levels consistent with long-term operational requirements.

## 7.2 TASK 2. PROOF-OF-CONCEPT TESTING

This task involved utilization of the most promising materials and processing techniques established in Task 1 for laboratory-scale TES charge/ discharge testing. The main objective of this work was to provide proof-of-concept testing essential to the improvement and further refinement of cost/ predictive performance evaluations for this advanced latent/sensible media direct contact heat exchange concept.

### 7.2.1 Subtask 2.1. Laboratory-Scale Module Design and Fabrication

To facilitate basic proof-of-concept cyclic stability assessments and preliminary performance data acquisition, the laboratory-scale TES unit was designed to operate as a randomly packed-bed array, instrumented to evaluate the key thermal discharge performance characteristics.

A computer code was developed to parametrically characterize the flow conditions through a packed bed as a function of temperature, pellet and bed geometry, packing density, and air mass flow rate. Another code evaluated the media mass requirements and calculated thermal capacities as a function of bed geometry, packing density, thermophysical salt and ceramic properties, actual pellet densities, and operating temperature transients.

The results in Figure 7-14 show that for ambient air (22°C or 72°F) with flow rates of 1.4 to 11 m<sup>3</sup>/h (50 to 400 standard cubic feet per hour or SCF/h, 1.7 to 13.5 kg/h, or 3.74 to 29.8 lbm/h), the typical flow through a 8.99-cm (3.54-in.) diameter bed (as a function of temperature) encompasses the laminar (<2500 N<sub>Re</sub>), transition, and turbulent (at low temperatures) flow regimes.

The system conditions assumed for these calculations include —

- Hydraulic diameter of packed bed of pellets = 0.64 cm (0.25 in.)
- Bed packing density = 65%
- Air working fluid
- Temperature ranging from 22° to 1093°C (72° to 2000°F) (with density and viscosity changes included)
- Initial air flow delivery at room temperature through 1.3-cm (0.5-in.) diameter pipe.

The calculated pressure drop per linear foot of packed bed (of diameter = 8.99 cm, 3.54 in.) ranges from 253 Pa/m (1.12 x 10<sup>-2</sup> psi/ft) [at 38°C (100°F) and an ambient air flow rate of 1.41 m<sup>3</sup>/h (50 SCF/h)] to 4,298 Pa/m (0.19 psi/ft) [at 1038°C (1900°F) and an initial cool delivery of 11.3 m<sup>3</sup>/h (400 SCF/h)] through a 1.3-cm (0.5-in.) diameter delivery pipe.

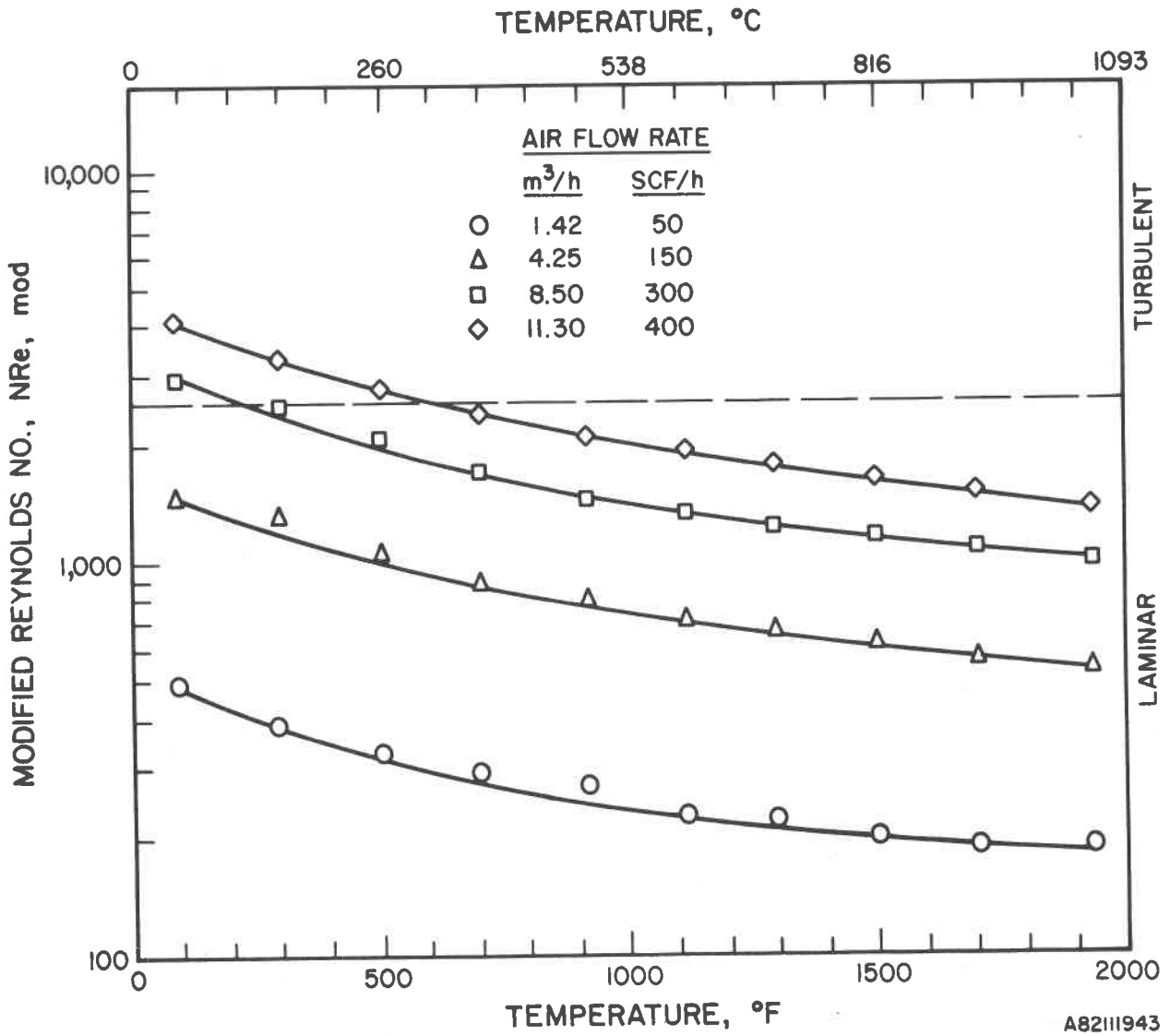


Figure 7-14. MODIFIED REYNOLDS NUMBER VERSUS TEMPERATURE  
 FOR VARIOUS AMBIENT INLET AIR FLOW RATES  
 THROUGH 3.54-INCH-DIAMETER BED



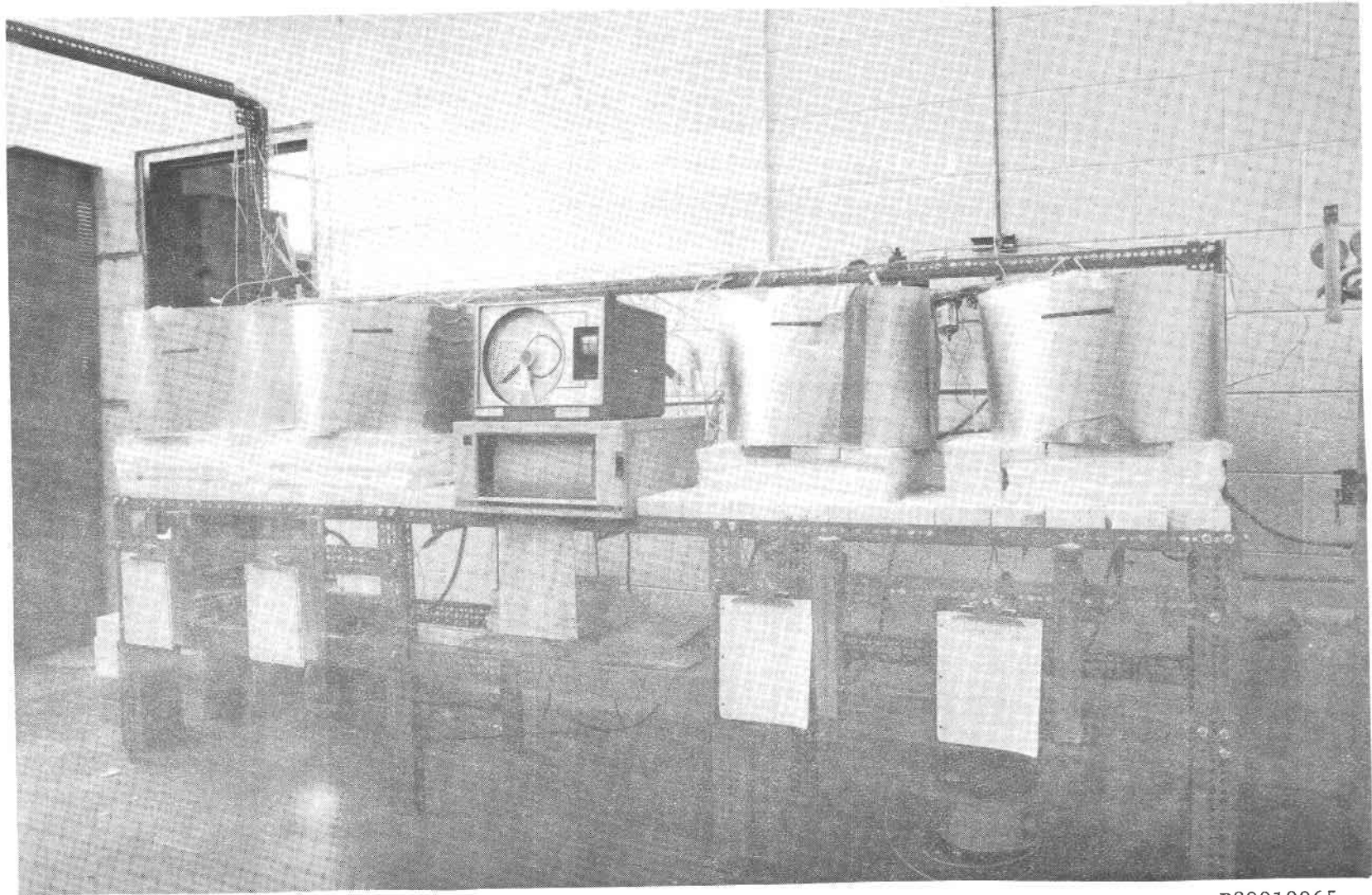
The final test unit fabricated for installation into the IGT laboratory-scale test-stand (Figure 7-15) was of AISI 316 stainless-steel construction: 9.65 cm OD and 8.99 cm ID (3.8-in. OD and 3.54-in. ID) x 18.9 cm (7.44 in.) in overall height. This allowed for a 8.99-cm (3.54-in.) diameter, 10.67-cm (4.2-in.) high, 672-cm<sup>3</sup> (41-in.<sup>3</sup>) total packed-bed volume (Figure 7-16). To facilitate radial and axial bed temperature monitoring, Swagelok fittings were butt-welded onto the cannister to seal four thermocouple wells, each of which housed three thermocouples. Three thermocouples were shielded within a vertical 316 stainless-steel sheath at a radius of 2.25 cm (0.887 in.), while three equi-spaced (radially from bed center) thin-wall thermocouples were located at 3.48-cm (1.37-in.) bed height intervals at radii of 0, 2.26, and 4.32 cm (0, 0.89, and 1.7 in.).

The cannister's top was drilled and welded to the heat exchanger outlet pipe and machined for a close fit (as shown in Figure 7-16) with the cannister lip and OD. During actual operation, it was found that 6.9 kPa (~1 psi) of holding force was sufficient to mechanically seal the top of the lip and OD. The removable Type 316 stainless-steel bed support plate was perforated in a staggered pattern to a 33% void area. A solid, tripod deflector plate and steel wool in the inlet gas plenum were used to distribute the gas uniformly throughout the bed. A pre-test photograph of the fabricated cannister is shown in Figure 7-17. Standard 1.3-cm (0.5-in.) Swagelok fittings connected the HX pipe to the TES system's air supply tubing.

For a media composition of 51 wt % carbonate salt (48 wt % Na<sub>2</sub>CO<sub>3</sub>-52 wt % BaCO<sub>3</sub>) and 49 wt % MgO, cycled over the temperature range 22° to 827°C (72° to 1521°F), this lab-scale module possesses a maximum storage capacity rating of 0.34 kWh (1182 Btu). As shown in Table 7-3, these calculations are based on an as-sintered pellet density of 87% of the theoretical, with a geometric bed volume packing density of 58.3%. Given this system configuration, the computations of Table 7-3 indicate a 0.41 MJ or 0.116 kWh (396 Btu) thermal capacity for a ±100°C (200°F) temperature swing about the Na<sub>2</sub>CO<sub>3</sub>-BaCO<sub>3</sub> salt mp of 716°C (1321°F).

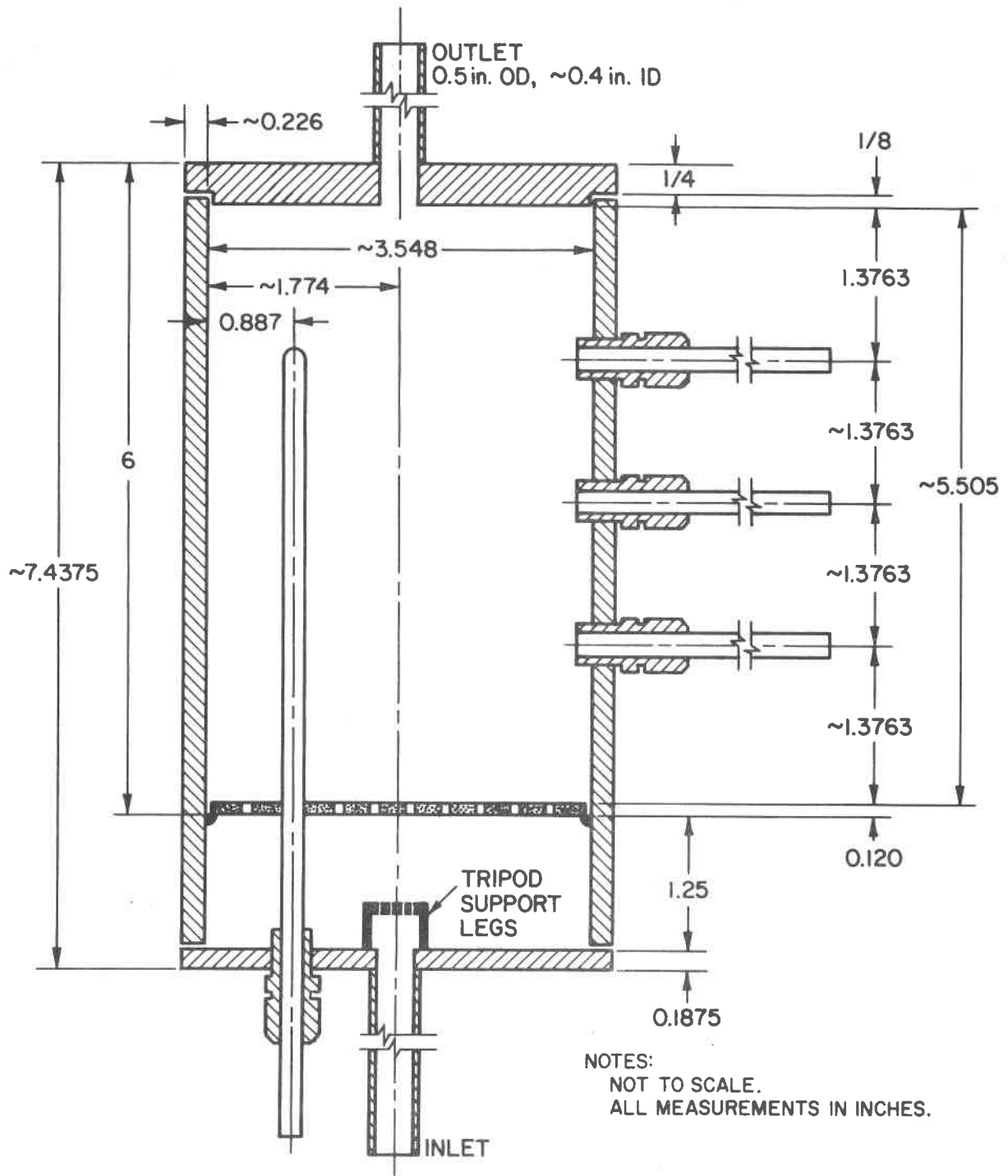
#### 7.2.2. Subtask 2.2. Laboratory-Scale Testing and Evaluation

Proof-of-concept testing of the composite media was conducted in one modified module of a four-station IGT lab-scale TES test-stand. Cooling discharge air was supplied through 1.3-cm (0.5-in.) diameter tubing manifolded to each station from a single house air supply source (Figure 7-15). Two external electrical-resistance clam-shell heaters [Thermal Corp., 825 watts, 1204°C (2200°F)] were used to charge the unit. The containers and heaters were wrapped with a 20-cm (8-in.) radial thickness of Johns-Manville Cerablanket high-temperature insulation of 128 kg/m<sup>3</sup> (8 lb/ft<sup>3</sup>) density, rated at a nominal thermal conductivity of 0.121 W/m-K (0.07 Btu/h-ft-°F) at 538°C (1000°F). The thermal barrier beneath the unit consisted of 6.35 cm (2.5 in.) of fire-bricks, 12.7 cm (5 in.) of insulation, and 6.35 cm (2.5 in.) of firebrick as a base. A 20.3-cm (8-in.) thick layer of insulation, was also used to minimize radiant heat losses from the top of the unit. A schematic of the TES module, comprised of the TES unit, heater, and insulation, is shown in Figure 7-18.



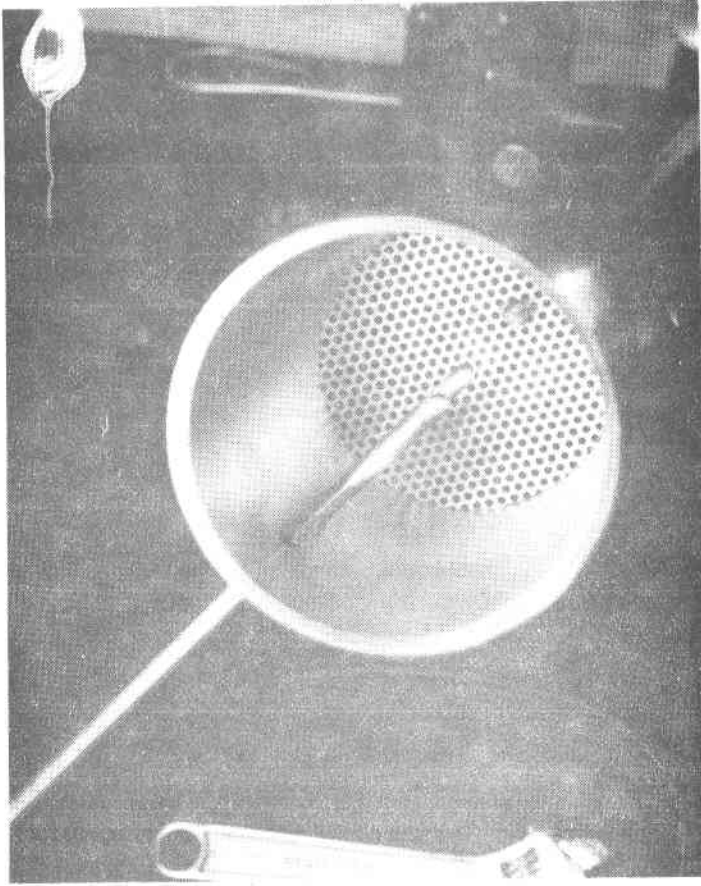
P80010065

Figure 7-15. FOUR-STATION TES LABORATORY-SCALE TEST STAND

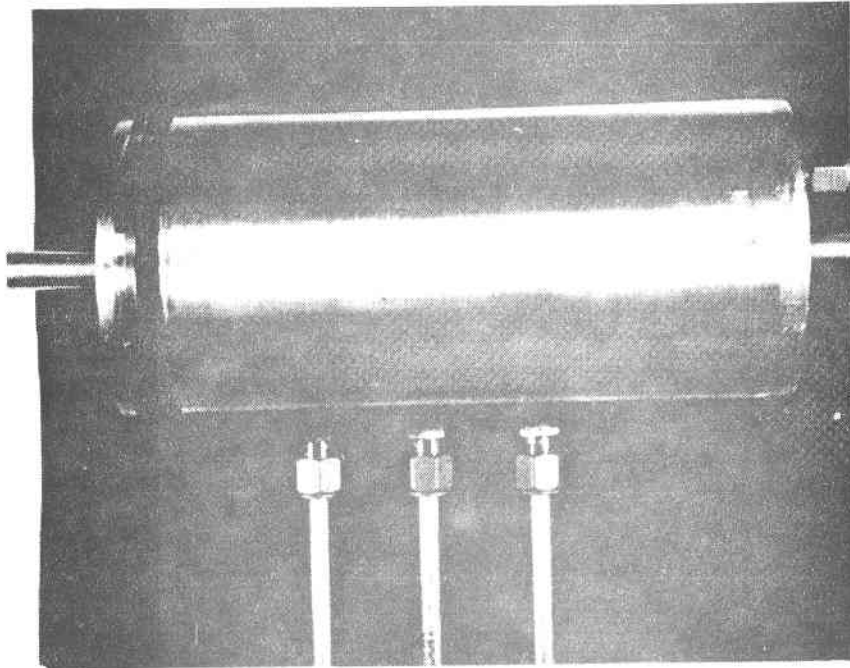


A83020289

Figure 7-16. CROSS SECTION OF LABORATORY-SCALE TES TEST CANNISTER



P83040430



P82030550

Figure 7-17. LABORATORY-SCALE TES TEST CANNISTER

Table 7-3. MASS AND THERMAL CAPACITY SIZINGS OF LABORATORY-SCALE TES BED

|                             |  |
|-----------------------------|--|
| Composite Material:         | 51 wt % NaBaCO <sub>3</sub> /49 wt % MgO |
| Bed Diameter:               | 0.30 ft                                  |
| Bed Height:                 | 0.344 ft                                 |
| Bed Volume:                 | 0.0236 ft <sup>3</sup>                   |
| Bed Void Fraction:          | 0.417                                    |
| Salt Density, theor:        | 203.4 lbm/ft <sup>3</sup>                |
| Avg Salt Heat Capacity:     | 0.317 Btu/lbm-°F                         |
| Salt Heat of Fusion:        | 74 Btu/lbm                               |
| Salt Melting Point:         | 1321°F                                   |
| Sensible Density, theor:    | 223.39 lbm/ft <sup>3</sup>               |
| Sensible Heat Capacity:     | 0.27 Btu/lbm/ft <sup>3</sup>             |
| Pressed-Pellet Density:     | 87% of theor                             |
| Composite Density, theor:   | 212.7 lbm/ft <sup>3</sup>                |
| Composite Density, pressed: | 185.1 lbm/ft <sup>3</sup>                |
| Mass Sensible Material:     | 1.25 lbm                                 |
| Mass Salt PCM:              | 1.30 lbm                                 |
| Total Mass Composite:       | 2.55 lbm                                 |

| $\Delta T$ ,<br>°F | Thermal<br>Capacity,<br>Btu | Thermal<br>Capacity,<br>kW-h |
|--------------------|-----------------------------|------------------------------|
| 50                 | 1.337E+02                   | 3.917E-02                    |
| 100                | 1.711E+02                   | 5.015E-02                    |
| 150                | 2.086E+02                   | 6.112E-02                    |
| 200                | 2.460E+02                   | 7.209E-02                    |
| 250                | 2.835E+02                   | 8.306E-02                    |
| 300                | 3.210E+02                   | 9.404E-02                    |
| 350                | 3.584E+02                   | 1.050E-01                    |
| 400                | 3.959E+02                   | 1.160E-01                    |
| 450                | 4.333E+02                   | 1.270E-01                    |
| 500                | 4.708E+02                   | 1.379E-01                    |
| 550                | 5.082E+02                   | 1.489E-01                    |
| 600                | 5.457E+02                   | 1.599E-01                    |
| 650                | 5.831E+02                   | 1.708E-01                    |
| 700                | 6.206E+02                   | 1.818E-01                    |
| 750                | 6.580E+02                   | 1.928E-01                    |
| 800                | 6.955E+02                   | 2.038E-01                    |
| 850                | 7.329E+02                   | 2.147E-01                    |
| 900                | 7.704E+02                   | 2.257E-01                    |
| 950                | 8.078E+02                   | 2.367E-01                    |
| 1000               | 8.453E+02                   | 2.477E-01                    |

Total heat stored in bed = 0.344075 ft high x 0.29567 ft diam  
 From room temperature (72°F) to salt (mp +200°F)

With 51 % NaBaCO<sub>3</sub>/49% MgO: 0.34 kWh (1182 Btu)

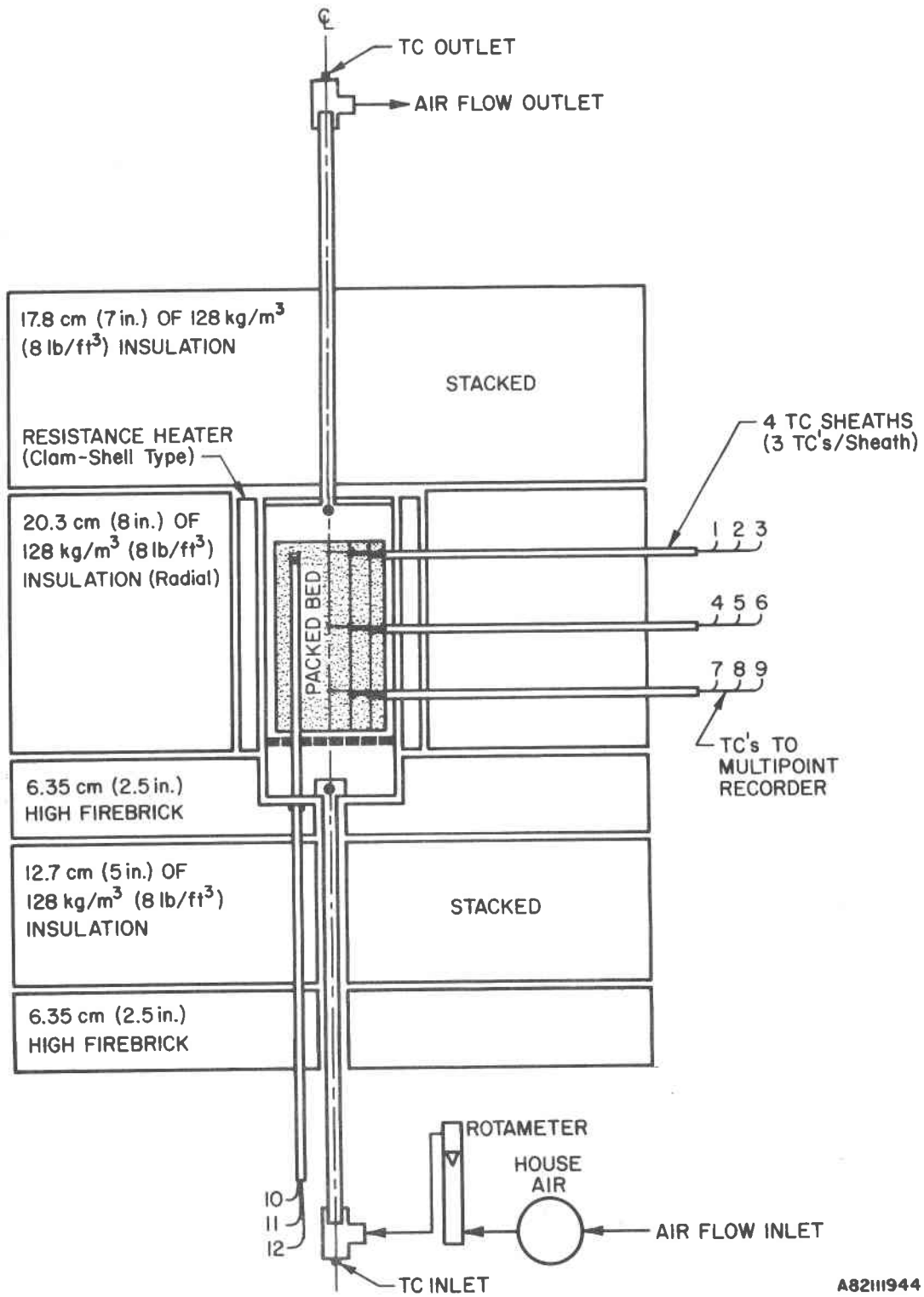


Figure 7-18. SCHEMATIC DIAGRAM OF LABORATORY-SCALE TES MODULE

Prior to installation into the module set-up, the cannister was filled in air with 1106 g (2.44 lb) of cold-pressed and sintered 51 wt %  $\text{Na}_2\text{CO}_3$ - $\text{BaCO}_3$ /49 wt %  $\text{MgO}$  composite pellets. The pellets had an average height of 0.82 cm (0.324 in.) and average diameter of 0.93 cm (0.365 in.) The overall geometric sizing resulted in a bed-to-pellet diameter ratio of about 10 to 1, which generally ensures uniform flow through the bed, thus minimizing preferential gas channeling up the container walls. The as-sintered pellets loaded into the unit possessed an average density of  $2,923 \text{ kg/m}^3$  or  $182.5 \text{ lb/ft}^3$  (~86% of theoretical) and volume packing density of 58.3%. As also shown in Table 7-4, pellets of this geometry represent  $0.26 \text{ m}^2$  ( $2.84 \text{ ft}^2$ ) of heat transfer surface area for charge/discharge thermal cycling. Figure 7-19 is a photograph of the composite pellets as they were loaded into the test unit. The unit was operated under varying cycling periods (a cycle consisting of a charge, discharge, and hold-time). The composite media bed studied in these tests was cycled from  $815^\circ\text{C}$  ( $1500^\circ\text{F}$ ; mp  $+100^\circ\text{C}$ ) to  $615^\circ\text{C}$  ( $1140^\circ\text{F}$ ; mp  $-100^\circ\text{C}$ ) for 17 cycles over 398 hours of operation.

As mentioned above, the packed bed was discharged by passing ambient air regulated by a Dwyer flowmeter (range 0 to 400 SCF/h) through it from bottom to top. The initial condition for a discharge was that all T/C's located within the bed were at mp  $+100^\circ\text{C}$  ( $180^\circ\text{F}$ ). At this point, power to the clam-shell heaters was cut, and air was passed through the bed at a constant flow rate, which varied from 1.42 to  $11.3 \text{ m}^3/\text{h}$  (50 to 400 SCF/h). Bed and air temperatures were continuously recorded on an Esterline Angus 24 point strip chart recorder throughout the cycle. A discharge run was ended when the slowest cooling bed-T/C attained the  $\text{Na}_2\text{CO}_3$ - $\text{BaCO}_3$  salt mp minus  $100^\circ\text{C}$ , or  $615^\circ\text{C}$ . Air flow was then shut off and the media was maintained at  $615^\circ\text{C}$  during the hold-time. The charging portion of the cycle was controlled by a thermocouple at bed mid-level, between the cannister OD and the heater coils. The temperature controllers were set to bring the temperature at this location to  $815^\circ\text{C}$  (mp  $100^\circ\text{C}$ ) in 6 hours, while initial heat-up was maintained at  $2^\circ\text{C}$  ( $3.6^\circ\text{F}$ ) per minute.

### 7.2.3 Performance Evaluation

The following parameters were used in assessing the applicability of this novel direct-contact concept and evaluating the composite's thermal performance in the laboratory-scale system:

- Average discharge heat flux during a discharge run
- Variation of the discharge heat flux during a discharge run
- Discharge bed temperature responses and characteristics
- Cycling stability — possible variations in discharge behavior resulting from composite instabilities during normal cycling
- Chemical stability of composite based on post-test chemical analyses (Subtask 2.3)

The heat flux,  $Q$ , from the composite pellets to the air working fluid was determined as a function of discharge time by monitoring the inlet and outlet air temperatures and calculating  $Q$  from the expression —

Table 7-4. PELLET AND PACKED-BED CHARACTERISTICS

|   | Average Pellet   | Packed-Bed                                       |
|---|--|--|
| Height, cm (in.)  | 0.8247 (0.3247)  | 10.487 (4.1289)                                  |
| Diameter, cm (in.)  | 0.9294 (0.3659)  | 9.011 (3.548)                                    |
| Volume, cm <sup>3</sup> (in. <sup>3</sup> )<br>m <sup>3</sup> (ft <sup>3</sup> )                        | 0.5572 (0.034)<br>5.58 X 10 <sup>-7</sup> (1.97 X 10 <sup>-5</sup> ) | 655.5 (40.82)<br>6.79 X 10 <sup>-4</sup> (0.024) |
| Heat Transfer<br>Surface Area, cm <sup>2</sup> (in. <sup>2</sup> )<br>m <sup>2</sup> (ft <sup>2</sup> ) | 3.74 (0.58)<br>3.42 X 10 <sup>-4</sup> (0.00368)                     | 2639 (409)<br>0.264 (2.84)                       |
| Density, kg/m <sup>3</sup> (lb/ft <sup>3</sup> )  | 2923 (182.5)   | --   |
| % Theoretical Density   | 86   | --   |
| No. Installed   | 704  | --   |
| Total Weight, kg (lb)   | 0.0016 (0.0036)  | 1.106 (2.439)                                    |
| Packing Density, %  | --   | 58.3   |
| Surface Area/Volume   | 17:1   | --   |

53ER/RPE/65055ta



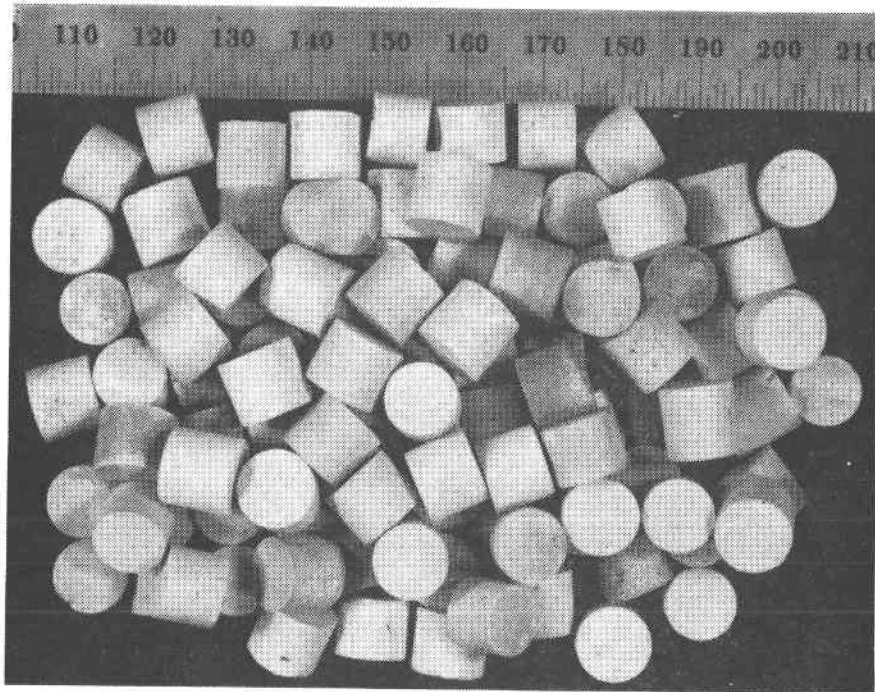


Figure 7-19. COLD-PRESSED AND SINTERED COMPOSITE  $\text{Na}_2\text{CO}_3\text{-BaCO}_3/\text{MgO}$   
TES PELLETS LOADED INTO TES TEST CANNISTER

$$Q = \frac{\dot{m} C_p \Delta T}{A}$$

$Q$  = heat flux,  $W/m^2$  (Btu/h-ft<sup>2</sup>)

$\dot{m}$  = air mass flow rate, kg/h (lb/h)

$C_p$  = heat capacity of air, J/kg-°C (Btu/lb-°F)

$\Delta T$  = air temperature differential =  $T_{out} - T_{in}$ , °C (°F)

$A$  = heat transfer area, m<sup>2</sup> (ft<sup>2</sup>)

The heat transfer area used to evaluate this heat flux was defined as the total surface area of all the pellets, which was calculated to be 0.26 m<sup>2</sup> (2.84 ft<sup>2</sup>). The air outlet temperature was measured at the center of the heat exchanger tube at the cannister exit, so as to result in heat fluxes that are not influenced significantly by radiant heat loss in the extended portions of the heat exchanger tube.

Characteristic discharge curves were determined as a function of discharge air flow rate over the range 1.42 to 11.3 m<sup>3</sup>/h (50 to 400 SCF/h). Figure 7-20 contains a plot of the discharge time required for the salt to solidify versus air flow rate. At air flow rates greater than 4.25 m<sup>3</sup>/h (150 SCF/h), the rate of discharge appears to be controlled mainly by heat transport through the solidified salt/composite pellets, thus resulting in data most indicative of the pellet's heat transfer characteristics.

Also, the decrease in total discharge time as a function of incremental increase in discharge air flow rate is in a region of diminishing marginal return in the regime of flow rates greater than 4.2 m<sup>3</sup>/h (150 SCF/h). This result indicates the optimum operating flow rate regime to be utilized in designing a cost-effective TES system for minimizing working fluid pump capital costs and parasitic power requirements. A flow rate of about 5.7 m<sup>3</sup>/h (200 SCF/h) was chosen as the standard, optimum flow condition, yielding ~20-minute discharge times for the slowest cooling T/C (near top of bed) to cool to 615°C (1139°F). As seen in Figure 7-21, flows above 1.4 m<sup>3</sup>/h (50 SCF/h) typically result in a turbulent flow condition within the inlet heat exchanger tube over the temperature range 22° to 982°C (72° to 1800°F), while Figure 7-14 indicates that flow through the actual packed bed is primarily laminar over the same temperature range. This laminar process condition will also lower pumping costs in scaled-up system applications.

Results obtained during Run 4 (149 hours of operation) and Run 13 (314 hours of operation) of the bed discharge temperature profile for an air flow rate of 5.7 m<sup>3</sup>/h (200 SCF/h) are plotted in Figures 7-22 and 7-23, respectively. The time-temperature responses of the bed thermocouples do indicate slight thermal arrests characteristic of congruent solidification, although they are not as distinct as that observed for the 48 wt % Na<sub>2</sub>CO<sub>3</sub>-52 wt % BaCO<sub>3</sub> molten salt alone when tested in a similar cannister with a single-pass heat exchanger tube at a discharge air flow rate of 180 SCF/h<sup>3</sup> (included here as Figure 7-24 for comparison). Discharge outlet delivery temperatures for the composite were very high (Figure 7-25), averaging from 815° to 560°C (1500° to 1040°F) compared with 190° to 90°C (374° to 194°F) for a similar salt temperature-

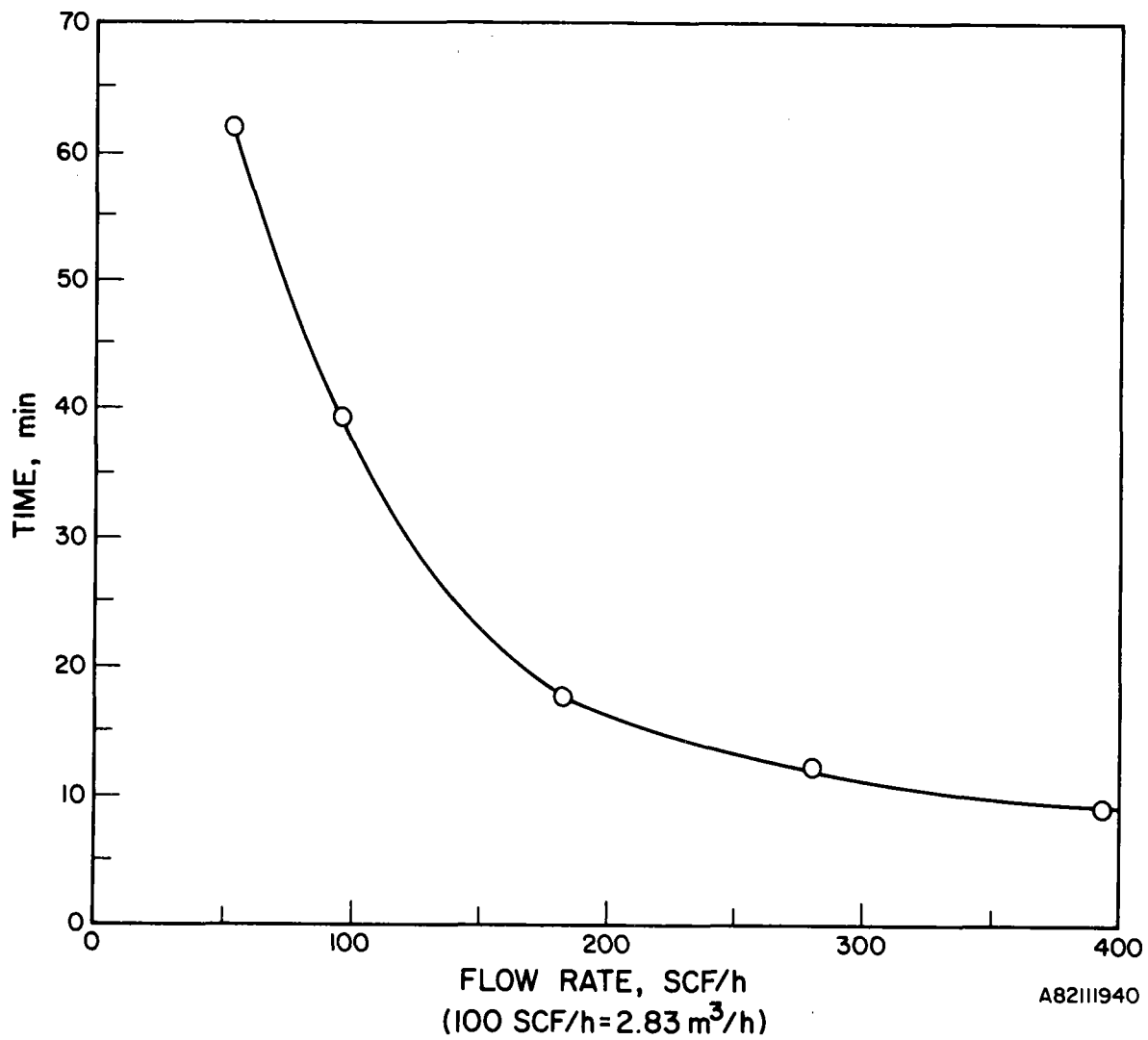


Figure 7-20. TYPICAL DISCHARGE PERFORMANCE OF LABORATORY-SCALE TES UNIT CONTAINING COMPOSITE 51 Wt % Na<sub>2</sub>CO<sub>3</sub>-BaCO<sub>3</sub>/49 Wt % MgO MEDIA

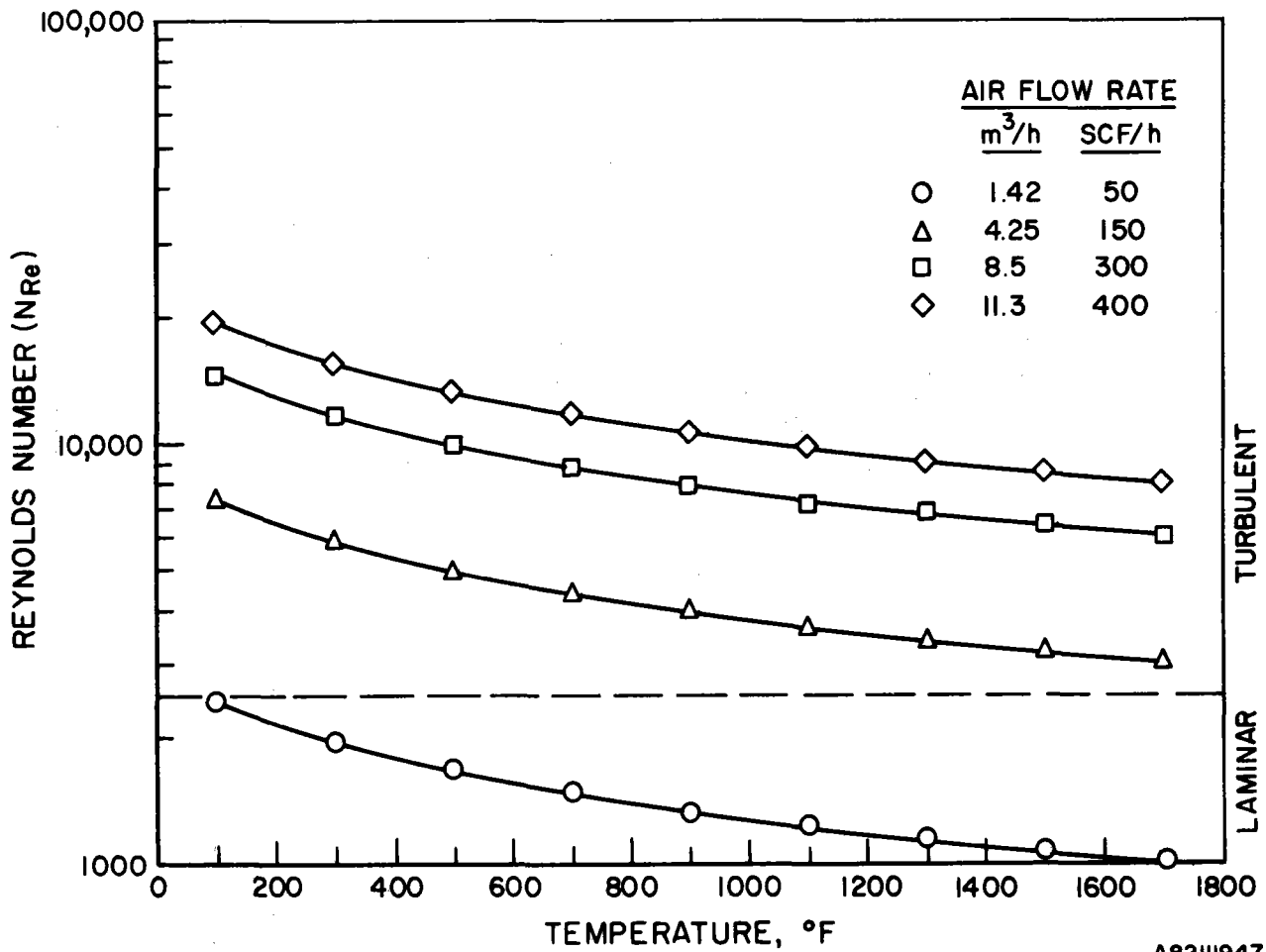


Figure 7-21. REYNOLDS NUMBER VERSUS TEMPERATURE  
FOR VARIOUS INLET AIR FLOW RATES  
THROUGH A 0.5-INCH TUBE

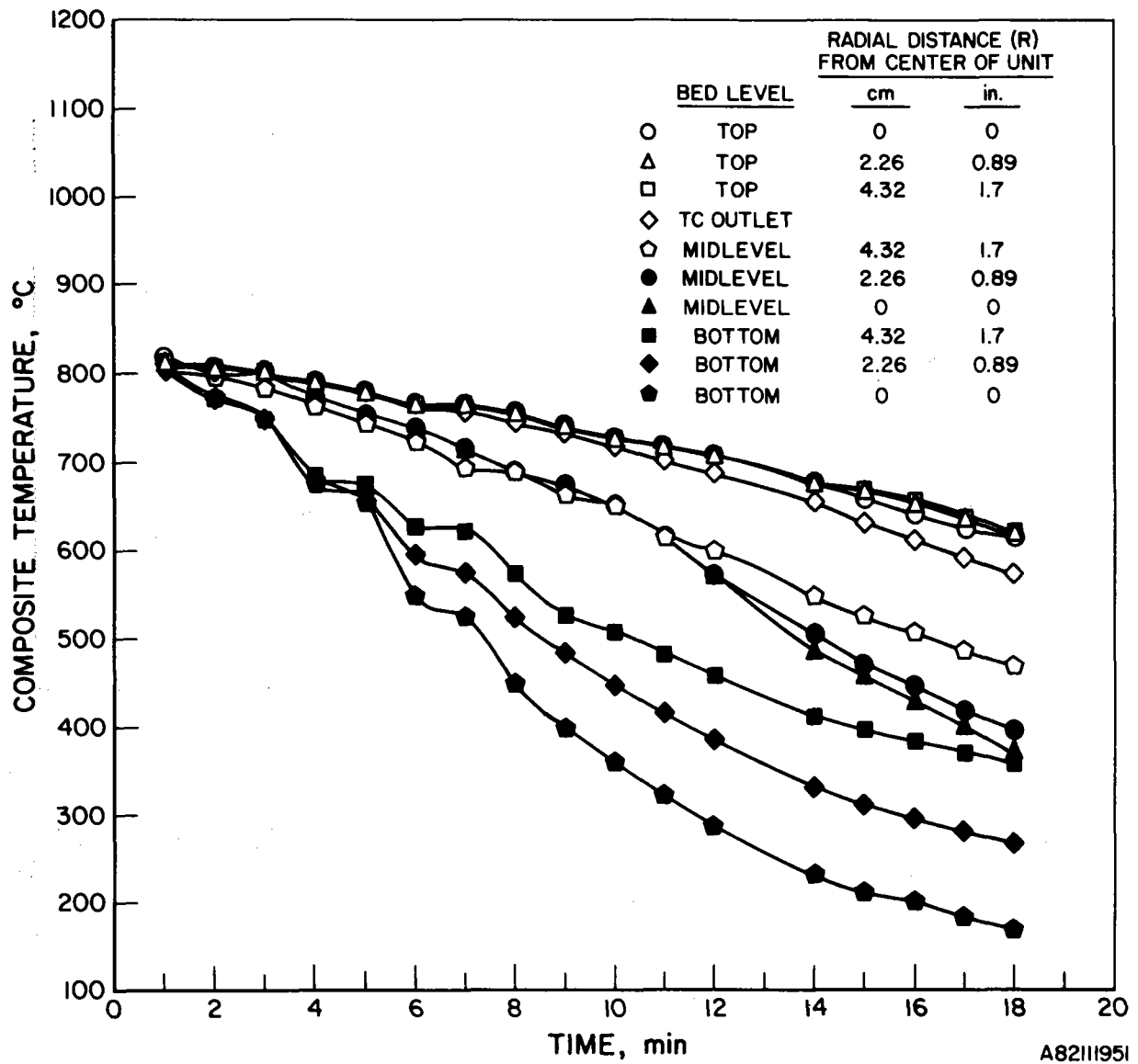
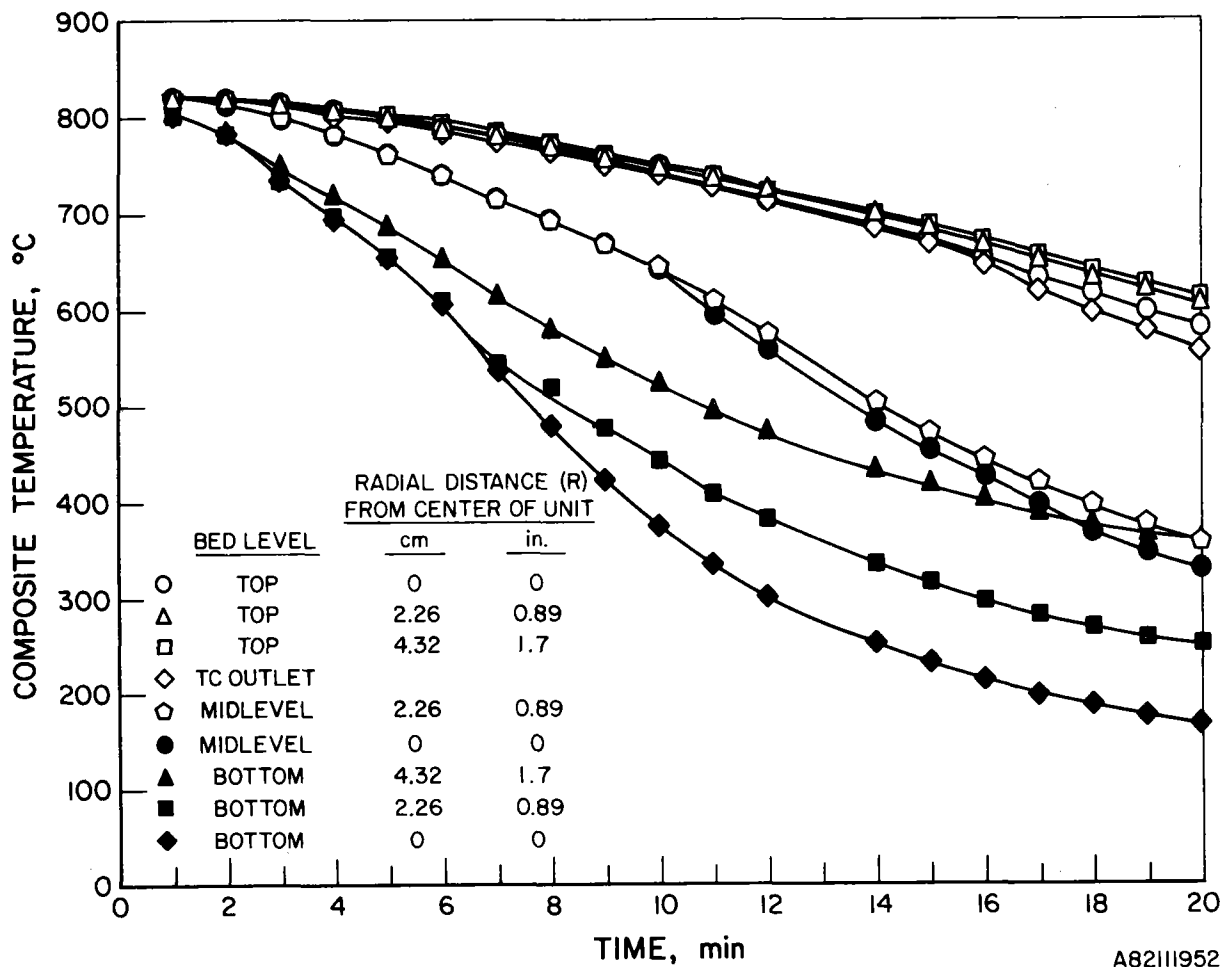
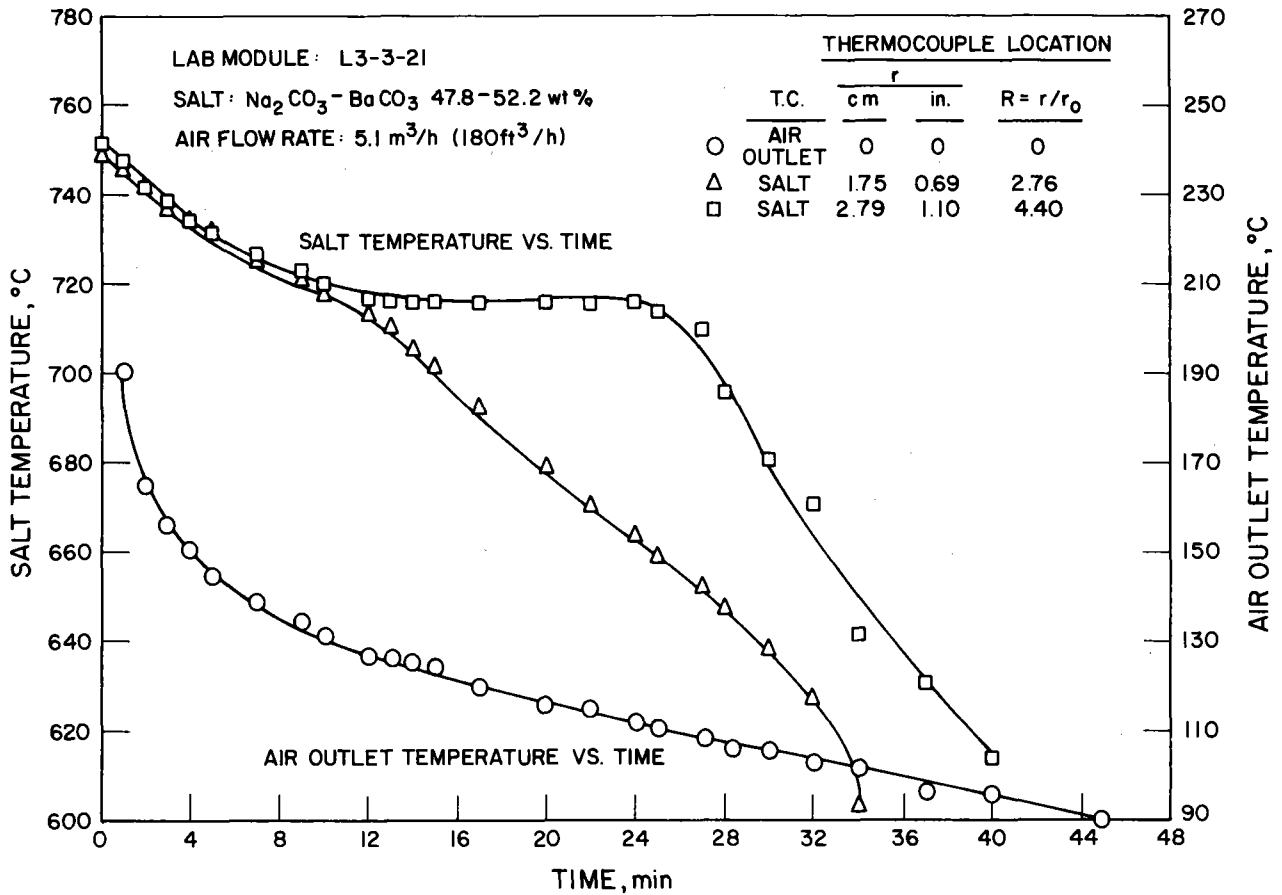


Figure 7-22. COMPOSITE MEDIA DISCHARGE PERFORMANCE AT 200 SCF/h AIR FLOW RATE ON RUN 4 (149 Hours of Operation)



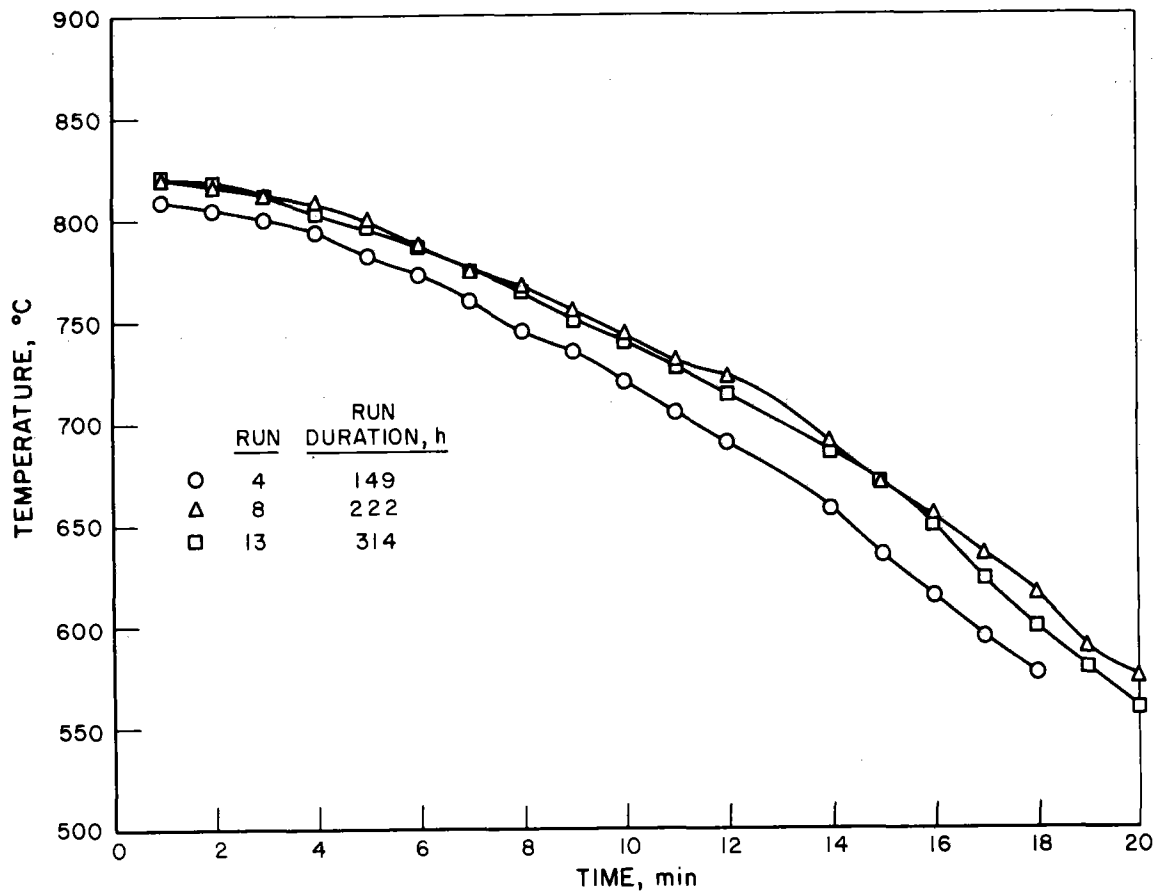
A82111952

Figure 7-23. COMPOSITE MEDIA DISCHARGE PERFORMANCE AT  
200 SCF/h AIR FLOW RATE ON CYCLE 13  
(314 Hours of Operation)



B80010253

Figure 7-24. TYPICAL DISCHARGE PERFORMANCE OF  $\text{Na}_2\text{CO}_3$ - $\text{BaCO}_3$  SYSTEM AT  $180 \text{ ft}^3/\text{h}$  AIR FLOW RATE



A83020286

Figure 7-25. DISCHARGE AIR OUTLET TEMPERATURES VERSUS TIME FOR 51 Wt %  $\text{Na}_2\text{CO}_3$ - $\text{BaCO}_3$ /49 Wt %  $\text{MgO}$  COMPOSITE SYSTEM AT 200 SCF/h AIR FLOW RATE



swing using a molten  $\text{Na}_2\text{CO}_3\text{-BaCO}_3$  in a single heat exchanger tube configuration.

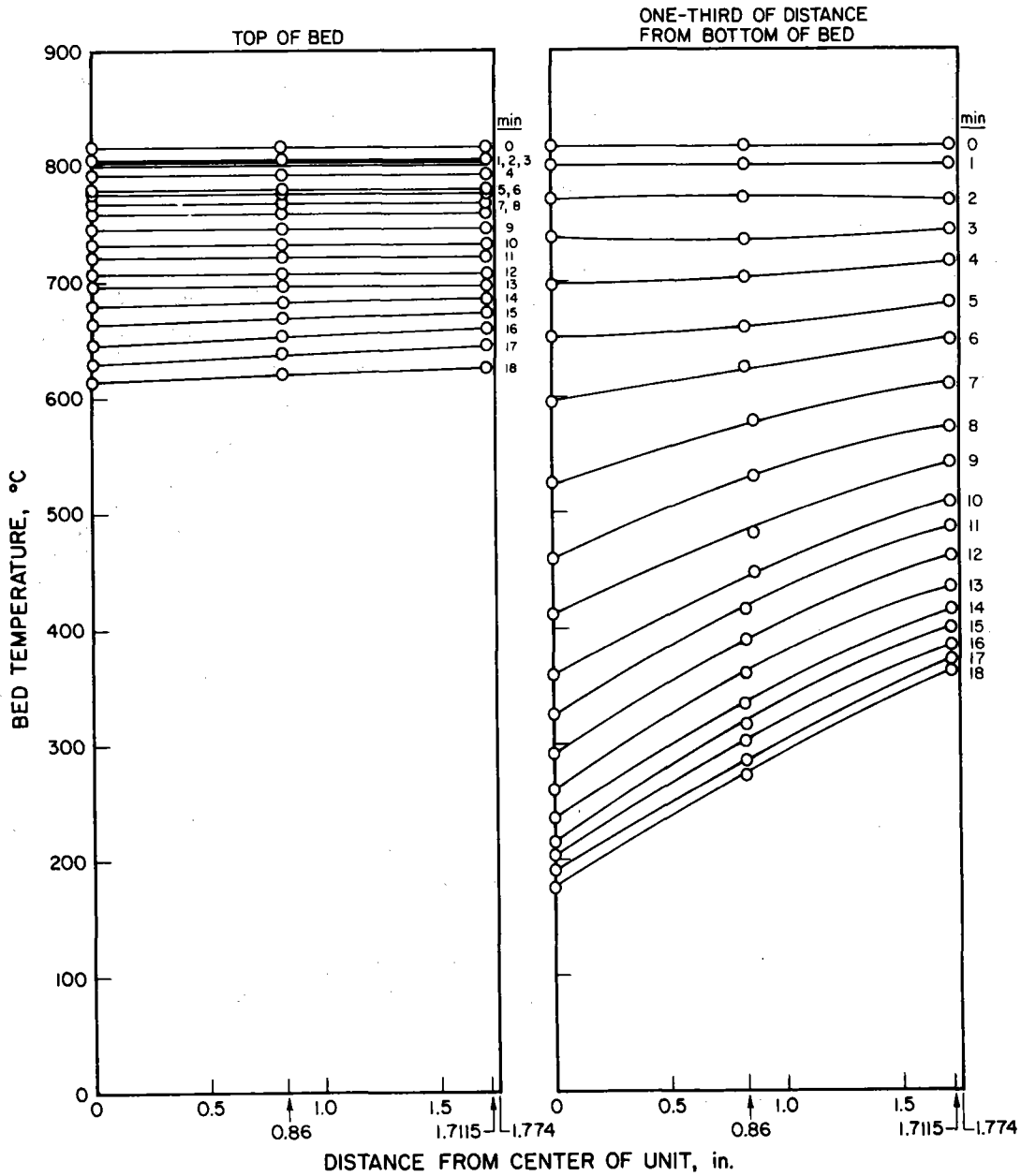
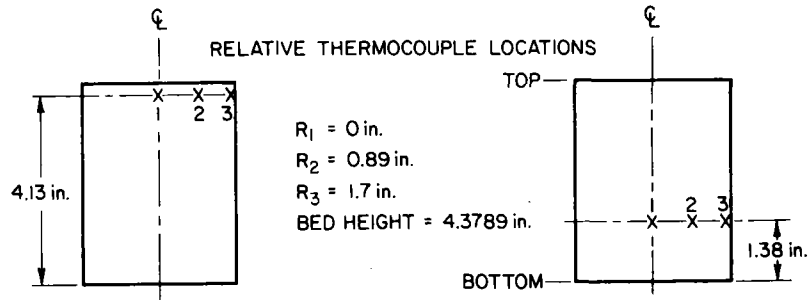
The observed radial thermal gradients along a given axial slice of the bed may have been caused by preferential flow channeling patterns in the bed, resulting in lower temperatures at the center thermocouples ( $R = 0$  cm, 0 in.). However, from Figure 7-26, which plots the radial bed temperature profile through the bed as a function of cooling time, it is seen that this apparent flow channeling occurs in the bottom third of the bed and flow becomes more uniform in the upper portions of the bed.

Figure 7-27 shows the variation of the instantaneous heat flux with discharge time for three cycles at different points during the lifetime of the unit. The slowly decreasing general shape of the curve remained unchanged, while defining a narrow lifetime discharge performance band, indicating no significant loss of composite thermal storage capacity or heat transfer capability during 398 hours of operation. From these results, a lifetime average heat flux of  $5,233 \text{ W/m}^2$  ( $1660 \text{ Btu/h-ft}^2$ ) was determined graphically as shown in Table 7-5.

The effect of salt heat of fusion/solidification on composite discharge performance became more pronounced when the time-related responses of axial bed temperature and instantaneous heat flux were united. Generally, the downward-curving instantaneous heat flux curves can be reduced to a locus that is piecewise (linear) continuous in three discrete regions, having different slopes which correspond to progressive time-temperature states within the composite bed:

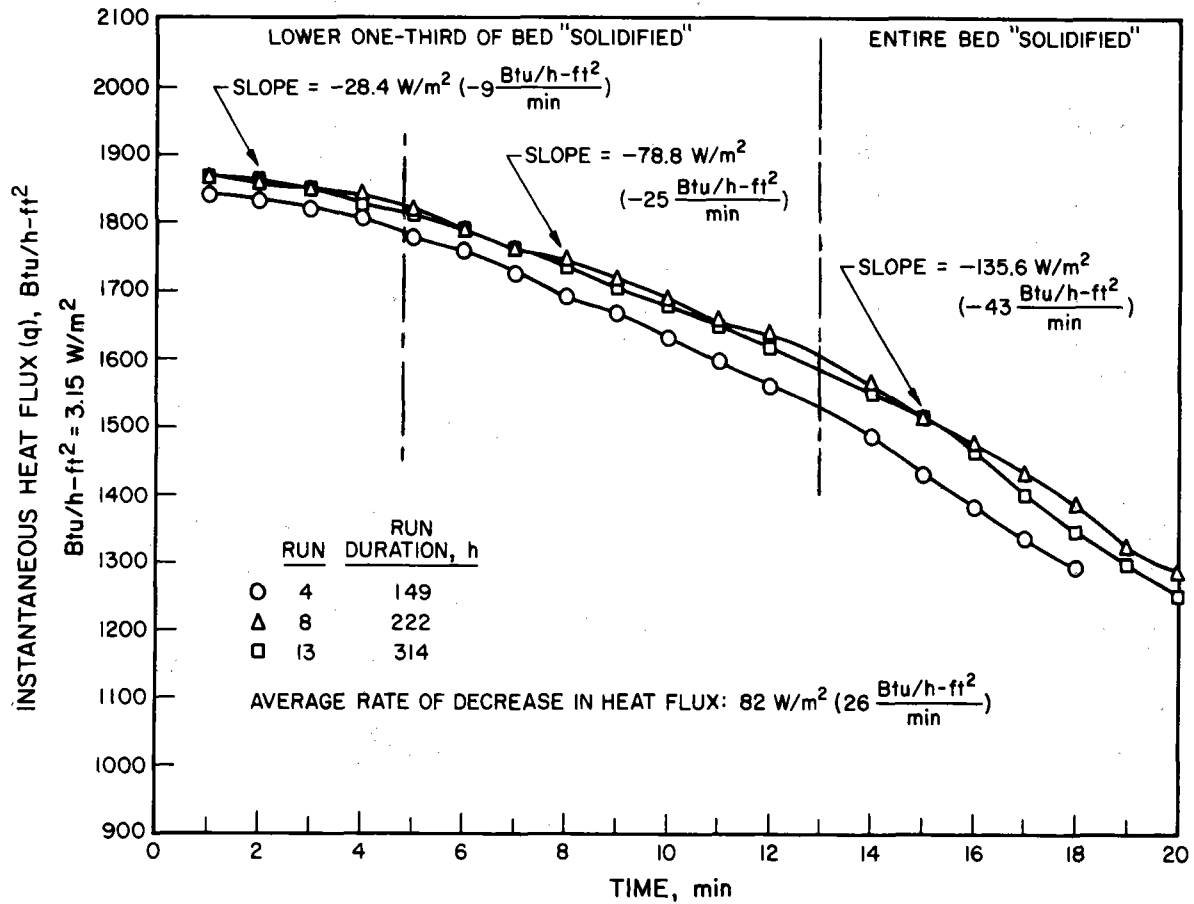
- 0 to 5 minutes
  - Liberation of sensible heat from liquid salt and  $\text{MgO}$
  - Initial solidification of salt in bottom third of bed
  - Heat flux slope =  $-28.4 \text{ W/m}^2/\text{min}$  ( $-9 \text{ Btu/h-ft}^2/\text{min}$ )
- 5 to 13 minutes
  - Gradual solidification of salt in bed
  - Liberation of sensible and latent heat from composite
  - Heat flux slope =  $-78.8 \text{ W/m}^2/\text{min}$  ( $-25 \text{ Btu/h-ft}^2/\text{min}$ )
- 13 to 20 minutes
  - Complete solidification of salt in bed
  - Release of sensible heat of solid salt and  $\text{MgO}$
  - Heat flux slope =  $-136 \text{ W/m}^2/\text{min}$  ( $-43 \text{ Btu/h-ft}^2/\text{min}$ )

The average rate of instantaneous heat flux decrease was  $82 \text{ W/m}^2$  ( $26 \text{ Btu/h-ft}^2$ ) per minute, which is 86% lower than the rate of heat flux decrease observed for solidification of molten  $\text{Na}_2\text{CO}_3\text{-BaCO}_3$  salt around a central heat exchanger tube in previous work at IGT.<sup>5</sup>



B83020290

Figure 7-26. TEMPERATURE PROFILE IN BED DURING FOURTH CYCLE  
AT 200 SCF/h AIR FLOW RATE



A83020288

Figure 7-27. LIFETIME DISCHARGE PERFORMANCE OF 51 Wt % Na<sub>2</sub>CO<sub>3</sub>-BaCO<sub>3</sub>/49 Wt % MgO MEDIA PACKED BED

Table 7-5. LIFETIME AVERAGE HEAT FLUX DISCHARGE PERFORMANCE FOR  
51 Wt % NaBaCO<sub>3</sub>/49 Wt % MgO COMPOSITE MEDIA

| Cycle   | Hours of<br>Operation | $\bar{Q}$   |               |
|---------|-----------------------|---|---------------|
|         |                       | mp +100°C →<br>mp -100°C<br>W/m <sup>2</sup> (Btu/h-ft <sup>2</sup> ) |               |
| 4       | 149                   | 5195  | (1648)        |
| 8       | 222                   | 5277  | (1674)        |
| 13      | 314                   | <u>5227</u>   | <u>(1658)</u> |
| Average |                       | 5233  | (1660)        |

53ER/RPE/65055ta

#### 7.2.4 Subtask 2.3. Post-Test Examination

After termination, the test module was dismantled to evaluate the stability of the composite and characterize the effects of direct-contact air-heat exchange, thermal cycling, and prolonged, high-temperature exposure. The pre- and post-test pressure drop as a function of air flow rate through the composite bed was relatively invariant, indicating a stable bed configuration and pellet integrity (Figure 7-28). Samples of the composite were taken from various locations in the bed to assess the geometric shape retention and density of the pellets. As shown in Table 7-6, the average pellet density decreased 1.5% while the total weight loss for the bed was only 0.94% in 398 hours and 17 thermal cycles in air. The chemical analysis for these samples, appearing in Table 7-7, revealed that there was a change in the composition of the composite due to partial salt decomposition, (during pre-test sintering or charge/discharge testing) or chemical reaction of salt with MgO support material or air working fluid. Evaluation of the effects of pre-test pellet sintering on composite chemical composition is under current investigation in the industrial TES program.

Figure 7-29 contains photographs of the terminated unit and post-test composite pellets. A slight discoloration was observed in the top pellet layer due to spalling of the oxide layer formed on the Type 316 stainless steel containment vessel on cooldown. The pellets remained otherwise intact and uniform.

The high degree of stability and high heat transfer characteristics of the composite media after 17 thermal cycles and 398 hours of operation serve as very encouraging lab-scale verifications of the initial latent/sensible direct-contact heat exchanger concept.

### 7.3 TASK 3. ECONOMIC ANALYSES

The purpose of this task was to improve and refine the initial cost and performance estimates as presented in our original proposal for composite salt/ceramic TES media. A composite carbonate salt/MgO ceramic medium was projected to offer an approximately 43% reduction in media cost and 35% reduction in system volume, compared to a baseline MgO refractory brick storage system proposed by Boeing [11]. Because the Boeing study showed that TES subsystem costs are dominated by storage media and containment vessel costs, these two parameters were focused upon in these analyses.

The cost of fabricated composite media will depend upon a number of factors, including raw materials costs, salt/ceramic chemical composition, heat of fusion and specific heat values, and processing costs. Raw materials costs were based on bulk-quantity prices of technical-grade salt and ceramic powders listed in the Chemical Marketing Reporter or quotes from industrial suppliers. Figure 7-30 shows the results of an evaluation of materials costs for Na<sub>2</sub>CO<sub>3</sub>-based composites containing various assumed ceramic support particles synthesized from technical-grade materials. Processing costs are not considered in this comparison.

It is more difficult to estimate costs associated with media processing operations such as spray drying of composite powders, pellet fabrication by

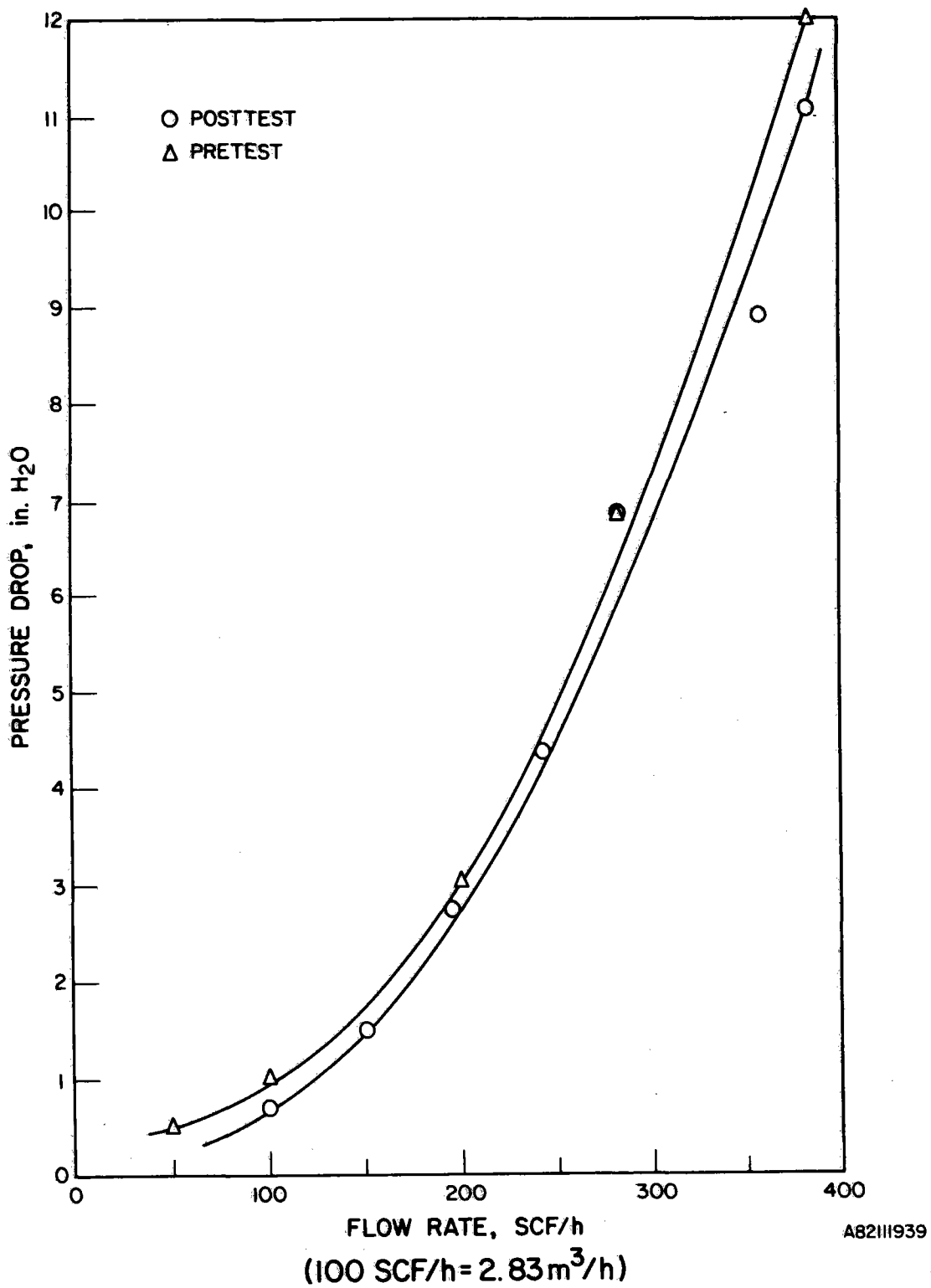


Figure 7-28. TES COMPOSITE BED PRESSURE DROP AS A FUNCTION OF AIR FLOW RATE FOR PRE- AND POST-TEST CONDITIONS

Table 7-6. PRE- AND POST-TEST COMPOSITE MEDIA CHARACTERISTICS

|  | Average Pellet      |                       |              |   | Total Bed<br>Weight, g |
|--|---------------------|-----------------------|--------------|---|------------------------|
|  | Height,<br>cm (in.) | Diameter,<br>cm (in.) | Weight,<br>g | Density,<br>kg/m <sup>3</sup> (lb/ft <sup>3</sup> ) |                        |
| Pre-Test<br>(Average)                  | 0.8222 (0.3237)     | 0.9268 (0.3649)       | 1.621        | 2923 (182.5)  | 1106.3                 |
| Post-Test<br>(Average)                 | 0.7986 (0.3144)     | 0.9205 (0.3624)       | 1.528        | 2877 (179.6)  | 1095.9                 |
| Average Change<br>Pre- to Post-Test, % | -2.9                | -0.69                 |              | -1.5  | -0.94                  |

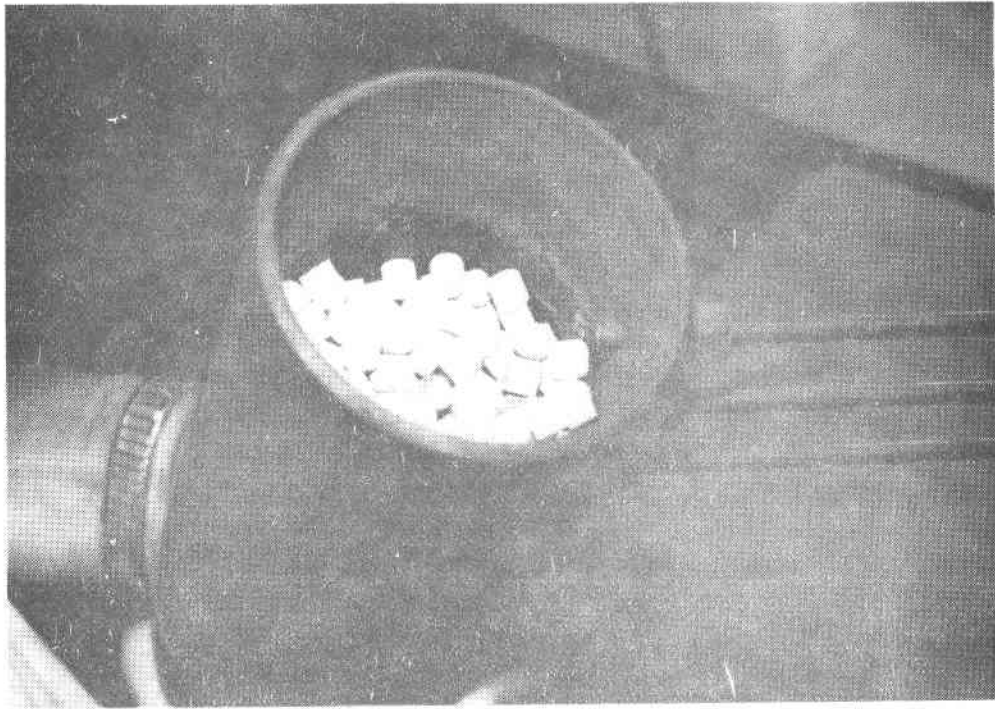
53ER/RPE/65055ta

Table 7-7. PRE- AND POST-TEST CHEMICAL ANALYSIS OF  
51 Wt % NaBaCO<sub>3</sub>/49 Wt % MgO COMPOSITE SYSTEM

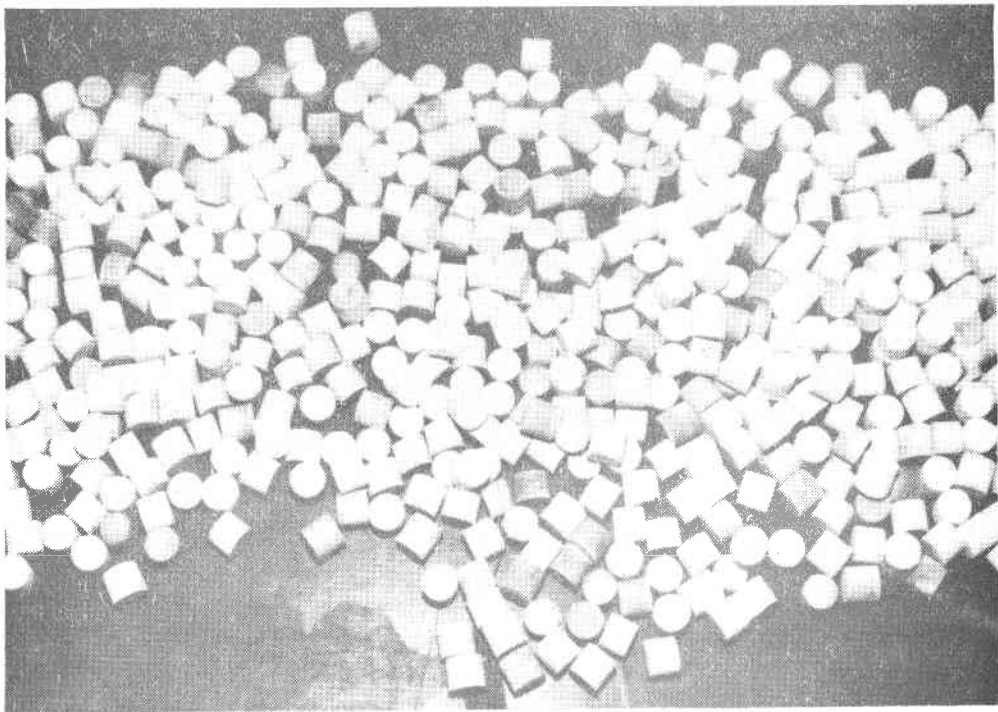
|                                     | Na <sub>2</sub> CO <sub>3</sub> ,<br>wt % | BaCO <sub>3</sub> ,<br>wt % | MgO,<br>wt % | Percent<br>Carbonation |
|-------------------------------------|---|-----------------------------|--------------|------------------------|
| Pre-Test: Powder                    | 25.1                                      | 29.3                        | 45.6         | 1.04                   |
| Post-Test:<br>Sintering Environment |   |                             |              |                        |
| 1. CO <sub>2</sub>                  | 23.9                                      | 27.4                        | 48.6         | 0.93                   |
| 2. CO <sub>2</sub>                  | 25.3                                      | 28.7                        | 46.0         | 0.89                   |
| 3. Air                              | 21.3                                      | 30.4                        | 48.3         | 0.90                   |

53ER/RPE/65055ta



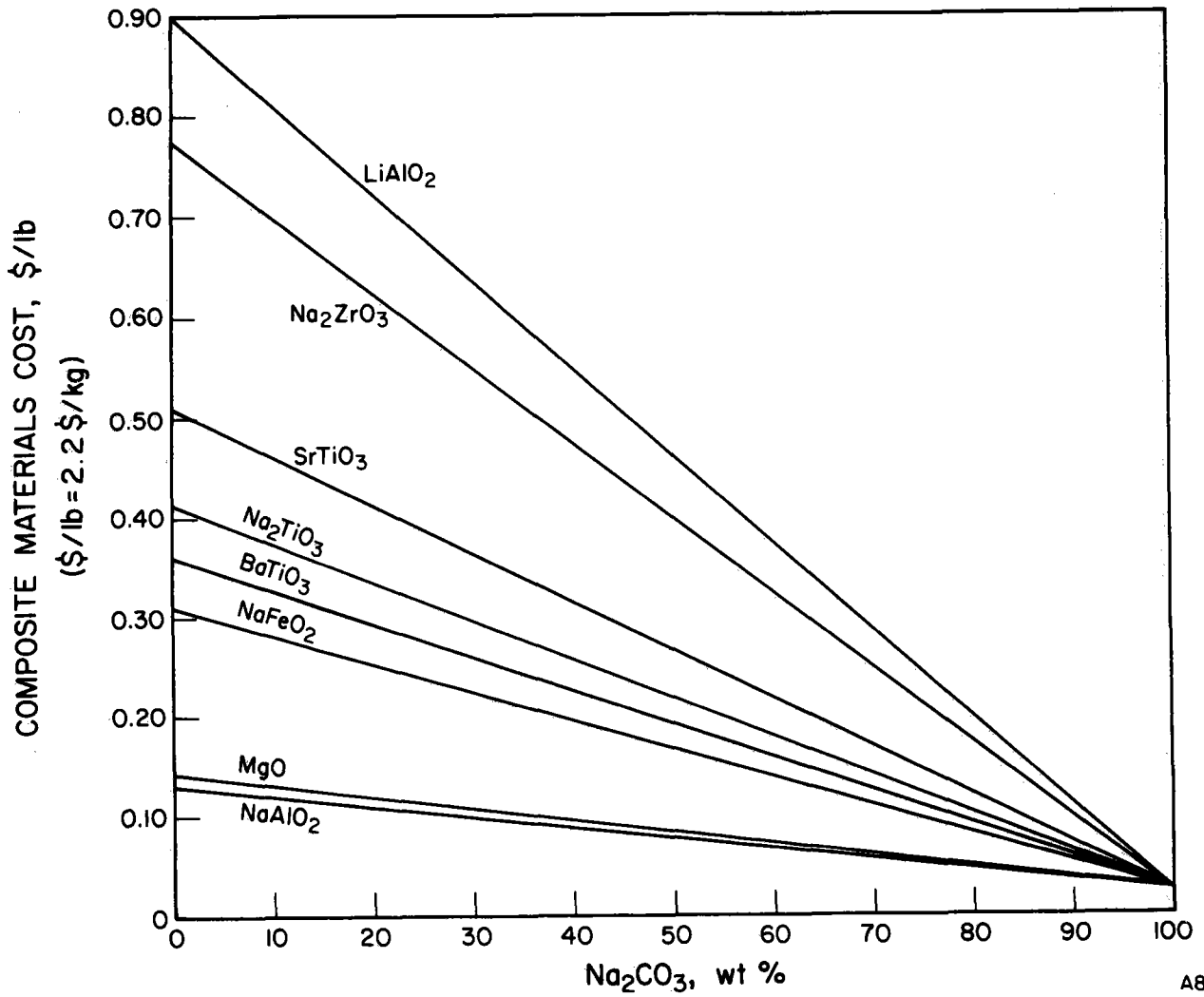


P83040428



P83040429

Figure 7-29. POST-TEST APPEARANCE OF TES TEST CANNISTER AND COMPOSITE MEDIA



A82111941

Figure 7-30. ESTIMATED MATERIALS COSTS FOR Na<sub>2</sub>CO<sub>3</sub>/CERAMIC COMPOSITES

extrusion or dry pressing, and pellet densification by high-temperature sintering. In general, each of these operations will have costs related to labor, energy consumption, and equipment requirements. Discussions were conducted with chemical processing companies that have extensive experience in commercial-scale production of ceramics, clays, and similar materials, for estimation of such processing costs.

Results of these materials and processing cost estimates were input to a BASIC computer program that was written to facilitate estimation of TES media and subsystem costs as a function of media composition, thermal properties, and TES operating temperature range. The computer code parametrically generates the key mass, volume, energy density, and cost requirements to store a given amount of heat over a given temperature swing for both the baseline sensible and composite materials.

Conceptually, the sensible and advanced-composite storage media TES systems may be envisioned to operate in either an arranged configuration with "fixed" gas flow passages (horizontal or vertical) or in a packed-bed mode with "random" void gas flow passages. To facilitate and simplify comparative evaluations of the sensible versus composite media, the system was taken to be in a packed-bed configuration.

Comparative media mass, volume, cost, and resultant system volume requirements were calculated on the following consistent bases:

- Storage of 1,055 MJ (1 million Btu) of heat
- Packed-bed void fraction = 0.4
- Temperature swing of media ( $\Delta T$ )
  - Considered as swing of  $\frac{\Delta T}{2}$  above and below salt mp
- Appropriate physical properties of sensible and composite media (e.g. density, heat capacity, heat of fusion, composition)
- Projected fabricated cost of composite media = \$/kg (\$/lb) unit cost of powders + 0.22 \$/kg (\$0.10/lb) for spray drying + 0.11 \$/kg (\$0.05/lb) for briquetting
  - The processing cost factors were obtained from discussions with industrial producers of ceramic powders and shapes
- Technical-grade materials are acceptable
- Individual media shape density = 100% of theoretical ( $3.41 \text{ g/cm}^3$ )

Figures 7-31 and 7-32 show the storage media cost in dollars and corresponding system interior volume requirements, respectively, per 1,055 MJ of stored energy as a function of temperature swing. Three baseline sensible media are plotted:

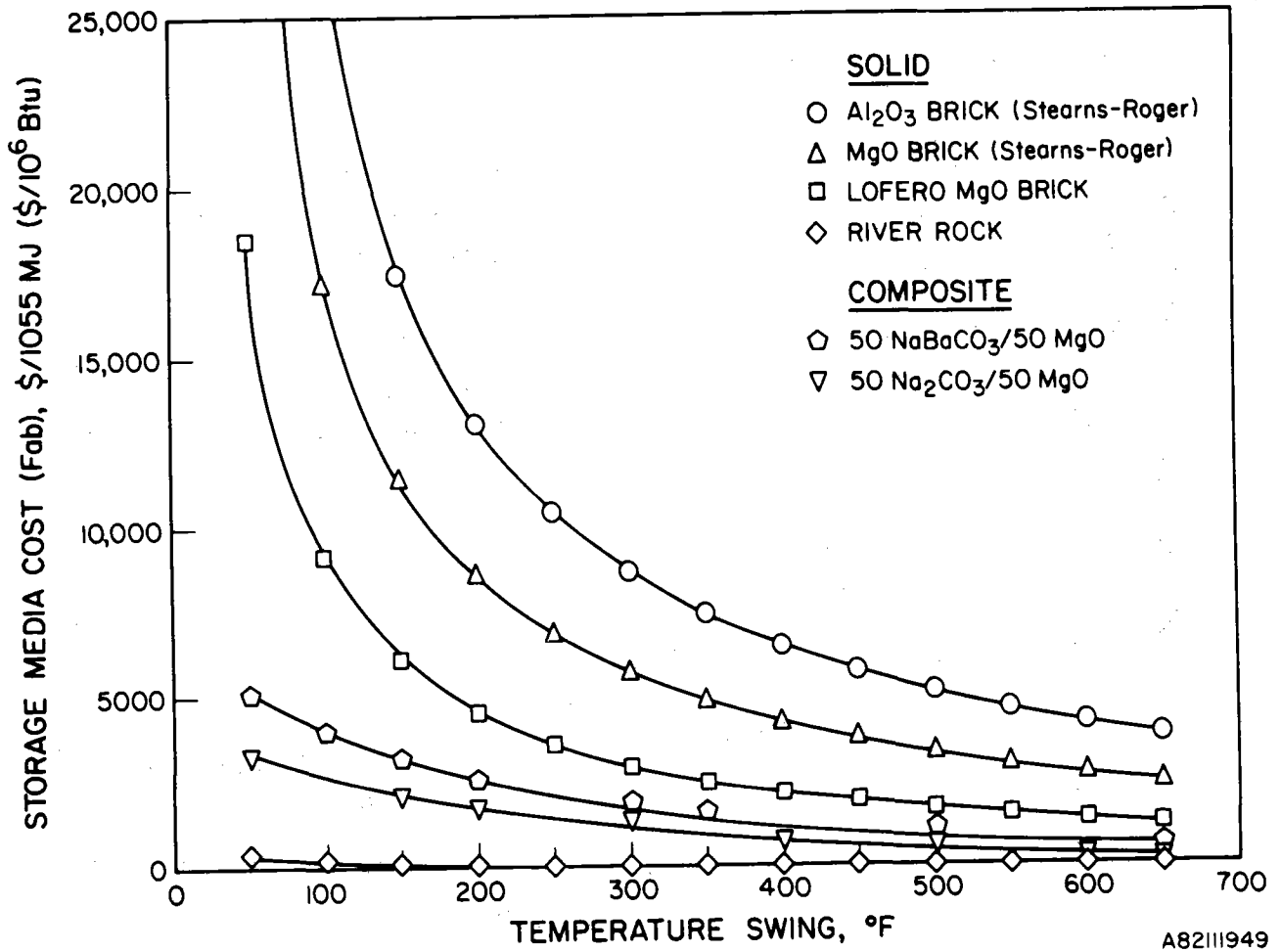
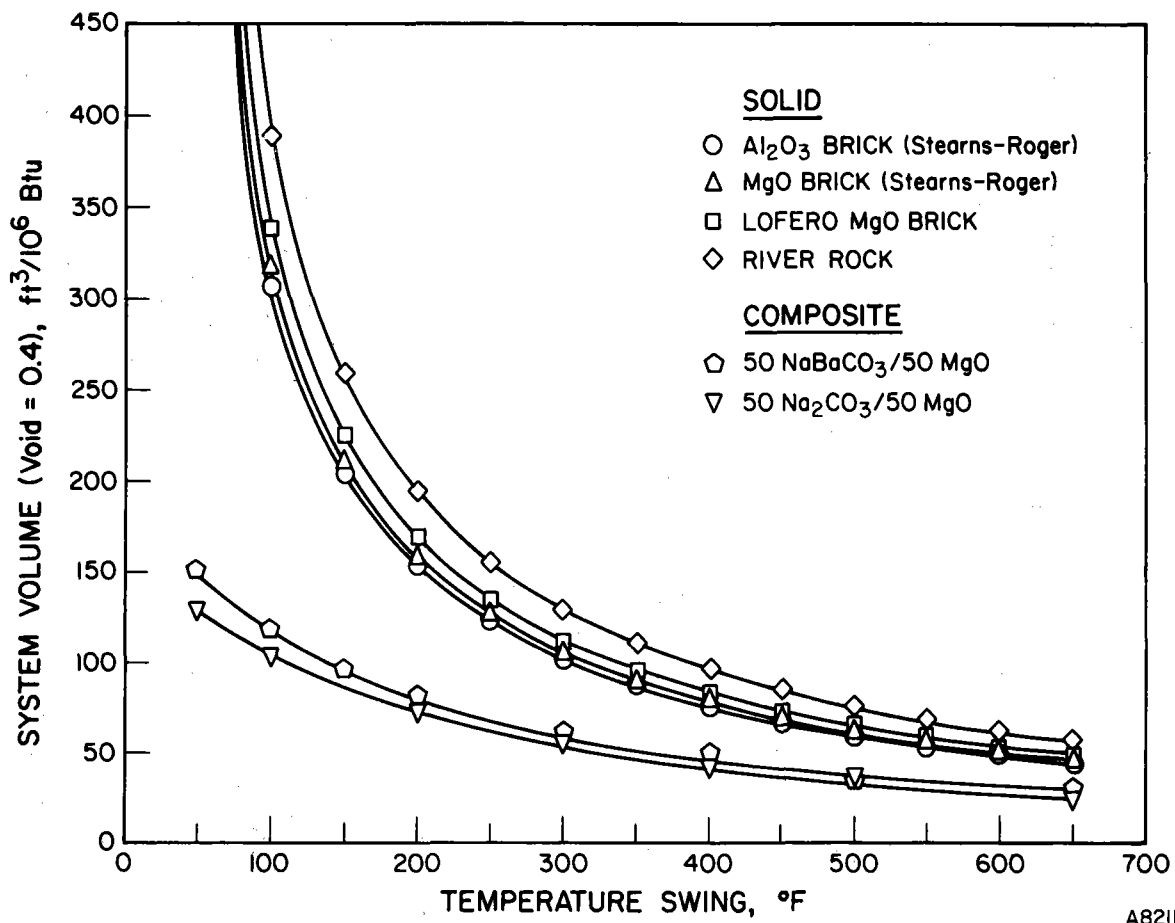


Figure 7-31. STORAGE MEDIA COST IN DOLLARS PER MILLION Btu STORED AS A FUNCTION OF TEMPERATURE SWING FOR BASELINE AND COMPOSITE MEDIA



A82111950

Figure 7-32. VOLUME REQUIREMENTS PER UNIT OF ENERGY STORED AS A FUNCTION OF TEMPERATURE SWING FOR BASELINE AND COMPOSITE MEDIA

- Al<sub>2</sub>O<sub>3</sub> Brick (95.1% purity): Data supplied from a Stearns-Roger [12] TES study study that screened a number of sensible-media-based conceptual TES designs.
- MgO Brick (95.1% purity): Data also from Stearns-Roger report [12]
- Lofero MgO Brick: Data supplied from Kaiser Refractories Co., for a high-temperature regenerator-quality brick.

River rock is also included (priced as random-sized shapes) in these figures as a "lowest cost/highest volume" requirement benchmark, although its long-term performance and mechanical and chemical stability in high-temperature, cyclic operation have yet to be established. Moreover, any special requirements for particle size uniformity or regional rock-type will result in increased cost of this sensible-heat system.

The two composites investigated were 50 wt % Na<sub>2</sub>CO<sub>3</sub>-BaCO<sub>3</sub>/50 wt % MgO (52 wt% BaCO<sub>3</sub>-48 wt% Na<sub>2</sub>CO<sub>3</sub> salt mp = 716°C) and 50 wt % Na<sub>2</sub>CO<sub>3</sub>/50 wt % MgO (Na<sub>2</sub>CO<sub>3</sub> salt mp = 858°C). These composite media were considered to cycle symmetrically about the respective salt mp's in a 250°C (450°F) temperature swing dynamic process. Property data and pertinent mass, volume, and cost results for these media are summarized in Table 7-8 and compared in Table 7-9.

Use of the 50 wt % Na<sub>2</sub>CO<sub>3</sub>-BaCO<sub>3</sub>/50 wt % MgO composite in a 250°C (450°F) temperature swing process results in a 21% (versus Lofero Brick) to 72% (versus Al<sub>2</sub>O<sub>3</sub> Brick) reduction in fabricated media costs and 29% (versus Al<sub>2</sub>O<sub>3</sub> Brick) to 37% (Lofero Brick) reduction in system volume requirements per 1055 MJ (million Btu) stored at 591° to 841°C (1096° to 1546°F).

Furthermore, a 50 wt % Na<sub>2</sub>CO<sub>3</sub>/50 wt % MgO composite results in a 45% (versus Lofero Brick) to 81% (versus Al<sub>2</sub>O<sub>3</sub> Brick) decrease in fabricated media costs and a 32% (versus Al<sub>2</sub>O<sub>3</sub> Brick) to 39% (versus Lofero Brick) decrease in system volume requirement per 1055 MJ (million Btu) stored at the elevated 732° to 932°C (1350° to 1800°F) temperature regime.

It is also particularly important to note that the decreases in system volume for the composite media relative to the sensible media translate directly into further system cost savings through reduced final containment vessel costs. A conservative rule-of-thumb in estimating industrial system costs is that the TES unit containment vessel cost will vary as the 0.6 power of the interior volume of the container [13]. Therefore, the relative cost of containment for composite media to that for the reference sensible system (with void fraction = 0.4) would be expressed by:

$$\frac{\text{Containment Vessel Cost, Composite}}{\text{Containment Vessel Cost, Baseline}} = \left[ \frac{\text{System Volume, Composite, m}^3 \text{ (ft}^3\text{)}}{\text{System Volume, Baseline, m}^3 \text{ (ft}^3\text{)}} \right]^{0.6}$$

The application of the 0.6 rule-of-thumb is an oversimplification of a valuable cost concept, because the actual values of cost-capacity factor may vary from less than 0.2 to greater than 1.0, depending on the actual types of equipment to which the factor is applied [13]. The 0.6 factor should only be used in the absence of other information and should not be used for estimating beyond a tenfold range of capacity.

Table 7-8. COMPARISON OF COMPOSITE MEDIA AND BASELINE (Solid Sensible) STORAGE REQUIREMENTS,  
 $\Delta T = 250^{\circ}\text{C}$  ( $450^{\circ}\text{F}$ )

|  | Al <sub>2</sub> O <sub>3</sub> Brick<br>(S&R) |         | MgO Brick<br>(S&R) |          | Lofero<br>MgO Brick<br>(Kaiser) |        | 50 Wt % Na <sub>2</sub> CO <sub>3</sub> -<br>BaCO <sub>3</sub> /50 Wt % MgO |  | 50 Wt % Na <sub>2</sub> CO <sub>3</sub> /<br>50 Wt % MgO |  |
|--|---|---------|--------------------|----------|---------------------------------|--------|---|--|--|--|
| Composite: Carbonate/MgO Wt Ratio  |   |         |                    |          |                                 |        | 1.0   |  | 1.0  |  |
| Melting Point (Salt), °C (°F)  |   |         |                    |          |                                 |        | 716 (1321)  |  | 858 (1576)   |  |
| Density, kg/m <sup>3</sup> (lb/ft <sup>3</sup> )                             | 3035  | (189.5) | 2867               | (179)    | 2915                            | (182)  | 3258 (203.4)  |  | 2762 (172.4)   |  |
| Heat of Fusion (Salt), J/kg (Btu/lb)   |   | 0       |                    | 0        |                                 | 0      | 172,124 (74)  |  | 255,860 (110)  |  |
| Sensible Heat (Salt + Ceramic), J/kg-K<br>(Btu/lb-°F)                        | 1197  | (0.286) | 1223               | (0.292)  | 1130                            | (0.27) | 1227 (0.293)  |  | 1495 (0.357)   |  |
| Media Unit Cost (Fabricated), <sup>a</sup> \$/kg (\$/lb)                     | 1.65  | (0.75)  | 1.11               | (0.5025) | 0.55                            | (0.25) | 0.62 (0.28)   |  | 0.53 (0.24)  |  |
| Media Mass, kg/1000 MJ (lb/10 <sup>6</sup> Btu)                              | 3340  | (7770)  | 2272               | (7610)   | 3538                            | (8230) | 2500 (5815)   |  | 2025 (4711)  |  |
| Media Volume, m <sup>3</sup> /1000 MJ (ft <sup>3</sup> /10 <sup>6</sup> Btu) | 1.1   | (41)    | 1.16               | (43)     | 1.2                             | (45)   | 0.78 (29)   |  | 0.72 (27)  |  |
| Bed Volume, m <sup>3</sup> /1000 MJ (ft <sup>3</sup> /10 <sup>6</sup> Btu)   | 1.83  | (68)    | 2                  | (71)     | 2.04                            | (76)   | 1.29 (48)   |  | 1.23 (46)  |  |
| M = Media Cost, \$/1000 MJ (\$/10 <sup>6</sup> Btu)                          | 5524  | (5828)  | 3624               | (3824)   | 1951                            | (2058) | 1543 (1628)   |  | 1072 (1131)  |  |

<sup>a</sup> Unit cost of composite media = cost of powders + \$0.10/lb for spray drying + \$0.05/lb for briquetting.

<sup>b</sup> System void volume fraction = 0.4.

B83040432

Table 7-9. COMPOSITE VERSUS BASELINE RATIO AND PERCENT SAVINGS  
FOR MEDIA (Fabricated),  $\Delta T = 250^{\circ}\text{C}$  ( $450^{\circ}\text{F}$ )

|                                     | 50 Wt % $\text{Na}_2\text{CO}_3\text{-BaCO}_3$ /50 Wt % MgO     |               | 50 Wt % $\text{Na}_2\text{CO}_3$ /50 Wt % MgO |               |               |               |
|-------------------------------------|---|---------------|---|---------------|---------------|---------------|
|                                     | Media<br>Cost   | Bed<br>Volume | Media<br>Mass                                 | Media<br>Cost | Bed<br>Volume | Media<br>Mass |
|                                     | Composite/Solid Sensible Scaling Ratio<br>Per $10^6$ Btu Stored |               |   |               |               |               |
| Solid Sensible Media                |   |               |   |               |               |               |
| $\text{Al}_2\text{O}_3$ Brick (S&R) | 0.28  | 0.71          | 0.75  | 0.19          | 0.68          | 0.61          |
| MgO Brick (S&R)                     | 0.43  | 0.68          | 0.76  | 0.30          | 0.65          | 0.62          |
| Lofero MgO Brick (Kaiser)           | 0.79  | 0.63          | 0.71  | 0.55          | 0.61          | 0.57          |
|                                     | Percent Savings Per $10^6$ Btu Stored,<br>Composite Over Solid  |               |   |               |               |               |
| $\text{Al}_2\text{O}_3$ Brick (S&R) | 72  | 29            | 25  | 81            | 32            | 39            |
| MgO Brick (S&R)                     | 57  | 32            | 24  | 70            | 35            | 38            |
| Lofero MgO Brick (Kaiser)           | 21  | 37            | 29  | 45            | 39            | 43            |

53ER/RPE/65055ta



However, for the purpose of this initial comparative evaluation, these conservative relations were computed and appear in Table 7-10 to serve as first-cut estimates of the further, volume-related systems cost advantage of composite media. In this context, the 50 wt%  $\text{Na}_2\text{CO}_3$ - $\text{BaCO}_3$ /50 wt % MgO system may result in a 19% (versus  $\text{Al}_2\text{O}_3$  Brick) to 24% (versus Lofero Brick) savings in TES containment vessel costs, while the 50 wt %  $\text{Na}_2\text{CO}_3$ /50 wt % MgO media may result in a 21% (versus  $\text{Al}_2\text{O}_3$  Brick) to 26% (versus Lofero Brick) savings in containment vessel costs. In addition, further cost and system volume reductions should be possible through optimization of media materials and processing techniques so that greater than 50 wt % molten salt can be retained.

A detailed economic analysis based on a conceptual TES system design utilizing the composite carbonate/ceramic media was beyond the scope of this program. However, a preliminary estimate of installed capital cost requirements was obtained for a TES system for a Brayton cycle solar thermal power system, using the costing approach outlined by Stearns-Roger [12]. This preliminary capital cost was based on substitution of  $\text{Na}_2\text{CO}_3$ - $\text{BaCO}_3$ /MgO media for the  $\text{Al}_2\text{O}_3$  brick reference media considered in the Stearns-Roger study.

The solar thermal power system selected for this analysis was a high-temperature central receiver system with a closed air Brayton cycle and storage subsystem, illustrated schematically in Figure 1. As mentioned earlier, the primary air flow circuit from the receiver is through the turbine, recuperator (low-pressure side), pre-cooler, compressor, and recuperator (high-pressure side), and back to the receiver.

The TES subsystem costed by Stearns-Roger for this Brayton application was based on the conceptual design proposed by Boeing. We considered the case of 6 hours of storage for two 75-MWe gross power modules. The TES subsystem was sized for charge/discharge rates of 360 MWt, thus providing a storage capacity of 2160 MWth-h for thermal cycling between 815° and 491°C (1500°F and 915°F). The TES system costed by Stearns-Roger consisted of  $\text{Al}_2\text{O}_3$  bricks [ $1.95 \times 10^7$  kg ( $4.3 \times 10^7$  lb) of Freyn shapes] arranged within internally insulated, welded carbon steel containers with a void fraction of 0.095. This sensible-heat storage concept required six storage tanks 6.22 m (20.4 ft) in diameter x 47.9 m (157 ft) long.

Based on a TES temperature swing of 815° to 491°C (1500°F to 915°F) ( $\Delta T = 325^\circ\text{C}$ , 585°F) and the known thermophysical properties of  $\text{Na}_2\text{CO}_3$ - $\text{BaCO}_3$  salt and MgO ceramic, it is estimated that the TES media can be reduced from  $1.95 \times 10^7$  kg ( $4.3 \times 10^7$  lb) for  $\text{Al}_2\text{O}_3$  to  $1.59 \times 10^7$  kg ( $3.5 \times 10^7$  lb) of  $\text{Na}_2\text{CO}_3$ - $\text{BaCO}_3$ /MgO composite (19% media mass reduction). Arrangement of composite brick shapes to the same packing density (90.5%) as utilized for the  $\text{Al}_2\text{O}_3$  media will result in a reduction of the media storage volume requirement from 7,116 m<sup>3</sup> (251,300 ft<sup>3</sup>) for  $\text{Al}_2\text{O}_3$  to 5,423 m<sup>3</sup> (191,500 ft<sup>3</sup>) for composite shapes. This reduced storage volume will lead to reduced energy-related equipment costs for storage tanks, tank insulation, and reinforced-concrete tank formation.

TES subsystem costs were estimated using the methodology outlined by Stearns-Roger. Using this approach, a total capital investment cost is obtained by incorporating a number of cost multipliers, based upon Stearns-Roger's experience, to convert costs of fabricated materials and factory equipment to

Table 7-10. COMPARATIVE IMPACT OF VOLUME REDUCTION ON  
 PROJECTED SYSTEM CONTAINMENT COST,  
 $\Delta T = 250^{\circ}\text{C}$  ( $450^{\circ}\text{F}$ )

| Solid Sensible<br>Media             | 50 Wt % $\text{Na}_2\text{CO}_3$ - $\text{BaCO}_3$ /50 Wt % MgO            |      |
|-------------------------------------|--|------|
|                                     | Section A,<br>Composite/Solid Sensible Scaling Ratio Per $10^6$ Btu Stored |      |
| $\text{Al}_2\text{O}_3$ Brick (S&R) | 0.71   | 0.79 |
| MgO Brick (S&R)                     | 0.79   | 0.77 |
| Lofero Brick (Kaiser)               | 0.76   | 0.74 |
|                                     | Section B,<br>Percent Savings Per $10^6$ Btu Stored                        |      |
| $\text{Al}_2\text{O}_3$ Brick (S&R) | 18.6   | 20.7 |
| MgO Brick (S&R)                     | 20.7   | 22.8 |
| Lofero Brick (Kaiser)               | 24.2   | 25.7 |

53ER/RPE/65055ta

direct field cost and total capital investment. The following cost equation was used:

$$CI = 1.95 [1.8 (CE + CP) + MEDIA]$$

where —

CI = capital investment

CE = energy-related equipment cost

CP = power-related equipment cost

MEDIA = media cost

1.8 = multiplier on equipment cost to arrive at direct field cost

1.95 = multiplier on direct field cost and media to arrive at total capital investment.

The 1.8 multiplier allows for the installation labor and provides the direct field costs. The 1.95 capital investment factor includes —

- Engineering (A/E)
- Interest during construction
- Fees, permits, state and local taxes
- Indirect field cost, including —
  - Field expense
  - Temporary facilities
  - Construction equipment
  - Payroll taxes, insurance
  - Performance bonds
- Contingency allowance.

For the purpose of this study it was assumed that the construction cost burdens used apply equally to all capital expenditures.

The storage media cost (MEDIA) was estimated to be  $\$9.83 \times 10^6$  for the  $\text{Na}_2\text{CO}_3$ - $\text{BaCO}_3/\text{MgO}$  composite.

The energy-related equipment cost (CE) corresponds to the costs for storage tanks, tank insulation, and tank foundation. Based on the 22% reduction in storage volume requirements for composite media, CE was estimated from the Stearns-Roger cost data to be  $\$11.31 \times 10^6$  for the composite case.

The power-related equipment cost (CP) is predominantly for air compressors, which Stearns-Roger had costed at  $\$1.77 \times 10^6$ .

The total capital investment cost was thus estimated to be approximately  $\$65 \times 10^6$  for a TES capacity of 2,160 MWth-h ( $7.37 \times 10^9$  Btu). Per unit of installed capacity, this figure corresponds to an installed capital cost of  $\sim \$30/\text{kWh}_c$ . Table 7-11 contains a comparison of the key economic components of the reference air/alumina and the advanced air/composite systems. By the standardized Stearns-Roger costing procedure, the  $\text{Na}_2\text{CO}_3\text{-BaCO}_3/\text{MgO}$  composite system results in the following savings over the reference alumina system:

- Energy-related equipment: 22%
- Media-related costs: 73%
- Capital investment costs: 51%

Table 7-11. PRELIMINARY THERMAL STORAGE ECONOMIC EVALUATION FOR SENSIBLE AND DIRECT-CONTACT COMPOSITE STORAGE SYSTEMS (Two 75-MWe Gross Power Modules)

| Storage Concept                     | Storage Hours | Cost, \$1000 (1980) |       |        |         |
|-------------------------------------|---------------|---------------------|-------|--------|---------|
|                                     |               | CE                  | CP    | Media  | CI      |
| Sensible <sup>12</sup>              |               |                     |       |        |         |
| Air to Alumina (Reference)          | 6             | 14,498              | 1,766 | 36,083 | 127,448 |
| Composite                           |               |                     |       |        |         |
| Air to $\text{NaBaCO}_3/\text{MgO}$ | 6             | 11,308              | 1,766 | 9,828  | 65,000  |
| % Savings Composite Over Reference  |               | 22                  | --    | 73     | 51      |

53ER/RPE/65055ta

## SECTION 8.0

### TASK 4. SUMMARY AND RECOMMENDATIONS

#### 8.1 SUMMARY

Technical accomplishments during this program include —

- Screened, identified, and investigated (from 10 candidate salt mixtures) one salt phase-change material with a composition of 48 wt %  $\text{Na}_2\text{CO}_3$ -52 wt %  $\text{BaCO}_3$  and an mp of  $713^\circ\text{C}$ , and two ceramic support materials ( $\text{NaAlO}_2$  and  $\text{MgO}$ )
  - Selected the  $\text{Na}_2\text{CO}_3$ - $\text{BaCO}_3$ / $\text{MgO}$  composition as model composite system for proof-of-concept and further development
- Developed an effective spray drying process for production of composite carbonate/ceramic (technical-grade) powders
- Formulated a composite pellet fabrication and sintering scheme for stability and proof-of-concept testing
- Demonstrated good thermal stability of  $\text{Na}_2\text{CO}_3$ - $\text{BaCO}_3$ / $\text{MgO}$  pellets containing 60 vol % molten carbonate during 1115 hours (>500 hours testing at  $800^\circ\text{C}$ ) in air with 22 thermal cycles to near room temperature
  - <1% weight loss
  - No dimensional change, deformation, or cracking
- Performed analysis of contact stresses in media pellets in packed-bed configuration. Two-body media mechanical stress analysis
  - Predicted a stable bed height of at least 1.5 m (5 ft) for 2.5-cm (1-in.) diam x 2.5-cm (1-in.) high cylindrical pellets
  - Maximum contact stress (point to point):
    - 3 MPa (440 psi), above salt mp
    - 70 MPa (10,000 psi), at room temperature
  - Minimum contact stress (face to face): < 7 kPa (1 psi)
- Successfully demonstrated stable proof-of-concept lab-scale media packed-bed charge/discharge performance with 17 thermal cycles over  $615^\circ$  to  $815^\circ\text{C}$  through 398 hours at operating temperature
  - 5,233  $\text{W}/\text{m}^2$  (1660  $\text{Btu}/\text{h}\text{-ft}^2$ ) average heat flux rate
  - 0.34  $\text{MWth}\text{-h}$  (1175  $\text{Btu}$ ) bed thermal capacity rating

- Refined economic evaluations of the 50 wt %  $\text{Na}_2\text{CO}_3$ - $\text{BaCO}_3$ /50 wt %  $\text{MgO}$  (salt mp =  $713^\circ\text{C}$ ) and 50 wt %  $\text{Na}_2\text{CO}_3$ /50 wt %  $\text{MgO}$  (salt mp =  $858^\circ\text{C}$ ) composites relative to the  $\text{Al}_2\text{O}_3$ ,  $\text{MgO}$ , and Lofero  $\text{MgO}$  sensible media TES systems

50 wt %  $\text{Na}_2\text{CO}_3$ - $\text{BaCO}_3$ /50 wt %  $\text{MgO}$   $\Delta T = 250^\circ\text{C}$  ( $450^\circ\text{F}$ )

- 19% to 30% reduction in media mass
- 22% to 37% reduction in media volume
- 21% to 72% reduction in media cost
- 51% reduction in "capital investment" vs. Stearns-Roger  $\text{Al}_2\text{O}_3$  "reference" TES system

50 wt %  $\text{Na}_2\text{CO}_3$ /50 wt %  $\text{MgO}$   $\Delta T = 250^\circ\text{C}$  ( $450^\circ\text{F}$ )

- 38% to 42% reduction in media mass
- 32% to 39% reduction in media volume
- 45% to 81% reduction in media cost
- 21% to 20% reduction in volume-related cost

## 8.2 RECOMMENDATIONS FOR FUTURE RESEARCH

- Determine critical composite properties to assess the long-term applicability of carbonate/ceramic composite media
  - Conduct TGA analysis of media decomposition and vaporization
  - Determine carbonate retention characteristics at higher volume fractions of molten salt
  - Determine thermomechanical behavior
  - Measure model media PCM component surface tension, viscosity, and thermal conductivity
- Conduct further research and development on  $\text{Na}_2\text{CO}_3$ -based composites to take advantage of low-cost and high energy storage density materials
  - Improve support materials and synthesis techniques
  - Conduct materials stability testing
- Model composite media behavior to optimize composition, microstructure, and stability
- Optimize media processing techniques

- Conduct long-term (>1000 hours) endurance testing of optimized media
- Model TES heat transfer and charge/discharge performance

## SECTION 9.0

### REFERENCES CITED

1. U.S. Department of Energy, Division of Energy Storage Systems and Division of Central Solar Technology, "Thermal Energy Storage Technology Development for Solar Thermal Power Systems: Multiyear Program Plan," Draft Report. Washington, D.C., March 13, 1979.
2. Maru, H. C., Dullea, J. and Huang, V. M., "Molten Salt Thermal Energy Storage Systems: Salt Selection," COO-2888-1. Chicago: Institute of Gas Technology, August 1976.
3. Maru, H. C. et al., "Molten Salt Thermal Energy Storage Systems: System Design," Report COO-2888-2. Chicago: Institute of Gas Technology, February 1977.
4. Maru, H. C. et al., "Molten Salt Thermal Energy Storage System," Report COO-2888-3. Chicago: Institute of Gas Technology, March 1978.
5. Petri, R. J. et al., "High-Temperature Molten Salt Thermal Energy Storage Systems," Report. Chicago: Institute of Gas Technology (NASA-CR159663), February 1980.
6. Petri, R. J., Claar, T. D. and Marianowski, L. G., "High-Temperature Molten Salt Thermal Energy Storage Systems for Solar Applications," Final Report. Chicago: Institute of Gas Technology, in preparation.
7. Janz, G. J., Conte, A. and Neuenschwander, "Corrosion of Platinum, Gold, Silver, and Refractories in Molten Carbonates," Corrosion 19, 292t-294t (1963).
8. Christie, J. R., Darnell, A. J. and Dustin, D. F., "Reaction of Molten Sodium Carbonate with Aluminum Oxide," J. Phys. Chem. 82, 33-37 (1978).
9. John, R. D., "Corrosion of Metals by Liquid Sodium Carbonate," Ph.D. Dissertation, Ohio State University, Columbus, Ohio, 1979.
10. Information Center for Diffraction Data, Powder Diffraction File — Inorganic Phases. Swarthmore, Pa., 1978.
11. Boeing Engineering and Construction, "Advanced Thermal Energy Storage Concept Definition Study for Solar Brayton Power Plants, Vol. 1," Report for U.S. Department of Energy Contract No. EY-76-C-03-1300. Seattle, Wash., November 1977.
12. Stearns-Roger Services, Inc., "Cost and Performance of Thermal Storage Concepts in Solar Thermal Systems — Conceptual Design Review," Report on work performed for SERI. Denver, September 1980.
13. Peters, M. S. and Timmerhans, K. D., Plant Design and Economics for Chemical Engineers. New York: McGraw-Hill, 1968.



Table A-1. CONVERSION FACTORS

| Non-SI Unit               | Operation                 | SI Unit              |
|---------------------------|---------------------------|----------------------|
| atm                       | X 1.013 X 10 <sup>5</sup> | Pa                   |
| Btu                       | X 1055.06                 | J                    |
| Btu/lb                    | X 2326.00                 | J/kg                 |
| Btu/lb-°F                 | X 4186.80                 | J/kg-K               |
| Btu/h-ft-°F               | X 1.731                   | W/m-K                |
| Btu/h-ft <sup>2</sup> -°F | X 5.678                   | W/m <sup>2</sup> -K  |
| Btu/h-ft <sup>2</sup>     | X 3.154                   | W/m <sup>2</sup>     |
| cal                       | X 4.18                    | J                    |
| °C                        | + 273.15                  | K                    |
| cP                        | X 0.001                   | Pa-s                 |
| °F                        | (5/9) (°F - 32)           | °C                   |
| ft                        | X 0.3048                  | m                    |
| ft <sup>2</sup>           | X 0.0929                  | m <sup>2</sup>       |
| ft <sup>2</sup> /h        | X 0.0000258               | m <sup>2</sup> /s    |
| ft <sup>3</sup>           | X 0.0283                  | m <sup>3</sup>       |
| in.                       | X 0.0254                  | m                    |
| in. <sup>2</sup>          | X 0.00064516              | m <sup>2</sup>       |
| lb                        | X 0.4536                  | kg                   |
| lb/ft <sup>3</sup>        | X 16.018                  | kg/m <sup>3</sup>    |
| lbm/ft <sup>2</sup> -s    | X 4.882                   | kg/m <sup>2</sup> -s |
| mil                       | X 0.0000254               | m                    |
| psia                      | X 6894.8                  | Pa                   |

53ER/RPE/65055ta

|  |   |   |                              |
|--|---|---|------------------------------|
| <b>Document Control Page</b>   | 1. SERI Report No.<br>SERI/STR-231-1860 | 2. NTIS Accession No.   | 3. Recipient's Accession No. |
| 4. Title and Subtitle<br>New Thermal Energy Storage Concepts for Solar Thermal Applications  |   | 5. Publication Date<br>April 1983                               |                              |
| 7. Author(s) R. Petri, E T. Ong, T. D. Claar,<br>L. G. Marianowski   |   | 6.  |                              |
| 9. Performing Organization Name and Address<br>Institute of Gas Technology<br>IIT Center, 3424 S. State Street<br>Chicago, Illinois 60616  |   | 8. Performing Organization Rept. No.                            |                              |
|  |   | 10. Project/Task/Work Unit No.<br>1298.12                       |                              |
|  |   | 11. Contract (C) or Grant (G) No.<br>(C) XP-0-9371-2<br><br>(G) |                              |
| 12. Sponsoring Organization Name and Address<br>Solar Energy Research Institute<br>1617 Cole Boulevard<br>Golden, Colorado 80401   |   | 13. Type of Report & Period Covered<br>Technical Report         |                              |
|  |   | 14.   |                              |
| 15. Supplementary Notes<br><br>Technical Monitor: Werner Luft  |   |   |                              |
| 16. Abstract (Limit: 200 words)<br>This report presents the results of an investigation into the feasibility of an advanced concept of composite salt/ceramic storage media for high-temperature solar thermal storage applications. This novel approach involves retention and immobilization of phase-change salts within porous ceramic matrices by capillary action. Composite media pellets, bricks, or other suitable shapes may be used in direct-contact heat recovery/storage applications with compatible fluids, thus eliminating the expensive heat exchanger tubes required in molten-salt storage systems utilizing shell-and-tube designs. Higher heat transfer rates are also expected because the thickness of solidified salt zones can be controlled and minimized. |   |   |                              |
| 17. Document Analysis<br>a. Descriptors Barium carbonates ; Brayton Cycle power systems ; carbonates ; ceramics ; cost ; economic analysis ; heat storage ; latent heat storage ; magnesium oxides ; molten salts ; phase change materials ; sensible heat storage ; sodium carbonates ;<br>b. Identifiers/Open-Ended Terms solar thermal power plants ; thermal energy storage equipment<br><br>c. UC Categories<br>62e   |   |   |                              |
| 18. Availability Statement<br>National Technical Information Service<br>U.S. Department of Commerce<br>5285 Port Royal Road<br>Springfield, Virginia 22161   |   | 19. No. of Pages<br>87  |                              |
|  |   | 20. Price<br>\$11.50  |                              |

UNITED STATES DEPARTMENT OF ENERGY

P.O. BOX 62  
OAK RIDGE, TENNESSEE 37830

OFFICIAL BUSINESS  
PENALTY FOR PRIVATE USE \$300

POSTAGE AND FEES PAID

UNITED STATES  
DEPARTMENT OF ENERGY



1158 FS- 1  
SANDIA NATIONAL LABS  
ATTN TECH LIB  
LIVERMORE, CA 94550